January 2016

Effect Of Bridging Group Of Dianhydride Precursor On Resulting Thermally Rearranged Polybenzoxazole For Removal Of Nitrogen From Natural Gas

Tucker Woock

EFFECT OF BRIDGING GROUP OF DIANHYDRIDE PRECURSOR ON
RESULTING THERMALLY REARRANGED POLYBENZOXAZOLE FOR
REMOVAL OF NITROGEN FROM NATURAL GAS

By

Tucker William Woock
B.S. Chemistry, University of Jamestown 2013
B.S. Mathematics, University of Jamestown 2013

A Thesis

Submitted to the Graduate Faculty

of the

University of North Dakota

in partial fulfillment of the requirements

for the degree of

Master of Science

Grand Forks, North Dakota

December
2016

This thesis, submitted by Tucker Woock in partial fulfillment of the requirements for the Degree of Master of Science from the University of North Dakota, has been read by the Faculty Advisory Committee under whom the work has been done and is hereby approved.

_____
Dr. Ali S. Alshami

_____
Dr. Brian Tande

_____
Dr. Edward Kolodka

This thesis is being submitted by the appointed advisory committee as having met all of the requirements of the School of Graduate Studies at the University of North Dakota and is hereby approved.

_____
Dr. Grant McGimpsey
Dean of the School of Graduate Studies

December 5, 2016
_____
Date

PERMISSION

Title   Effect of Bridging Group of Dianhydride Precursor on Resulting Thermally Rearranged Polybenzoxazole for Removal of Nitrogen from Natural Gas

Department   Chemical Engineering

Degree   Master of Science

In presenting this thesis in partial fulfillment of the requirements for a graduate degree from the University of North Dakota, I agree that the library of this University shall make it freely available for inspection. I further agree that permission for extensive copying for scholarly purposes may be granted by the professor who supervised my thesis work or, in his absence, by the Chairperson of the department or the dean of the School of Graduate Studies. It is understood that any copying or publication or other use of this thesis or part thereof for financial gain shall not be allowed without my written permission. It is also understood that due recognition shall be given to me and the University of North Dakota in any scholarly use which may be made of any material in my thesis.

Tucker Woock
12/5/2016

TABLE OF CONTENTS

LIST OF FIGURES

LIST OF TABLES

ACKNOWLEDGMENTS

ABSTRACT

Membrane separation is an excellent potential method for purification of natural gas. Multiple polymers have been studied for use in natural gas separation, and two stand above the rest: polyimide and polybenzoxazole. It was found that the selection of monomer precursors could influence the separation properties and resistances of the resultant polyimide and polybenzoxazole membranes. Polybenzoxazole has even better separation properties than polyimide due to the size and distribution of its free volume elements. Methods to influence these properties are similar to those used with polyimides. The intent of this thesis was to compare different dianhydride precursors. My research attempted to compare the permeabilities and selectivities of polybenzoxazole membranes thermally rearranged from hydroxyl-polyimides formed from four dianhydride precursors. The hydroxyl-polyimides were formed by the azeotropic synthesis method, cast into membranes, thermally rearranged into polybenzoxazoles, and underwent permeation testing using a manifold constructed in-house. It was found that hydroxyl-polyimides were indeed formed, but not completely thermally rearranged, and the setup for permeation testing was insufficient to fulfill the goal of this thesis. Thus no conclusions on the effect of the dianhydride bridging group could be made.

CHAPTER I

INTRODUCTION

Every year, enormous volumes of natural gas are released along with oil during drilling across the United States and the rest of the world. More and more of this gas is being flared off due to being unusable. It is unusable because it is highly contaminated with gases such as nitrogen and carbon dioxide, which can't be processed to create electricity or heat, thus decreasing the natural gas' heating value[1]. When researchers began looking for alternatives to the overly large and expensive methods of natural gas purification, they turned to polymer membranes.

Eventually it was found that a form of the polymer polyimide, which is formed by the condensation reaction between diamine and dianhydride monomers, has excellent gas separation properties, especially with respect to natural gas purification. It was also found that by using different diamine and dianhydride precursors, researchers could influence the separation properties of the membranes. By picking diamines or dianhydrides with bulkier pendant groups or more rigid bridging groups, researchers could impact the polymer chain packing efficiency and the polymer chain rigidity of the polymer matrices[2].

Recently researchers found that polyimides containing a hydroxyl group located ortho to the imide functional group, called hydroxyl-polyimides, could be

1

thermally rearranged into a new polymer, called polybenzoxazole.

Polybenzoxazole has even better separation properties than polyimide. This is

because the cavities within the polymer matrix of the polyimide tend to meld

together during thermal rearrangement, which creates larger cavities with a

bottleneck shape[3].

Please see the literature review in the next chapter for extensive

descriptions and discussions about polyimide and polybenzoxazole.

Hypothesis

Despite an abundance of studies examining the effect of the structure of

the diamine precursor on the resulting thermally rearranged polybenzoxazole,

there is a surprising dearth of analogous studies dealing with the dianhydrides.

My thesis project attempts to determine, out of four candidate

dianhydrides with varying bridging groups, which one will produce a

polybenzoxazole with the best separation properties. The four candidate

dianhydrides are:

4,4'-oxydiphthalic anhydride (ODPA)
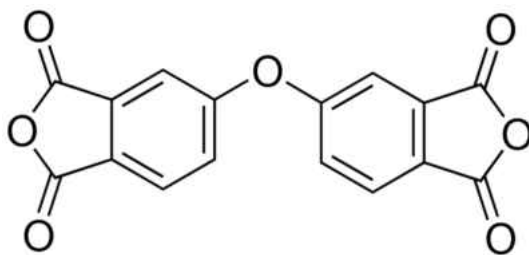
3,3',4,4'-benzophenone tetracarboxylic dianhydride (BTDA)
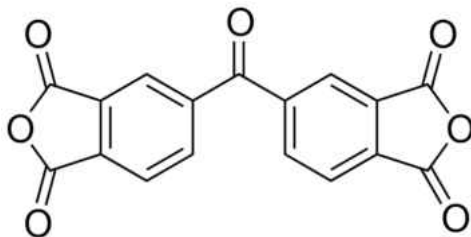
3,3',4,4'-biphenyl tetracarboxylic dianhydride (BPDA)
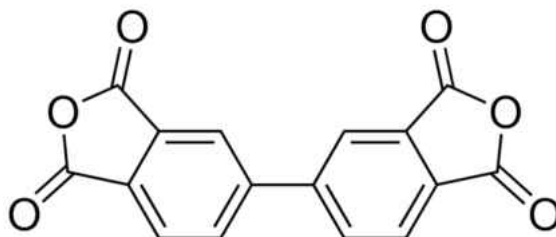
Benzene-1,2,4,5-tetracarboxylic dianhydride or pyromellitic dianhydride (PMDA)
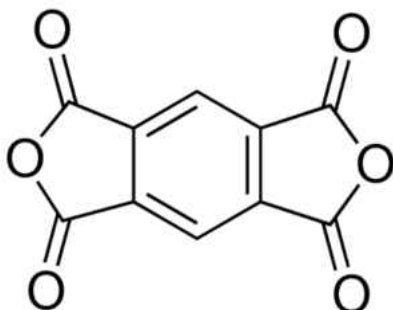
These dianhydrides will all be combined with the diamine 2,2'-bis(3-amino-4-hydroxyphenyl) hexafluoropropane (bisAPAF), pictured below.
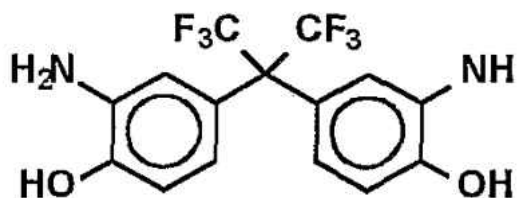
My hypothesis is that the BPDA will produce the polybenzoxazole with the best separation properties, because it has a bridging group that will give the most polymer chain rigidity out of the four candidates.

Outline of Thesis

This thesis consists of seven chapters. Chapter one is the introduction, which introduces the problem my research is focused on and my hypothesis. Chapter two is a literature review of polyimides and thermally rearranged polybenzoxazoles and their evolution with regards to separating nitrogen and other gases from natural gas, along with some general history of membrane separation. Chapter three consists of the synthesis and membrane formation portions of the research. Chapter four discusses more of the membrane formation, including thermal rearrangement, and the permeation testing. Chapter five contains detailed additional information regarding the synthesis and membrane formation covered in chapter three. Similarly to chapter five, chapter six has more detailed information than covered in chapter four. Chapter seven offers a general conclusion and provides the endcap for the thesis.

CHAPTER II

LITERATURE REVIEW

Introduction

From February to July of 2015 alone, approximately 16 trillion cubic feet of natural gas was released from reservoirs due to oil drilling throughout the U.S.[4]. While the nitrogen content of this crude natural gas is usually no more than 8-15%, most pipelines can transport natural gas only if it contains less than 4-6% nitrogen, so some nitrogen has to be removed[5]. This removal of nitrogen and other impurities from natural gas serves four purposes: 1) to increase the fuel heating value, 2) to reduce corrosion within the pipeline, 3) to decrease atmospheric pollution, and 4) to reduce the volume of gas that needs to be transported[1].

One method of separating the nitrogen from natural gas is fractionation, which requires a large amount of energy and other resources. The gas stream has to be liquefied, which means that enough carbon dioxide and water vapor would have to have been previously removed to prevent freezing. The liquefaction consists of compression and expansion of the gas stream. Other methods include cryogenic separation and pressure swing adsorption. Cryogenic distillation involves distillation towers that cool the gases to liquefy the gas in the stream with the higher boiling point, and allowing them to be separated. Pressure swing adsorption uses molecular sieves that selectively adsorb nitrogen

to remove it. Both of these processes, along with fractionation, are better suited for larger scale gas fields. Operators of smaller gas fields often cannot process their natural gas because they cannot afford these methods, and even for large scale fields they are very expensive.

Researchers began examining membrane separation as an alternative to these methods because of its high energy efficiency relative to earlier methods, operational simplicity, and small footprint. Membrane separation has no heating element, so much less energy is needed. Membranes are made of polymers that are usually inexpensive, especially when compared to the costs of the processes described above. Membrane separation also uses considerably less equipment overall.

Membrane processes have been studied since at least the 1750s[6], and continued to be studied for hundreds of years until multiple breakthroughs in the 1980s and 1990s. One of the most important breakthroughs was in 1994, when Paul *et al.* produced high flux asymmetric membranes, called Loeb-Sourirajan membranes, with nanoscale thicknesses. These membranes were limited due to various defects that formed during their production[7]. In the early 1990s new processes emerged that allowed the fabrication of various membrane macro-geometries, such as hollow fiber and spiral wound, which were able to vastly increase the ratio of surface area to volume of membranes[8].

Over the last two decades, studies researching gas separation membranes, specifically polyimide membranes, have increased greatly, with almost fivefold articles published in 2007 than in 1985. Polyimides emerged as

the forerunner due to their high permeability, selectivity, chemical and thermal resistance, and mechanical strength. Even before polyimides became popular research subjects, they were recognized as highly effective separation membranes by Du Pont Co. in the United States as far back as 1962, when Du Pont began testing polyimides for the separation of helium from natural gas[6].

Over the years it has been found that the permeability and selectivity of polyimide membranes can be controlled by modifying their molecular structure[2]. In 2007, it was found that even further adjustments can be made to polyimide membranes to produce even more desirable properties. Specifically, they are thermally rearranged into polybenzoxazole, which has even higher permeability and selectivity than its progenitor polyimide[9]. This review will focus on the evolution of the polyimide as a gas separation membrane, its subsequent transformation into polybenzoxazole, and various studies done to optimize the separation ability of polybenzoxazole.

Theory and Background

In 1866, Sir Thomas Graham presented his model for solution-diffusion, which is generally regarded as the foremost model of gas molecules being transported through polymeric membranes[10]. This model states that the transport of a gas molecule begins with its dissolution into the face of the membrane, then diffusion through the membrane itself, then desorption from the opposite face at a lower pressure. The rate-limiting step in this process is the diffusion step, which

is controlled by the movement of the individual polymer chains. As the chains shift, the gas molecules move through the open spaces between the chains[11].

Solution-Diffusion Model

Membrane separation is governed by the following equation for volumetric flux (j_i)[12]:

$$j_i = \frac{P_i(p_{io} - p_{il})}{l}$$

where j_i is the steady state flux through the membrane in (cm^3 of component i)/(cm^2 s), P_i is the membrane permeability for component i, given in Barrer ((10^{-10} cm^3 cm)/(cm^2 s cmHg)), p_{io} is the partial pressure of component i on the entrance side of the membrane (cmHg), p_{il} is the partial pressure of component i on the exit side of the membrane (cmHg), and l is the thickness of the membrane (cm). The term P_i can be found by the following equation[12]:

$$P_i = D_i S_i$$

Where D_i is the effective concentration-averaged diffusion coefficient (cm^2/s), and S_i is the gas solubility coefficient (cm^3 of component i)/(cm^3 of membrane cmHg).

The membrane selectivity for ideal gases i and j ($\alpha_{i/j}$) is given by the following equation[12]:

$$\alpha_{\frac{i}{j}} = \frac{P_i}{P_j} = \frac{D_i S_i}{D_j S_j}$$

The term D_i/D_j is the ratio of diffusivity of gases i and j, which reflects to the ratio of sizes of the molecules of gases i and j. This is because the diffusivity through the free volume elements of the membrane is determined by the size of the molecules, and the smaller molecules are favored. The term S_i/S_j reflects the

8

ratio of condensabilities of the two gases in the polymer matrix and the relative affinity of the gases for the polymer matrix. This is because higher condensability generally causes higher gas sorption through a polymer membrane, so the gas with higher condensability will be favored[12].

The K_i/K_j term for the mixture of nitrogen and methane (K_{N2}/K_{CH4}) generally ranges from 0.2 to 0.4[12], which means that it will change very little as the type of polymer used for the membrane changes. The diffusivity ratio D_{N2}/D_{CH4}, which can change greatly depending on the polymer used, generally ranges from 1 to 6[12].

Fractional Free Volume

Gas molecules diffuse through a membrane by traveling through spaces between the moving polymer chains. The sum of these spaces is called the free volume, and the fractional free volume (FFV) is given by the equation:

$$FFV = \frac{V - V_0}{V}$$

where V is the total volume of the membrane and V_0 is the volume occupied by polymer chains[6].

Free volume is created by the constant vibration of the individual polymer chains and the tendency of the chains to tangle and untangle. Hence the diffusion of gas molecules is controlled by the size of the molecule, the amount and distribution of free volume in the membrane, and the mobility of the polymer chains[1].

Positron annihilation spectroscopy (PALS) is utilized to measure the free volume. Orthopositronium (o-Ps) is inserted into the polymer matrix and the time

it takes for the o-Ps to decay is recorded. The decay of o-Ps occurs more quickly

in the free spaces of the matrix, so the decay time is proportional to the amount

of free volume in the matrix[13]. Although PALS provides fairly accurate insight into

the free volume of a membrane, it is not as accurate as it could be. Since the

introduction of gas molecules into the polymer matrix affects the positions of the

polymer chains and therefore the amount and distribution of free volume, there is

no way to produce an exact representation of what happens to the free volume

during the actual diffusion process[1].

Limitations of Membrane Separation

Permeability/Selectivity Trade-off

The ultimate goal is to produce membranes with both high selectivity and

high permeability. A membrane with higher selectivity will produce a product

stream with fewer impurities. A membrane with higher permeability will produce a

larger product stream per area membrane. Both of these will decrease capital

costs by using less of the polymer and create more revenue by creating more

product with higher purity.

Although it is desirable to have both high selectivity and high permeability,

there is a trade-off between the two. This trade-off is best described by the

following equations[14]:

$$\propto_{\frac{i}{j}} = \frac{\beta_{\frac{i}{j}}}{(P_i)^{\frac{\lambda_i}{j}}}$$

and

$$\ln\left(\alpha_{\frac{i}{j}}\right) = \ln\left(\beta_{\frac{i}{j}}\right) - \lambda_{\frac{i}{j}} * \ln(P_i)$$

where $\beta_{i/j}$ is an empirical parameter based on the condensability of the gas

mixture, and is similar to the S terms previously discussed. The $\lambda_{i/j}$ is an empirical

parameter based on the sizes of the gases and is related to the diffusivity (D)

terms discussed previously[14].

A graph of $\alpha_{i/j}$ vs P_i shows a negatively sloped curve that is an upper

bound for the points indicating values for different types of polymers[14]. This

relationship was shown by Robeson in 1991 with an update in 2008 for the

CO_2/CH_4 gas pair in Figure 1[15].
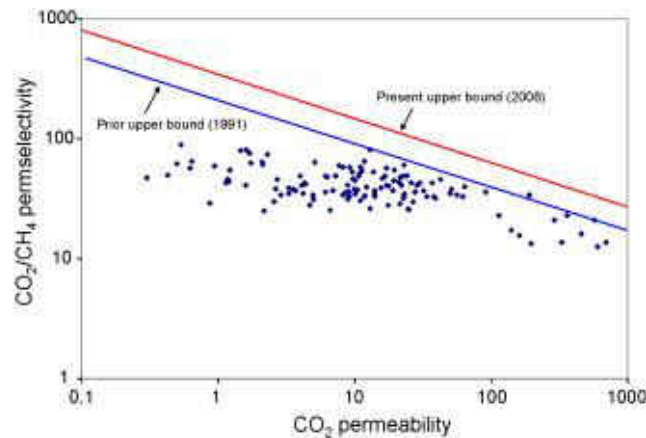
Figure 1: Experimental pure gas data for CO_2/CH_4 separation[15]

This trade-off can also be seen in the relationship between the

permeability and selectivity of the polymer poly(1-trimethylsilyl-1-propyne)

(PTSMP), which has the highest permeability of all known polymers[9]. It has very

large pores, upwards of 0.6-0.7 nm[9], and they are highly interconnected. These

large and plentiful pores allow many molecules to pass through, granting high

permeability but very low selectivity. This shows that the most important factor in

the permeability and selectivity of a polymer membrane is the free volume size and distribution

Physical Aging

Polymer chains move in order to minimize free volume, which leads to an increase in density. This is antithetical to optimizing gas separation, which requires ample amounts of free volume.

There are currently two mechanisms that are regarded as the foremost method of physical aging in membranes. The first mechanism entails the diffusion of free volume to the surface of the membrane, where it is lost to the atmosphere[16]. This diffusion of free volume is dependent on the thickness of the membrane, with thinner membranes having more loss of free volume due to a smaller distance that it has to travel to leave the membrane. The second mechanism involves lattice contraction, in which the entire polymer matrix contracts and compresses the free volume elements within it. Unlike free volume diffusion, lattice contraction occurs at the same rate for different thicknesses of the membrane. Often the two mechanisms combine, with lattice contraction accelerating free volume diffusion out of the polymer by creating a pressure difference within the membrane[17].

These mechanisms lead to the conclusion that membranes with more free volume and less efficient chain packing will lose free volume at a higher rate than membranes with better chain packing. This can be seen in a study by Kim *et al.* in 2006, in which they studied the loss of free volume in polyimide membranes. They found that the membranes with higher amounts of free volume underwent

faster physical aging[18]. Faster physical aging leads to a decrease in permeability and introduces time-dependent separation properties. This is one of the reasons these polymer membranes are not used more in industry, as the ability of the membrane to separate gas molecules will decrease over time[1].

The thickness of the membrane film also affects its physical aging. A study by Wang *et al.* in 2014 found that thinner films had a higher rate of physical aging than thicker films, as can be observed by the decrease in permeability over time seen in Figure 2. The thick and thin films had a similar rate of plasticization with respect to CO_2 exposure time for approximately one hour, after which the rate of plasticization of the thin films decreases greatly[19]. This trend is also shown in Figure 2.
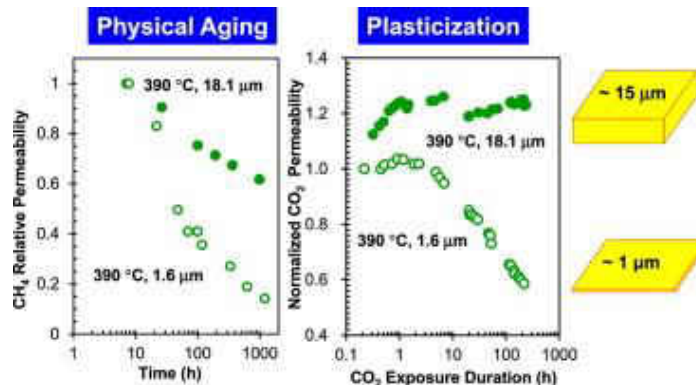
Figure 2: Physical aging of thick and thin membranes with respect to time and plasticization of thick and thin films with respect to CO_2 exposure time[19]

Plasticization

When a gas diffuses through a polymer membrane, gas molecules do not immediately exit through the other side of the polymer. They remain within the structure of the polymer for an amount of time. If the concentration of gas inside the membrane gets high enough, plasticization may occur. Plasticization is the

increase in free volume and chain motion within the polymer that results from excess molecules pushing the chains apart. Plasticization causes an increase in permeability for every type of molecule, and therefore the selectivity drastically decreases. Plasticization causes the permeability of a gas to increase as the upstream partial pressure of that gas increases. For CO_2 and N_2 separation from natural gas, specifically, plasticization occurs because the permeability of the membrane for CH_4 increases at a faster rate than its permeability for CO_2 or N_2 as the upstream pressure increases[20]. Plasticization can also be caused by impurities in the gas stream, especially if they have higher sorption than the desired gas molecules[21].

Polyimide Synthesis

There are two methods of fabricating polyimide membrane systems. The first is creating a pure polyimide by synthesizing various dianhydrides and diamines. The second is combining a polyimide system with another type of polymer, which will not be discussed in this review. There are also methods for improving desired properties by manipulating the finished polyimide, either by thermal annealing or by cross-linking.

Design of Polyimide

The general monomer of a polyimide is shown in Figure 3.
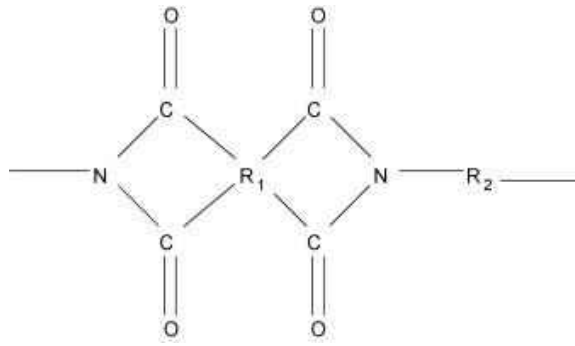
Figure 3: General Structure of Polyimide[1]

This structure is created by the condensation reaction of a dianhydride with a diamine. The structure of the dianhydride will dictate the R_1 group and the structure of the diamine will determine the R_2 group in Figure 3. The properties of a polyimide can be altered by selecting different dianhydrides and diamines to use as precursors[1]. The properties of interest for membrane separation are inter-chain spacing and chain mobility, which control the permeability of the membrane, and the chain rigidity, which controls the selectivity. Hence the three factors to examine are the type of pendant groups (polar or bulky), the type of spatial linkage (meta or para), and the type of bridging group, since these factors have the greatest effect on the aforementioned properties.

The polarity of a side group will affect interchain interactions and impact the chain rigidity and packing efficiency. Pendant groups with higher polarity increase chain rigidity and packing efficiency, which increases selectivity while decreasing permeability. This was confirmed by Tanaka *et al.* in 1995, when they showed that a polyimide with the more polar carbonyl group displayed higher selectivity and lower permeability than a polyimide with a methyl group in the same place[22]. The bulkiness of a side group has a similar effect because bulkier

15

side groups increase chain rigidity and packing efficiency. This was demonstrated by multiple teams, with Tanaka *et al.* showing that increasing pendant group bulk increased permeability and decreased selectivity. They showed this by comparing polyimides containing methylenedianiline (MDA, hydrogen as pendant), isopropylidenedianiline (IPDA, methyl as pendant), and 2,2-bis(4-aminophenyl) hexafluoropropane (6FpDA, carbon trifluoride as pendant). The permeability followed the pattern MDA<IPDA<6FpDA and the selectivity followed the pattern 6FpDA<IPDA<MDA. These fit with the pattern of the size of the side groups, which is MDA<IPDA<6FpDA[23]. Another study, comparing polyimides made up of 3,6-diaminocarbazole, which has hydrogen as a pendant, and N-ethyl-3,6-diaminocarbazole, which has an ethyl pendant group, produced similar results as Tanaka *et al.*[24].

The two previously mentioned studies also found that polyimides with meta- spatial linkage configurations had higher chain packing efficiency and more rigid chains, which led to higher selectivity and lower permeability in membranes[23,24]. This relationship was also studied by Coleman *et al.* by comparing 6FpDA and its meta counterpart, 2,2-bis(3-aminophenyl) hexafluoropropane (6FmDA). It was found that the 6FmDA version of the polyimide possessed higher selectivity for the gas pair CO_2/CH_4, with a selectivity coefficient of 63, while 6FpDA had a selectivity coefficient of 39.9. The 6FpDA had a much higher CO_2 permeability, however, with a permeability coefficient of 63.9, while the 6FmDA had a permeability coefficient of 5.1[25].

Increasing the chain rigidity and packing efficiency of the polyimide membrane will increase its selectivity and decrease its permeability. These properties are also affected by the rotational energy of the bridging groups between aromatic parts of the polymer. Chains with lower rotational energy move more easily and therefore allow more free volume, thus increasing permeability and decreasing selectivity. In addition to examining the effect of different spatial linkage configurations, Coleman *et al.* (1990) also studied the effect of bridging groups with higher and lower rotational energies. They compared MDA, which contains CH_2 as the bridging group between two phenyls, and 4,4'-oxydianiline (ODA), which contains an oxygen atom as the bridging group. Their results did not follow the expected paradigm, since the polyimide containing MDA had both a lower permeability and lower selectivity[25]. This was further studied by Xu *et al.* in 1997 who added a polyimide containing phenylene thioether (PPTI-1), which has a sulfur atom as a bridging group. This PPTI-1 produced higher selectivity than the ODA[26]. Comparing the results of these two studies shows that the selectivity of the membrane corresponds with the electronegativity of the bridging group, with higher electronegativity causing stronger interchain interactions and therefore higher selectivity.

To summarize, a membrane with optimal selectivity needs to have bulky and/or polar pendant groups, meta linkages, and bridging groups with high rotational energy barriers and electronegativity.

Thermal Annealing

Since polyimide membranes have time dependent separation properties due to physical aging, methods of mitigating physical aging have been tested. The first of these is thermal annealing, which involves heating the polymer to a high temperature and quickly quenching it. This would, in theory, cause a stiffening of the polymer chains, thereby rendering the free volume immobile and able to retain constant separation properties for a longer period of time. This idea was investigated by Fuhrman *et al.* in 2004 by creating polyimides out of hexafluoroisopropylidine-diphthalic anhydride (6FDA) and 6FmDA or 6FpDA, then heating and quenching them. These quenched polyimides showed much higher permeabilities than their unquenched counterparts, with the 6FDA-6FmDA having up to 90% more permeability. The quenched samples also retained their separation properties for much longer[27].

Cross-linking

Cross-linking of polyimides can be performed by many methods, the main four of which are ultraviolet radiation, ion beam radiation, thermal treatment, and chemical treatment. These treatments can have large impacts on the properties of the polyimide membrane. The most important of these impacts are increasing the stability of the membrane, attaining better gas separation abilities, and decreasing plasticization caused by CO_2.

Kita *et al.* found in 1994 that an improvement in selectivity could be attained through periods of ultraviolet irradiation, although this increase was accompanied by a decrease in permeability. This was speculated to be due to

the polymer chains decreasing in mobility and the consequent increase of density

of the polymer matrix. This difference in selectivity and permeability increased

with increasing duration of exposure to the ultraviolet radiation[28]. In 2000, Won *et*

al. found an analogous shift in selectivity and permeability with exposure to ion

beam radiation, although this method was deemed disadvantageous for industrial

utilization due to its high cost and the great inconvenience of irradiating entire

sheets of membrane or hollow fiber membranes[29].

Thermal annealing has also been shown to initiate cross-linking in

polyimide membranes containing 6FDA[30]. It was ascertained that polyimides

comprised of acetylene groups were able to undergo Diels-Alder cross-linking

when thermally treated. This cross-linking increased selectivity while having a

small decrease in permeability, and also greatly slowed CO_2 plasticization[31].

Thermal treatment intended to induce cross-linking often occurs concurrently with

chemical treatment. Chemical treatment is performed by combining the

polyimides with oligomers or monomers that terminate in cross-linkable reactive

groups. The majority of chemical treatments designed to cross-link polyimides

take place at elevated temperatures. For example, Rezac *et al.* (1997)

successfully cross-linked a polyimide comprised of 6FDA and IPDA with a

diacetylene oligomer. This reaction was carried out at a temperature of 340°C

and the cross-linking improved the selectivity and the permeability of the

polyimide[32]. The impact of cross-linking is heavily dependent on the structure of

the cross-linking agents and the temperature at which the reaction is performed.

The above example is a special case, as usually cross-linking decreases

permeability in addition to increasing selectivity. However, cross-linking

polyimides containing carboxylic groups with ethylene glycol can increase the

permeability of the membrane without decreasing its selectivity[1]. In 1991, Hayes

et al. discovered a method of cross-linking that incorporated creating a solution of

polyimide with a diamine that did not require elevated temperature[33].

Summary of Polyimide Performance

Table 1 summarizes the performances, in permeability and selectivity, of

the various designs of PI membranes from studies examined in this review.

Table 1: Gas permeability and selectivity of PI membranes

Diamine	P_{CO2} (barrer)	P_{N2} (barrer)	CO_2/CH_4 Selectivity	N_2/CH_4 Selectivity	Ref
MDA	19	-	45	-	23
IPDA	30	-	43	-	23
6FpDA	640	-	400	-	23
6FmDA	5.1	-	63	-	25
ODA	23	-	61	-	25
PPTI-1	23	-	35	-	26
Kapton	0.263	0.035	84	11.2	34
bisAPAF-BTDA	10.10	0.45	45	2.00	35
bisAPAF-ODPA	1.7	0.071	85	3.55	36

Thermally Rearranged Polybenzoxazole

Overview

First introduced by Hill *et al.* in 2007, polybenzoxazole (PBO) has become

a staple of the field. PBO is formed by thermal rearrangement of aromatic

polyimides with hydroxyl groups occupying the spot ortho- to the carbon-nitrogen

bond of the imide ring. This thermal rearrangement occurs when the polyimide is

subjected to a high temperature, generally 300-500°C, for an extended period of

time. This method of thermal rearrangement also negates the high insolubility of

PBO by beginning with precursors that are workably soluble[9]. The general

mechanism for this reaction is shown in Figure 4, and the entire mechanism is

shown in Figure 5.
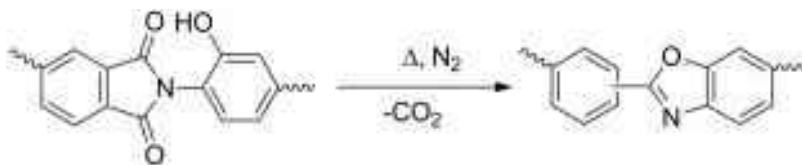
Figure 4: General mechanism for thermal rearrangement of hydroxyl-polyimide

(HPI) to PBO[6]
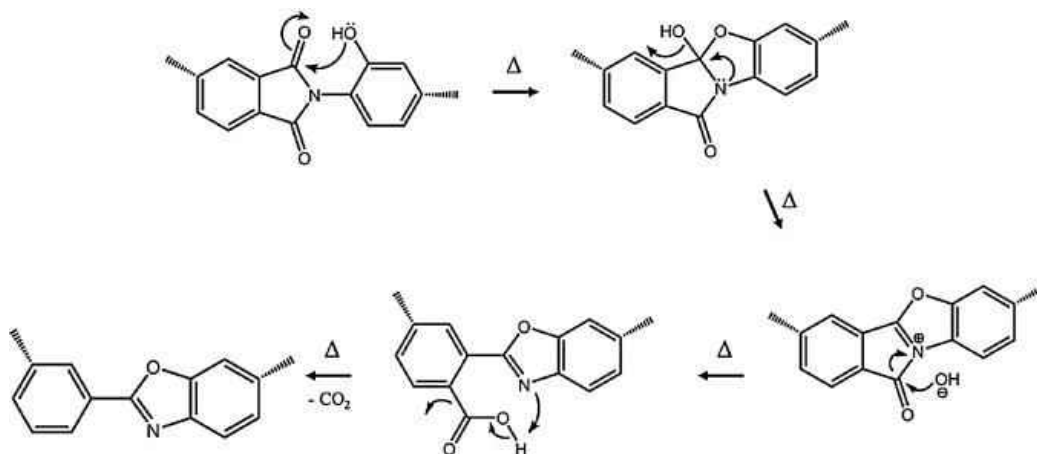
Figure 5: Complete mechanism for thermal rearrangement of HPI to PBO[37]

The reaction starts with an attack by the lone pair of electrons on the

ortho-hydroxy oxygen towards the near carbonyl carbon, which makes one of the

bonds of the carbonyl reacts with the hydrogen from the ortho-hydroxyl. Then the

lone pair from the nitrogen forms a double bond with the carbon that used to be

the carbonyl carbon, and this separates the hydroxide. The wandering hydroxide

is then attracted to the opposite carbonyl carbon, forcing the bond between the

carbonyl carbon and the nitrogen to retreat as a lone pair to the nitrogen. The last

step of the reaction consists of the rearrangement and departure of the chimera

molecule containing the original opposite carbonyl and the displaced hydroxyl group as carbon dioxide.

This rearrangement increases the fractional free volume, diminishes the free volume distribution, and leads to a more homogeneous membrane[9]. This change can be shown by PALS and small-angle X-ray scattering (SAXS), with an example shown in Figure 6.
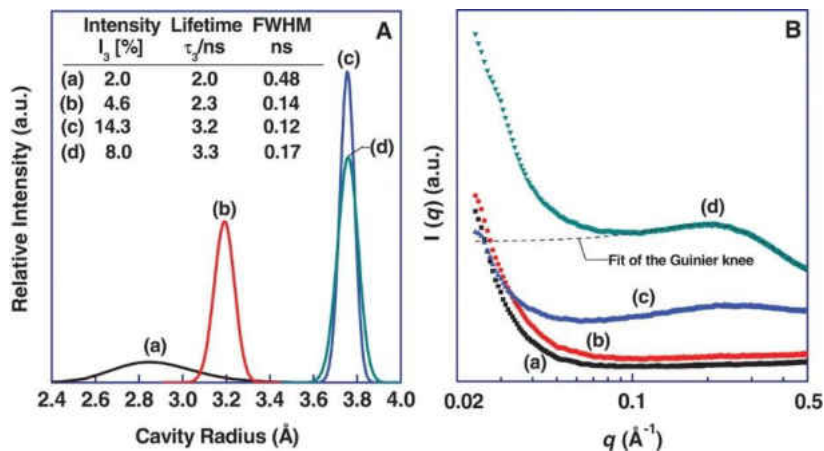
Figure 6: (A) Change of cavity radius (Å) distribution, measured by PALS as a function of treatment temperature, and (B) SAXS profiles for (a) PIOFG-1 thermally rearranged at (b) 350ºC, (c) 400ºC, and (d) 450ºC[9]

Figures 2-6A and 2-6B show the change in the distribution of different pore sizes as a polyimide is thermally rearranged. The curves for (a) are the original polyimide PIOFG-1, which was formed from 6FDA and 2,2'-bis(3-amino-4-hydroxyphenyl) hexafluoropropane (bisAPAF). The curves for (b), (c), and (d) are PIOFG-1 after thermal rearrangement at 350ºC, 400ºC, and 450ºC, respectively[9]. It can be ascertained from these results that the thermal rearrangement results in fewer but larger cavities, with the polymer formed at 450ºC having the fewest and largest cavities. Hill *et al.* (2007) theorizes that the

smaller cavities from the original PIOFG-1 meld together as heat is applied to them[9].

This combination of larger but fewer cavities and the elevated rigidity of polymer chains are what gives PBO its exceptional ability to surpass the upper bound in both selectivity and permeability, as shown in Figure 7 for the gas pair CO_2/CH_4. As seen in Figure 7, PBO is currently the best separation tool for separating CO_2 from CH_4. In addition to high selectivity and permeability, PBO also has excellent resistance to plasticization and chemicals[9].
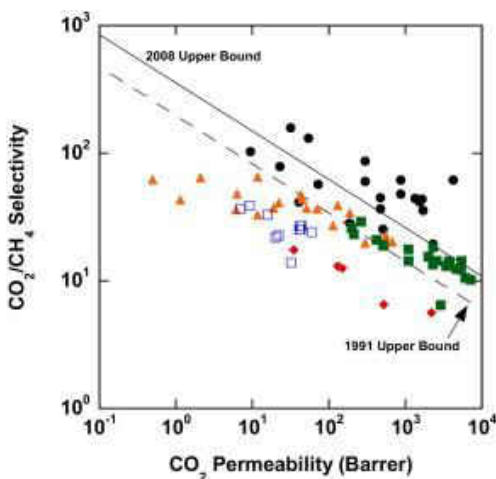
Figure 7: CO_2/CH_4 upper bound with separation properties for various TR-PBO (circles), perfluoropolymers (diamonds), PIMs (solid squares), polyimides (triangles), and PRTILS (empty squares)[38]

Design of Polybenzoxazole

The gas transport properties of PBO depend on the network structures/cross-linking and rigidity of the polyimide precursors, the method of imidization of the polyimide precursor, the temperature of thermal treatment, the physical state of the polyimide, the glass transition temperature of the polyimide,

and the incorporation of non-thermally rearrangeable diamines into their structures. These factors also have an effect on the plasticization resistance of the membrane.

The flat aromatic units in the network structures of the polymers used in the formation of membranes pack very efficiently and thus reduce the amount of free-volume elements that may permit unwanted penetrants. The depressed structure also allows the molecules to arrange themselves in a columnar fashion[9]. The rigidity of these units prevents twisting of the polymer chains upon thermal rearrangement so they stay flat and well packed as desired[9].

In 2013, Calle *et al.* added 3,5-diaminobenzene (DABA) to their precursor polyimides and were able to activate cross-linking of the resulting polyimide (HPIDABA) by adding a step after the azeotropic imidization in which the HPIDABA reacted with 1,4-butylene glycol. These cross-linked HPIDABA were then thermally rearranged in the normal manner[39].

Polybenzoxazoles with 0%, 5% (XTR-PBO-5), 10% (XTR-PBO-10), 15% (XTR-PBO-15), and 20% (XTR-PBO-20) were synthesized and compared by Calle *et al.* in 2013. The PBOs showed the following trend of increasing permeability of CO_2 and N_2, respectively: TR-PBO<XTR-PBO-20<XTR-PBO-15<XTR-PBO-5<XTR-PBO-10 and TR-PBO<XTR-PBO-20<XTR-PBO-5<XTR-PBO-15<XTR-PBO-10. For nitrogen, the permeability of XTR-PBO-5 and XTR-PBO-15 were very close, with values of 29.6 and 29.8, respectively. The following trend for increasing selectivity for the gas pair CO_2/CH_4 was found: XTR-PBO-10<XTR-PBO-15<TR-PBO<XTR-PBO-20<XTR-PBO-5, with all the

values fairly close, having a standard deviation of 2.88. For the gas pair N_2/CH_4, the selectivities of the five membranes were very close, with values from 1.5 to 1.7, with TR-PBO having the highest value at 1.7. All of the cross-linked PBOs transcended the 2008 upper bound for the permeability/selectivity trade-off mentioned earlier. The group's explanation for the excellent transport properties of the XTR-PBOs was that the cross-linking allowed an increase and setting of the free volume elements, which increased cavity size while retaining high rigidity[39].

The effect of the imidization route on the properties of PBO was studied by Han *et al.* in 2010. The method of imidization influences the chemical structure of the polyimide, which in turn affects the structure of the PBO. The three types of imidization studied by Han *et al.* were thermal, chemical, and azeotropic. Thermal imidization occurs when the intermediate polyamic acid is kept at an elevated temperature ($>200^o$C) and the solvent and water are evaporated out as the reaction continues. Azeotropic imidization involves dissolving the monomers in a polar aprotic solvent and adding organic solvents that form azeotropes with water, such as o-xylene. This mixture is then refluxed at slightly elevated temperatures (140-200^oC). Chemical imidization could not form hydroxyl-polyimides, instead substituting the hydroxyl group with an acetate group to form an acetic polyimide (AcPI)[40].

The PBO formed from the thermally imidized HPI (tPBO) showed a 48% increase in FFV. The PBO formed from the azeotropically imidized HPI (aPBO) showed a 29% increase in FFV. The PBO formed from the chemically imidized

AcPI (cPBO) showed a very large 96% increase in FFV. The resulting PBOs had the following order of increasing permeability and selectivity,respectively for CO_2/CH_4 and N_2/CH_4: aPBO<tPBO<cPBO and cPBO<tPBO<aPBO. The differences between the aPBO and tPBO can be explained by the mechanism of their creation, since the tHPI undergoes cross-linking while it is heated, while the aHPI remains linear[40].

It was also shown that the temperature at which the precursor was heated had an effect on the pore size and distribution, with membranes formed at a higher temperature having larger and fewer pores, while those formed at lower temperatures had smaller and more pores[9].

Another study by Calle *et al.* in 2012 found that the state of the precursor before thermal rearrangement affected the amount of PBO formed. Precursors in powder form produced very low conversion, while those in film form produced high conversion, even near 100%. The reason provided was that the rearrangement kinetics are a lot slower for powder samples than for film samples. Another possibility provided was that the CO_2 diffusion is rate-limiting[41].

In 2012, Calle *et al.* studied the relationship between the glass transition temperature of the precursors and the thermal rearrangement temperature necessary to produce PBO. Thermal gravimetric analysis of polyimide precursor showed that the first of two weight loss peaks occurred between 300 – 500°C, as shown in Figure 8.
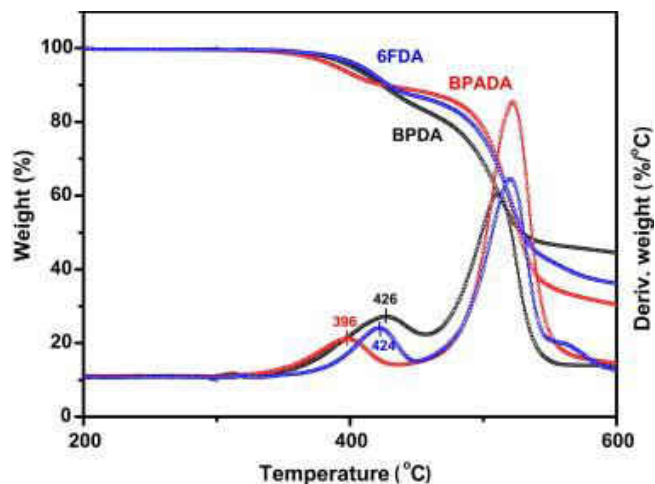
Figure 8: TGA (bottom curves) and DTG (top curves) of polyimides containing

1,4-bis(4-amino-3-hydroxyphenoxy)2,5-di-*tert*-butylbenzene (TBAHPB)[42]

This indicated the loss of a CO_2 molecule that is produced during the

transition to PBO, as shown by mass spectrometry by a loss of weight 44 g/mol.

The second peak is the decomposition of the main polymer chain, which occurs

from 500 – 600°C, which is also shown in Figure 8. Precursor polymers with

more rigid structures showed a higher glass transition temperature, as evidenced

by DSC. The DSC results showed a glass transition within the range of 375 –

475°C for all of the polymers tested, as shown in Figure 9.
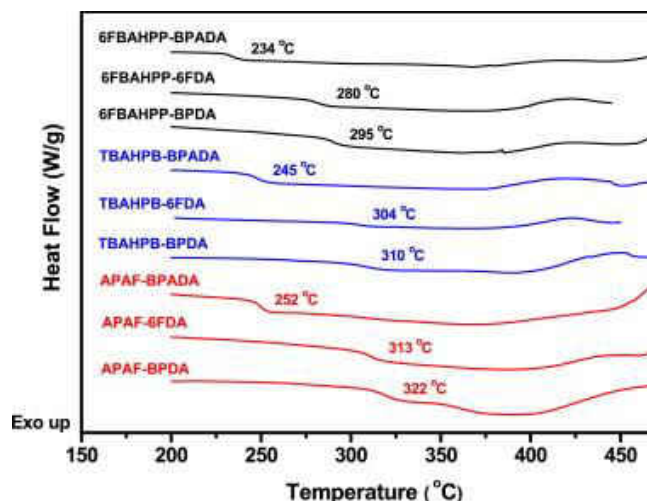
Figure 9: DSC curves of HPI membranes, labeled by glass transition
temperature[42]

Calle *et al.* showed that the thermal rearrangement temperature was
proportional to the glass transition temperature[42].

In 2013 Jo *et al.* studied the effect of network structure on the gas
separation properties of PBO membranes. They tested ten PBO membranes
formed from ten different polyimide precursors. These precursors were formed
from eight non-thermally rearrangeable aromatic diamines, one dianhydride, and
one thermally rearrangeable hydroxyl diamine, all with different structures. The
structures of these diamines and dianhydrides are shown in Figure 10.
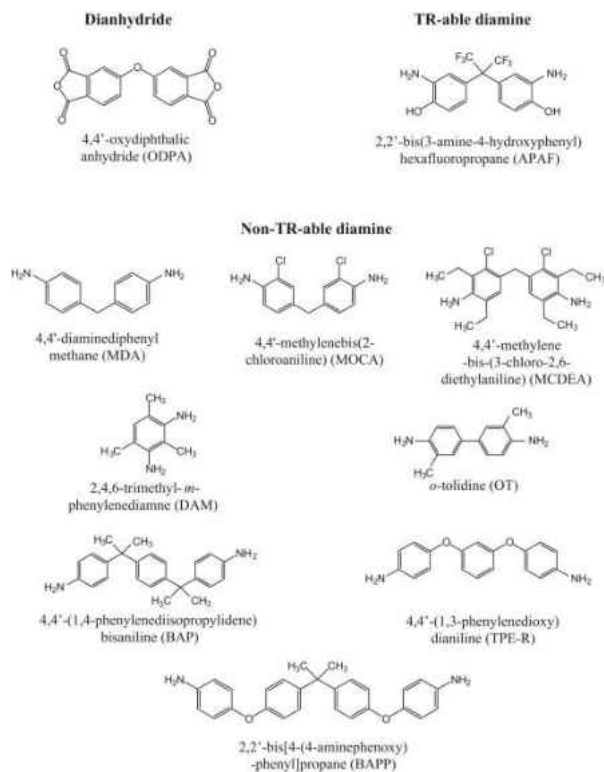
Figure 10: Chemical structures of monomers used in synthesis of HPIs to

compare effects of diamine structure on gas separation properties[43]

The thermally rearrangeable hydroxyl amine and dianhydride formed 90%

of the main structure of the polymide, with one of the eight non-thermally

rearrangeable diamines comprising the other 10%[43]. Since these diamines do not

undergo thermal rearrangement, they can be used in conjunction with other

precursors that do in order to influence the separation properties of the resulting

PBO. PBOs formed in this manner are referred to as polybenzoxazole-co-

polyimides (PBO-co-PIs).

The selectivities and permeabilities of the ten membranes were

determined by Jo *et al.* using a constant volume, variable pressure time-lag

method. The PBO membranes were split into the following three groups: those

with two benzenes connected by a methylene group (A), those with multiple

benzene rings connected directly to each other (B), and those with relatively long

structures with connections consisting of oxygen and/or isopropylidine molecules

(C). Jo *et al.* also compared them to a PBO homopolymer[43].

Jo *et al.* found the molecular weight distributions, glass transition

temperatures, and other general properties of the ten polymers using various

methods including GPC, TGA, and DSC. The results showed that none of the

groups of polymers or the polymers themselves stood out, except for two of

them, which had much higher number average molecular weights than the

others[43]. A pattern arose within the glass transition temperature results, which

showed that the more rigid polymers lacking flexible connecting groups tended to

have higher glass transition temperatures than their more flexible counterparts[43].

Another pattern was that the polymers whose precursors contained bulky side

groups had lower densities after thermal rearrangement, and therefore had a

higher fractional free volume[43].

Jo *et al.*'s experiments examining the gas transport properties of the

various membranes resulted in clear patterns. As stated earlier, the polymers

with more and bulkier side groups caused more inefficient packing, which in turn

increased the FFV and permeabilities of those membranes. The reverse effect

was seen for their selectivities. Jo *et al.* reiterated that flat and less sterically-

hindered structures had the most efficient packing and higher selectivities[43].

Jo *et al.* compared the polymers in group C and showed that para-

linkages tended to result in higher permeabilities than meta-linkages, because

the para-linkages would allow more space within the structures. Meta-linked polymers also have lower rotational mobility, which decreases the spaces through which gas molecules can diffuse[43].

Overall, the polymer with the highest permeability was 4,4'-methylene-bis-(3-chloro-2,6-diethylaniline) (MCDEA)[43], whose base structure is shown in Figure 10. This follows the same pattern, since none of the other polymers have as many or as bulky side groups as MCDEA. MCDEA also had high selectivity due to its rigid structure[43].

The thermally rearranged PBO from Jo *et al.* in 2013 was formed by heating a small amount of polyimide solution on a glass plate at 60°C for one hour, then 100°C for one hour, then 150°C for an hour, and so on until 250°C. It was then heated at 5°C/min to 300°C and held for an hour, then heated at the same rate to 400°C and held for two hours[43]. The majority of studies examined thus far[39-43] have formed the polyimide in this same manner and performed thermal rearrangements to form PBO using the same method. This method was introduced by Doherty *et al.* in 2010[40], and is widely regarded as the most effective method of polyimidization and thermal rearrangement into PBO. This amount of heating and time caused approximately 90 – 99% conversion of the precursors into PBO. The conversion had little effect on the FFV or gas transport properties of the membranes[43].

Various techniques have been developed to mitigate the effects of physical aging and plasticization. Cross-linking both the precursor polyimide[31,32] and the thermally rearranged polybenzoxazole[39] enormously increase the

resistance of the membrane to physical aging and plasticization. The resistance of PBO-co-PIs to aging and plasticization can be increased by using non-thermally rearrangeable diamines that are highly rigid and have aromatic structures[43]. The method of imidization also has an effect on the resistances to aging and plasticization, with polyimides formed by the azeotropic method showing the highest resistance[40].

Industrial Viability of Polybenzoxazole Membranes

Industrial use of polybenzoxazole membranes would involve processing it into usable forms, namely hollow fibers. According to a study by Kim *et al.* in 2012, it is very easy to form the PBOs into different shapes. This is because the thermal rearrangement from polyimide to polybenzoxazole is done when the polyimide is already in its final membrane form. Since polyimides are highly soluble in organic solvents, this shaping of the precursor membrane is straightforward. The polyimide will be dissolved in a solvent then formed into its desired shape, such as hollow fibers via spinning, then the hollow fibers will be thermally rearranged while retaining their shape. These thermally rearranged hollow fibers performed similarly to previous TR-PBO membranes in terms of permeability and selectivity[44].

Summary of Polybenzoxazole Performance

Table 2 summarizes the performances, in permeability and selectivity, of the various designs of PBO membranes from studies examined in this review.

Table 2: Gas permeability and selectivity of PBO membranes

Polymer	Structure	Permeability (barrer)			Selectivity		Ref
		CO_2	N_2	CH_4	CO_2/CH_4	N_2/CH_4	
tPBO	6FDA+bisAPAF	4201	284	151	28	1.88	40
aPBO	6FDA+bisAPAF	398	19	12	33	1.58	40
cPBO	6FDA+bisAPAF	5568	431	252	22	1.71	40
TR-PBO	6FDA+bisAPAF	261	12.6	7.5	35	1.68	39
XTR-PBO-5	6FDA+bisAPAF+DABA(5)	746	29.6	19.9	37	1.49	39
XTR-PBO-10	6FDA+bisAPAF+DABA(10)	980	50.9	33	30	1.54	39
XTR-PBO-15	6FDA+bisAPAF+DABA(15)	668	29.8	19.4	34	1.54	39
XTR-PBO-20	6FDA+bisAPAF+DABA(20)	440	19.7	12.4	35	1.59	39
PBO-MCDEA	ODPA+bisAPAF(8)+MCDEA(2)	35.3	1.36	0.86	41	1.58	43
PBO-MDA	ODPA+bisAPAF(8)+MDA(2)	18	0.66	0.41	44	1.61	43
PBO-DAM	ODPA+bisAPAF(8)+DAM(2)	23.5	0.79	0.43	55	1.84	43
PBO-OT	ODPA+bisAPAF(8)+OT(2)	16.8	0.57	0.32	53	1.78	43
PBO-BAP	ODPA+bisAPAF(8)+BAP(2)	11.9	0.39	0.22	54	1.77	43
PBO-BAPP	ODPA+bisAPAF(8)+BAPP(2)	18.8	0.62	0.41	46	1.51	43
PBO	ODPA+bisAPAF	15.7	1.25	1.74	9.0	0.72	43

Other High Performance Polymers

Along with polybenzoxazole, two other polymers have been recently
identified as having exceptional gas separation properties, especially for the
N_2/CH_4 pair. These are perfluoropolymers and polymers of intrinsic microporosity
(PIMs). These alternative polymers will be discussed briefly.

Perfluoropolymers

Perfluoropolymers employ the very powerful bond strength of carbon-
fluorine bonds to increase the stability, mechanical resistance, thermal
resistance, and chemical resistance of polymers. The structure of a
perfluoropolymer is very similar to that of a polyimide or polybenzoxazole but
highly augmented with fluorine molecules[6]. Several research groups[45-48] have
shown that perfluoropolymers are highly capable of specifically separating

nitrogen from natural gas, second only to the thermally rearranged

polybenzoxazole, as shown in Figure 11[6].
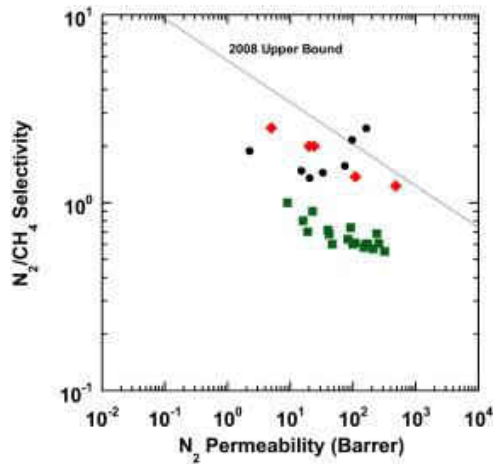
Figure 11: N_2/CH_4 upper bound with separation properties for various TR-PBO

(circles), perfluoropolymers (diamonds), and PIMs (squares)[6]

This high selectivity and permeability is due to the ability of fluorinated

polymers to dissolve light gases while blocking hydrocarbons[49]. This trait also

decreases susceptibility to hydrocarbon-induced plasticization[6].

Polymers of Intrinsic Microporosity (PIMs)

Breaking down the name of these polymers, microporosity refers to the

size of the free volume elements throughout the membrane, which are very small

compared to conventional membranes. The microporosity is created by

extremely rigid, yet contorted, corkscrew structures, which interrupts their chain

packing and results in high selectivity and permeability[6]. These micropores are

intrinsic due to their independence from any thermal or mechanical modifications

on the membrane. PIMs were first presented by Budd *et al.* in 2004 as a

simulacrum of the structure of zeolites constructed of a combination of inorganic

and organic compounds[50]. As shown in Figure 11, PIMs adequately separate

34

nitrogen from natural gas, although not as well as PBOs or perfluoropolymers. Budd *et al.*[50] and others[51-53] demonstrated this over the last decade.

Future Outlook and Conclusions

Purification of natural gas via polymer membrane separation has vastly improved since its conception. The first generation of polyimides possessed good separation properties, which were improved by varying their monomers, implementing thermal annealing, or creating cross-linking. The selectivity and permeability of the polyimides are affected by the free volume elements and rigidity of the polymer chains. These two properties are governed by the size and polarity of side groups, the spatial configuration of linkages, and the type of bridging groups. The best values of selectivity and permeability were attained with large and/or polar pendant groups, meta linkages, and bridging groups with high rotational energy. The membranes are also resistant to plasticization and physical aging.

The polyimide membranes were improved via thermal rearrangement to polybenzoxazole. Polybenzoxazole has better gas transport properties than polyimide, which are determined by the same structural concepts. In general, PBO exhibits much better separation ability than polyimide, due to increased free volume and backbone rigidity, and decreased free volume distribution. Many studies were done to further improve the properties of PBO, including changing the monomers used in the structure of the precursor polyimide, utilizing different imidization routes, and instituting cross-linking.

Thermally rearranged PBO, along with other emerging separation methods including perfluoropolymers and polymers of intrinsic microporosity have consistently exceeded the upper bound for the trade-off between selectivity and permeability, with PBO and PIMs showing the greatest values for both. Perfluoropolymers, while showing magnificent ability to separate nitrogen from natural gas, are outclassed by PBO. All these methods also have excellent resistance to plasticization and chemical and thermal degradation.

However, industrial processes still require great amounts of membranes to efficiently separate gases. Further studies will need to be done to continue to enhance the selectivity and permeability to make large-scale applications more economically feasible.

CHAPTER III

POLYIMIDE SYNTHESIS AND MEMBRANE FORMATION

Materials and Equipment

Materials were purchased from Sigma Aldrich Co. LLC (USA) except for bisAPAF, which was purchased from Matrix Scientific (USA). These materials are the candidate dianhydrides listed in Chapter I of the thesis, bisAPAF, N-methyl-2-pyrrolidinone (NMP), and o-xylene (OX). All materials were of reagent grade and used without further purification or pretreatment. The oven used was a Ney Vulcan 3-550, shown in Figure 12. The reflux apparatus comprised of a hot plate, a 1 L beaker filled with approximately 700 mL of mineral oil (Sigma Aldrich Co. LLC (USA)), a 300 mL round-bottom flask, a dean stark trap, and a condenser column. All glassware was purchased from Fisher Scientific (USA).

Figure 12: Ney Vulcan 3-550 oven

Synthesis

Hydroxy-Polyamic Acid Synthesis

The procedure, adapted from Soo et al. from 2013[43], began with dissolving 10 mmol of bisAPAF in enough NMP to fully dissolve, then cooling the solution to below 3°C. Then 10 mmol of the selected dianhydride and enough NMP to dissolve it was added and the solution was left at below 10°C for 12 hours. This solution had a viscous yellow appearance.

Hydroxy-Polyimide (HPI) Synthesis

The solution was then transferred to a round-bottom flask, along with OX in an equal volumetric amount to the NMP, and set up with a dean stark trap with a water-circulated condenser and a thermometer. The flask was heated in an oil bath to between 160-180°C, held at about 165°C, while distilling off water formed by the condensation reaction. Once all the water was removed, the solution was left to react for 6 hours. The solution was then cooled and the HPI was precipitated with a 3:1 water:methanol solution then vacuum filtered (the vacuum filtration apparatus is shown in Figure 31 in Chapter V). The powder was washed in a 3:1 water:methanol solution for 12 hours, and then dried in the oven at 110°C for 12 hours.

Membrane Formation

After drying, the HPI powder was dissolved in NMP to make a 30wt% solution and cast on a glass plate wrapped in Teflon™ and levelled within the oven using aluminum foil and a bubble level. This plate was then heated in the oven at 1°C/min to 250°C, spending 1 hour each at 60, 100, 150, 200, and

250°C. It was then allowed to cool to room temperature and the dry membrane was peeled off.

Thermal Rearrangement

To perform the thermal rearrangement, the membrane was placed between two ceramic plates to prevent curling of the membrane and heated in the oven at a rate of 5°C/min to 300°C and held there for an hour, then at a rate of 5°C/min to 400°C and held there for two hours. After thermal rearrangement, the membrane was cooled to room temperature.

HPI Characterization

The HPI powders were characterized using attenuated total reflectance Fourier transform infrared spectroscopy (ATR-FTIR, referred to henceforth as FTIR) and thermal gravimetric analysis (TGA). The FTIR was a Nicolet IR200 and the TGA was a Simultaneous DSC-TGA (SDT) Q600/2960 from Thermo Fisher Scientific. The temperature program run on the TGA matched that of the procedure for thermal rearrangement, with heating at 5°C/min to 300°C and holding for one hour, then heating at 5°C/min to 400°C and holding for two hours. The number average and weight average molecular weights of the HPIs were found using a Varian ProStar Gel Permeation Chromatograph (GPC).

Results

FTIR Data

All FTIR spectra for the HPI samples were similar, and the spectrum for sample 22 was chosen to represent all of the spectra, since it has the clearest peaks. Figure 13 shows the FTIR spectrum for sample 22.
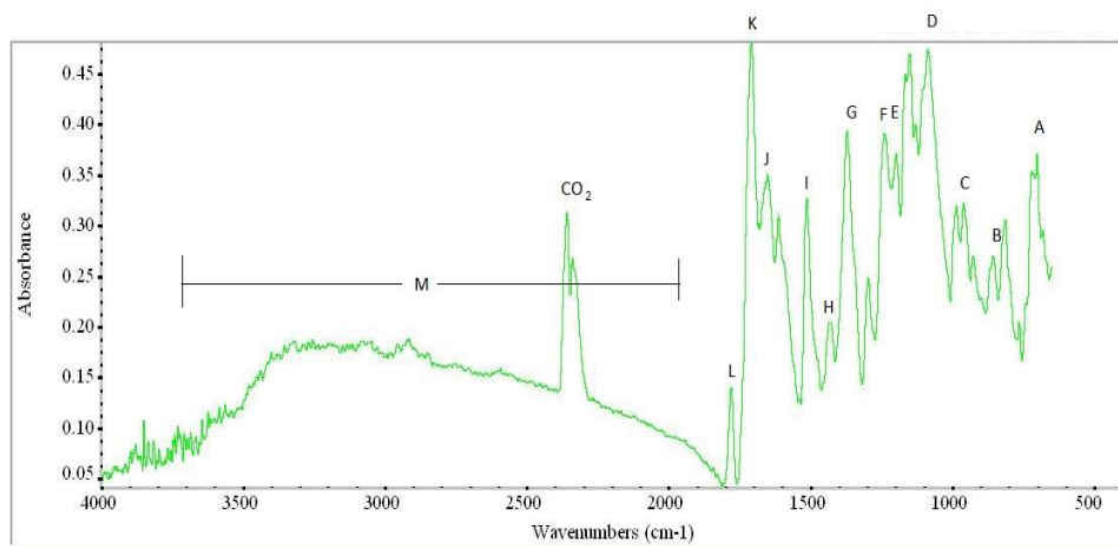
Figure 13: FTIR data for HPI sample 22

The analysis tool included with the Nicolet IR200 software provided peak wavenumber measurements for each sample. The provided wavenumbers of important peaks varied slightly from sample to sample, so approximate averages were found by eye, so the values may not be exact. The wavenumbers of important peak locations from Figure 13 along with their corresponding bonds and/or functional groups are shown in Table 3.

Table 3: Wavenumbers of important peaks and their corresponding bonds and/or functional groups for HPIs

Location	Absorption peak (cm^{-1})	Type of bond[54]
A	700	C-X
B	860	para/meta-disubstituted benzene
C	1000	fluoroalkane
D	1100	trifluoromethyl
E	1200	trifluoromethyl
F	1250	C-N
G	1370	aromatic nitro
H	1450	aromatic C=C
I	1520	aromatic C=C/C-N

40

Table 3 cont.

J	1650	aromatic C=C/N-C=O
K	1720	carbonyl
L	1790	carbonyl
M	2000-3700	alcohol/phenol

TGA Data

The TGA data for the samples was similar. The TGA data for HPI sample 3 (HPI-ODPA) is shown below in Figure 14. Sample 3 was chosen as a representative graph because the values of the weight percent are approximately at their average.
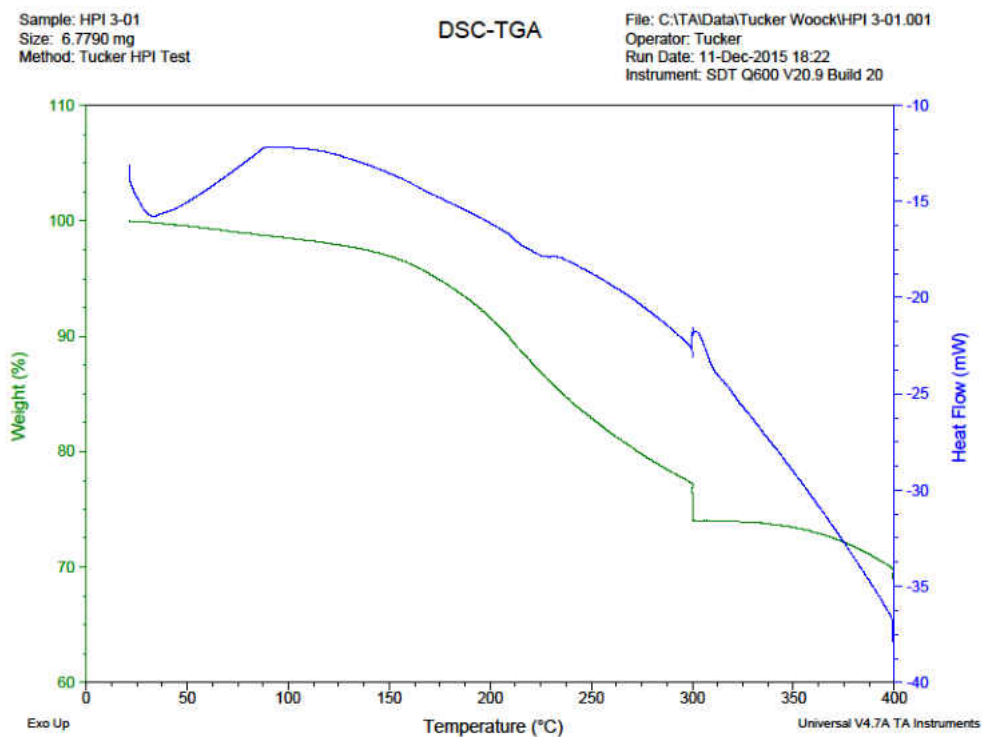
Figure 14: TGA data for HPI sample 3

This TGA curve shows a gradual weight loss until approximately 160°C, where it starts decreasing more sharply. Then at 300°C, where the sample was

held for one hour, the weight decreased almost 10%. At 400°C the sample was held for two hours and the weight decreased another 10%, for a total of 32% weight loss.

GPC Data

The GPC was used to find the number average molecular weights (Mn) and weight average molecular weights (Mw) of three HPI-ODPA, three HPI-BTDA, and three HPI-PMDA samples. The averages of these values for each HPI, along with the average polydispersity index (PDI) for each HPI, are shown in Table 4.

Table 4: Average Mn, Mw, and PDI for each HPI sample

HPI	Mw (g/mol)	Mn (g/mol)	PDI	Mw StDev	Mn StDev
HPI-ODPA	55000	31000	1.8	2200	820
HPI-BTDA	16000	7600	2.1	470	590
HPI-PMDA	14000	5900	2.4	470	50

Discussion

FTIR Data:

The majority of the spectra show a peak at 2300-2400 cm^{-1}, corresponding to CO_2, which shows that the apparatus used was easily contaminated by CO_2.

All of the bonds and functional groups in Table 3 show that the synthesized samples had characteristic structures of polyimides. Figure 15 shows the structure for the HPI made from bisAPAF and ODPA (bisAPAF+ODPA), and it can be seen that all of the bonds listed in Table 3 are present in the structure. This is analogously the same for HPIs made from bisAPAF and BTDA and those made from bisAPAF and PMDA, as BTDA and

42

PMDA have no bonds or functional groups that are different from those in bisAPAF+ODPA. According to Guierrez-Wing *et al.*, peaks at 1718 cm^{-1} and 1788 cm^{-1} are indicative of symmetric and asymmetric C=O stretching, respectively. This shows that the hydroxyl-polyamic acid was imidized into hydroxyl-polyimide[40,41,55,56]. More peaks characteristic of polyimides are those at 1649 cm^{-1} and 1538 cm^{-1}, which indicate the presence of O=C-N and C-N bonds, respectively[56,57].
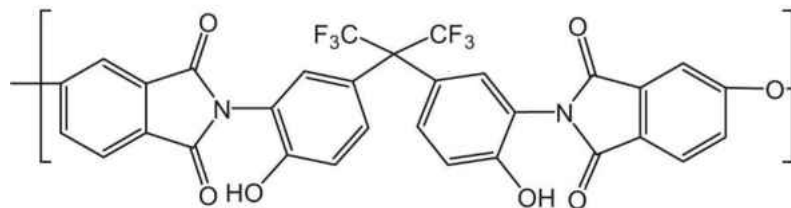
Figure 15: bisAPAF+ODPA structure[43]

In addition to the specific peak values, most of the FTIR spectra generally match part a of the following Figure 16, which shows the spectrum for a hydroxyl-polyimide and its thermally rearranged polybenzoxazole[58].
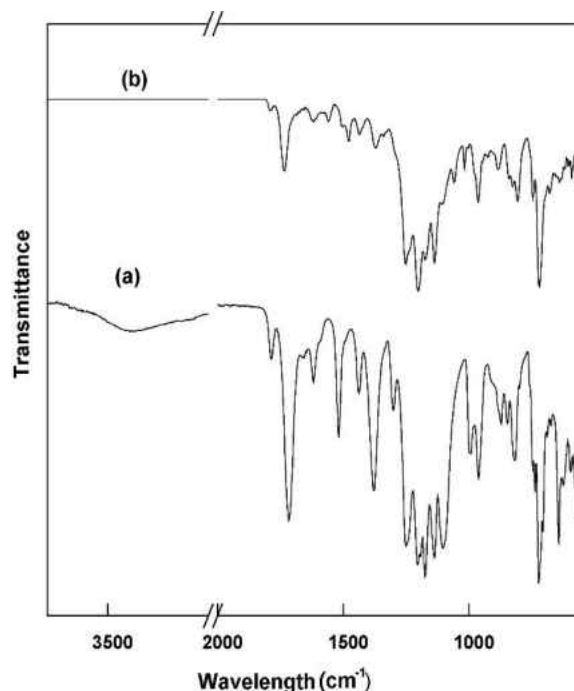
Figure 16: (a) FTIR spectrum for HPI, and (b) FTIR spectrum for thermally

rearranged PBO from HPI in (a)[58]

TGA Data

The TGA curves are generally consistent with that of the literature

(example TGA curves for HPI are shown in Figures 17 and 18), indicating that all

samples should undergo some degree of thermal rearrangement under similar

conditions. The weight loss shown in the TGA curves corresponds to the loss of

CO_2, which is expected from thermal rearrangement according to the mechanism

in Figure 19. This weight loss does not fully occur in many of the TGA curves,

indicating that some of the HPIs synthesized may not have fully undergone

thermal rearrangement. This is most likely due to the membranes being much

thicker than those studied in literature.
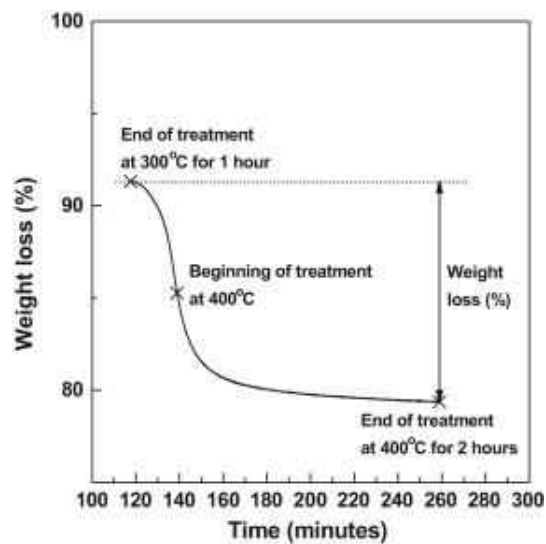
Figure 17: TGA curve for HPI at 400°C for 2 hours with respect to time[43]
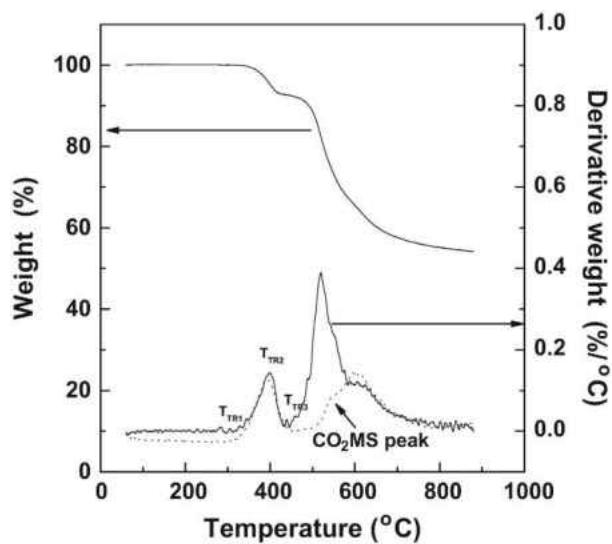
Figure 18: TGA curve for HPI with respect to temperature[43]
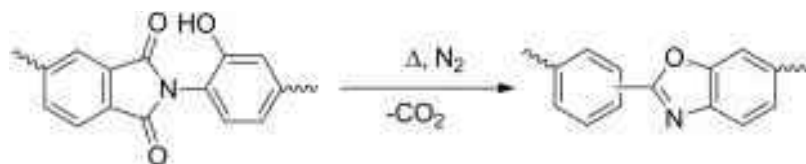
Figure 19: General mechanism for thermal rearrangement of HPI to PBO[9]

45

GPC Data

The Mn and Mw values for the HPI-BTDA and HPI-PMDA agreed with values obtained by Calle *et al.* in 2012 for HPIs made from bisAPAF and 6FDA using azeotropic imidization[41]. The molecular weight values for HPI-ODPA found in this study were close to those of the homopolymer, which was made from bisAPAF and ODPA, found by Soo *et al.*[43]. The HPI-ODPA had a higher molecular weight due to the ether oxygen present in its structure. This ether oxygen is highly electron donating and can share its unbonded electrons with the amine groups in the diamine structure[59], thus facilitating bond creation between the diamine and dianhydride monomers. This means that there will be more monomers per polymer chain and therefore the HPI-ODPA will have a higher molecular weight. The HPI-BTDA, on the other hand, contains a bulkier pendant group in its carbonyl group. This bulkiness creates an obstacle that prevents other monomers from approaching close enough to the BTDA to bond with it. This will result in fewer monomers per polymer chain and thus a lower molecular weight.[43]. The carbonyl group in the BTDA is also moderately electron withdrawing, which also reduces reactivity of the dianhydride[59]. PMDA is the most reactive of the dianhydrides studied in this project, but it is also has the smallest molecular weight, so equivalent chain lengths have lower molecular weights[60]. The PDIs found in this study were very close to the normal PDI for polyimides, which is 2.0[60].

<div align="center">

Conclusion

</div>

Following the azeotropic imidization method, HPIs containing the diamine biAPAF and one of four dianhydrides, which were ODPA, BTDA, BPDA, and PMDA, were synthesized. Judging by the FTIR and TGA data, hydroxyl-polyimides were indeed created, and they should successfully thermally rearrange into polybenzoxazole.

Multiple samples of HPI were synthesized and cast into membranes to be thermally rearranged for use in permeation testing.

CHAPTER IV

THERMAL REARRANGEMENT AND PERMEATION TESTING

Materials and Equipment

The materials used for this section of the project were the membranes cast previously described in Chapter 3. The oven used for thermal rearrangement was the Ney Vulcan 3-550 used in Chapter 3. The permeation test cell used was a PTC 700 1" Test Cell For Vapor Phase Testing purchased from Pesce Labs, Inc. (USA). The manifold was built in-house using off the shelf components. The gas sampling bags were Standard FlexFoil® Gas Sample Bags purchased from SKC, Inc. (USA). Gas chromatograph use was provided by the Energy and Environmental Research Center (EERC) in Grand Forks, ND. The gas chromatograph was an Agilent Technologies 7890A Refinery Gas Analyzer Gas Chromatograph. All gases were purchased from Praxair (USA). The ceramic plates were 6 in by 6 in Duran Laboratory Glass Ceramic Lab Protection Plate, purchased from Fisher Scientific (USA).

Thermal Rearrangement

To perform the thermal rearrangement, the membrane was placed between two ceramic plates and heated in the oven at a rate of 5°C/min to 300°C and held for an hour, then at a rate of 5°C/min to 400°C and held for two hours[43]. After thermal rearrangement, the membrane was cooled to room temperature. The thermally rearranged membranes were characterized using

attenuated total reflectance Fourier transform infrared spectroscopy (ATR-FTIR,

referred to henceforth as FTIR).

Permeation Testing

Figure 20 shows a diagram of the manifold and its connections.
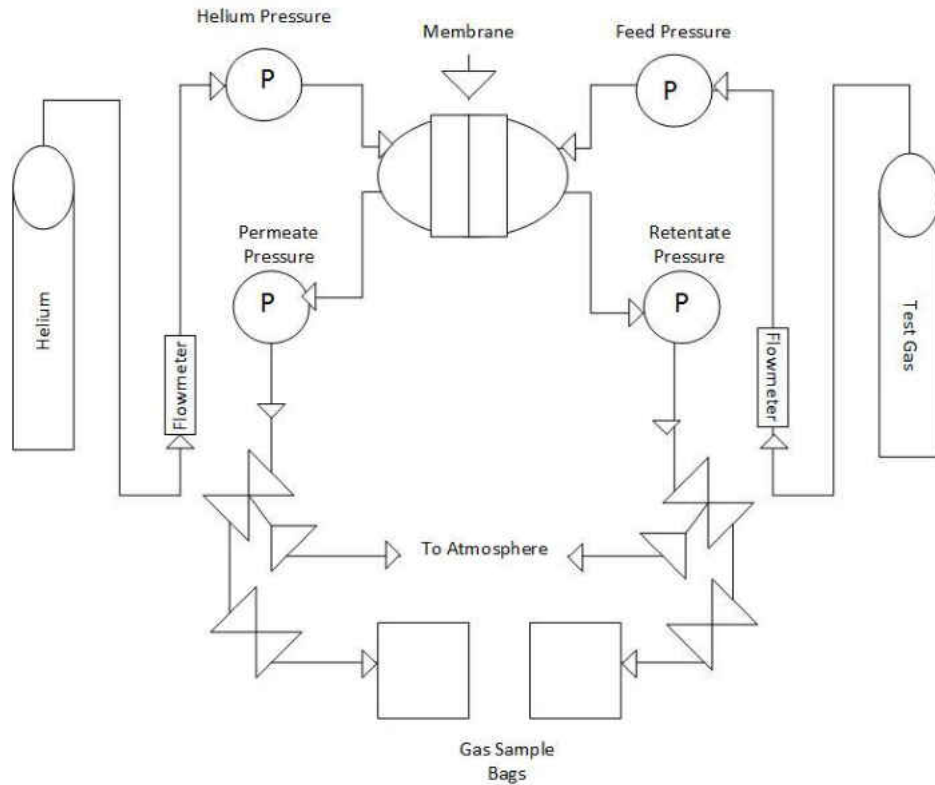
Figure 20: Diagram of in-house constructed gas permeation manifold setup

Each half of the manifold consisted of a flowmeter to control the flow of

gas, a pressure gauge to measure inlet pressure, connecting tubes going to and

from the permeation test cell (shown in Figures 21 and 22), another pressure

gauge to measure outlet pressure, a three-way valve to control the direction of

gas flow (open, closed, and vent), and a two-way valve to control gas flow to the

sample bag. The test gas, which was a mixture of 20.1% methane and 79.9%

nitrogen, flowed through one half of the manifold. Through the other half of the

manifold flowed the carrier gas, which was helium.
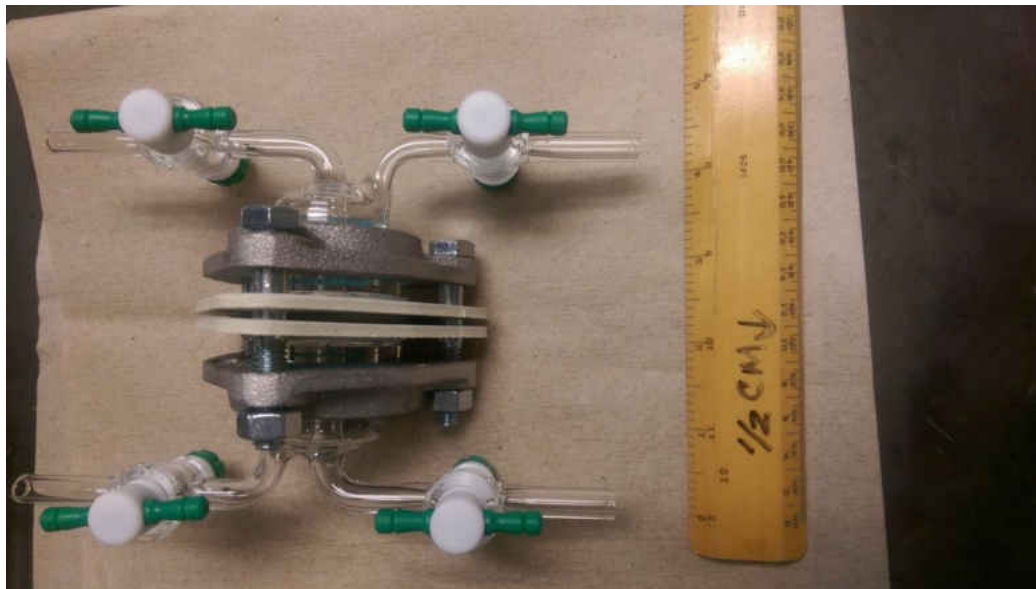
Figure 21: Top view of closed PTC 700 1" Test Cell for Vapor Phase Testing

from Pesce Labs, Inc.

Figure 22: Open PTC 700 1" Test Cell for Vapor Phase Testing from Pesce Labs,

Inc.

This manifold setup is standard for membrane flux quantification, and was constructed by the author of this thesis with assistance from a few people in the department.

A membrane was placed in the permeation test cell, which was then connected appropriately to the manifold. Each gas was turned on at a specified flow rate, both of which are listed in Table 13 in Chapter VI, and allowed to flow across opposite sides of the membrane for 5-10 minutes, while the three-way valve vented them to atmosphere, in order to reach steady state, then the three-way and two-way valves were positioned to allow flow into the gas bags on the permeate and retentate sides. While the gas bags were filling, pressure readings were recorded for later use in the permeation equation. When the gas bags were full, they were closed and the flow was vented again.

A gas chromatograph was then used to analyze the permeate and retentate gases.

Results

Twenty-one HPI membranes were partially thermally rearranged into polybenzoxazole (PBO) via the thermal rearrangement process outlined above. Seven HPI-ODPA, seven HPI-BTDA, and seven HPI-PMDA were partially thermally rearranged into PBOs.

Polybenzoxazole Characterization

Three of each PBO-dianhydride (PBO-DA) were subjected to FTIR. All FTIR spectra for the PBO samples were similar. FTIR spectra for HPI samples have been overlaid on spectra for their respective PBOs in Figures 23 through

25. Figure 23 shows sample 20, which is an HPI-BTDA, and sample PBO-BTDA-03, Figure 24 shows sample 26, which is an HPI-ODPA, and sample PBO-ODPA-02, and Figure 25 shows sample 34, which is an HPI-PMDA, and sample PBO-PMDA-03. These pairs of spectra have been chosen because they give the clearest contrast between the HPIs and their respective PBOs and allow for the easiest comparison. The peaks that are most relevant to thermal rearrangement are marked on each spectra, and shown in Table 5.
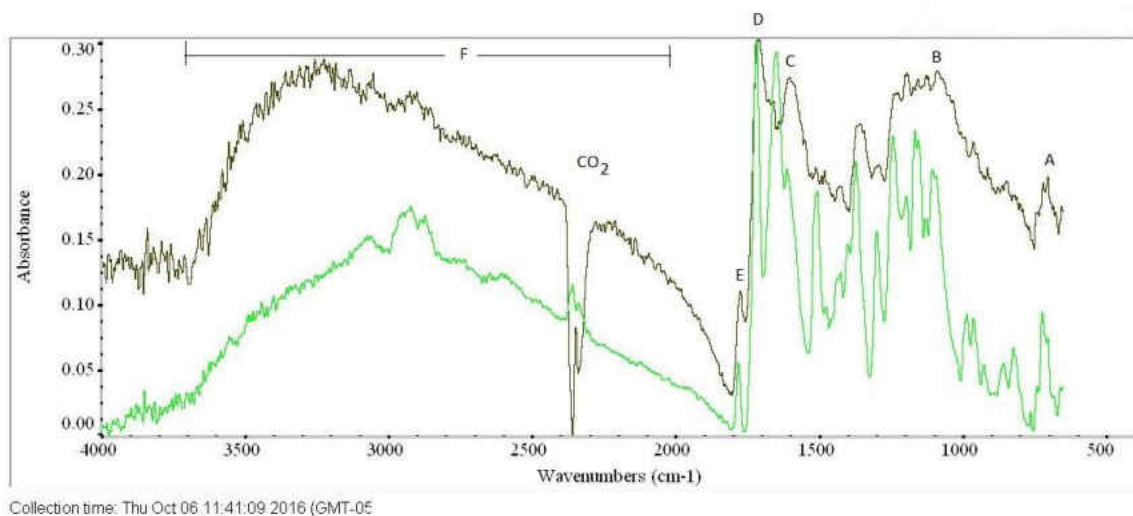
Figure 23: FTIR spectra for samples 20 (HPI-BTDA, lighter spectrum) and PBO-BTDA-03 (darker spectrum)
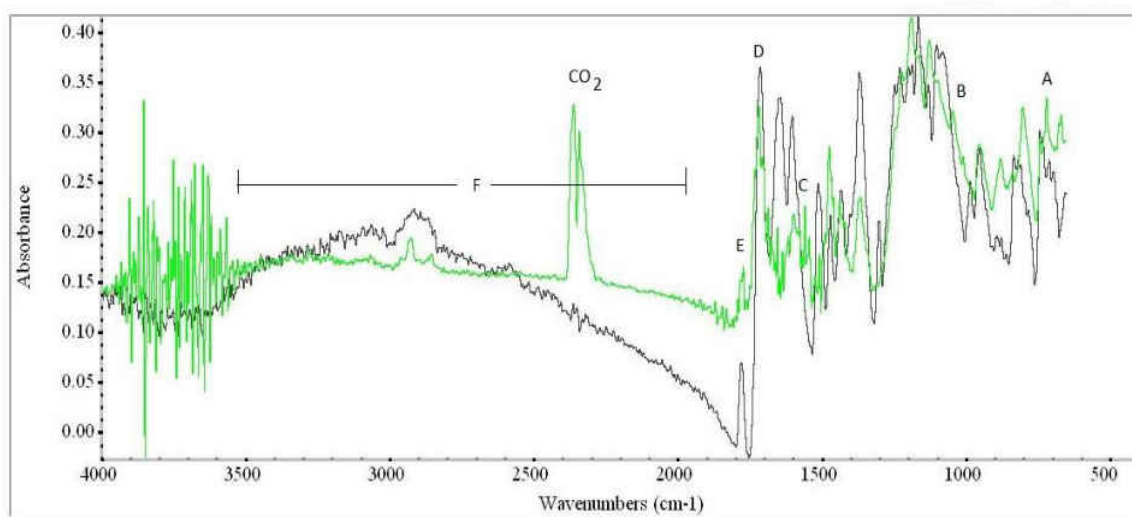
Figure 24: FTIR spectra for samples 26 (HPI-ODPA, darker spectrum) and PBO-

ODPA-02 (lighter spectrum)
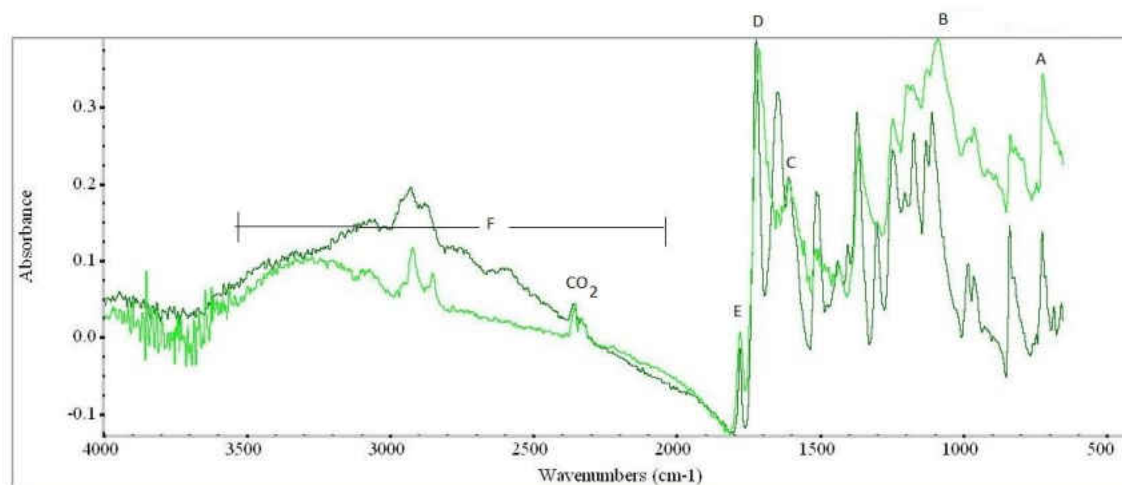
Figure 25: FTIR spectra for samples 34 (HPI-PMDA, darker spectrum) and PBO-

PMDA-03 (lighter spectrum)

Table 5 shows the important peaks found by the Nicolet IR200 software

and their corresponding functional groups. These peaks were found in the same

manner as the peaks in Chapter III. Each PBO spectrum had similar, but not

53

exactly the same, peak locations, so a general average for each set of similar peak locations was found by eye. The peaks marked with letters in Figures 23-25 are also denoted in Table 5.

Table 5: Wavenumbers of important peaks and their corresponding bonds and/or functional groups for PBOs

Location	Absorption peak (cm^{-1})	Type of bond[54]
A	720	benzoxazole ring
	860	para/meta-disubstituted benzene
	1000	fluoroalkane
B	1060	benzoxazole ring
	1200	trifluoromethyl
	1250	C-N
	1370	aromatic nitro
	1450	aromatic C=C
	1500	aromatic C=C
C	1600	benzoxazole ring
D	1720	carbonyl
E	1790	carbonyl
F	2000-3700	alcohol/phenol

Permeability Calculations

The flow rates for the gases were controlled with the regulators on the respective gas cylinders. The regulator for the helium cylinder directly measured the helium flow, so the value for the helium flow rate was used directly. The regulator for the test gas cylinder did not read the flow of the test gas directly, but it did show the flow of Argon, so the flow measurement for Argon was used and later converted into flow of the test gas. This was done using the following equation[61]:

$$Q_2 = Q_1 * \sqrt{SG_1/SG_2}$$

Where Q_2 is the converted flow rate of test gas, Q_1 is the observed flow rate of Argon, SG_1 is the specific gravity of Argon (1.379), and SG_2 is the specific gravity of the test gas. The specific gravity of the test gas was found using the following equation:

$$SG_2 = x_{methane} * SG_{methane} + x_{nitrogen} * SG_{nitrogen}$$

Therefore,

$$SG_2 = 0.201 * 0.5537 + 0.799 * 0.9669 = 0.8838$$

Substituting this into the flow rate conversion equation gives:

$$Q_2 = Q_1 * \sqrt{\frac{1.379}{0.8838}} = 1.249 Q_1$$

The following equation[62], was used for permeability calculation:

$$P_i = \frac{l * x_{perm\,i} * 273\,K * p_{atm}}{A * \left(x_{feed\,i} * p_{feed} - x_{perm\,i} * p_{perm}\right) * T * 76\,cmHg} * \frac{dV}{dt}$$

Where P_i is the permeability of species i in $(cm^3(STP) * cm)/(cm^2 * s * cmHg)$, l is the thickness of the membrane in cm, $x_{perm\,I}$ is the molar concentration of species i in the permeate gas, p_{atm} is the atmospheric pressure in cmHg, A is the surface area of the membrane in cm^2, $x_{feed\,I}$ is the molar concentration of species i in the feed gas, p_{feed} is the pressure of the feed gas in cmHg, p_{perm} is the pressure of the permeate gas in cmHg, T is the temperature of the system in K, and dV/dt is the flow rate of the feed gas in cm^3/s.

Table 6 shows the calculated permeabilities and selectivities for the various runs of testing for each membrane, along with literature values for the permeabilities. The N_2/CH_4 selectivity ($\alpha_{N2/CH4}$) was found using the following equation:

$$\propto_{N_2/CH_4} = \frac{P_{N_2}}{P_{CH_4}}$$

Table 6: Run number, type of membrane, calculated permeabilities and

selectivities for various membranes, and literature values for permeabilities

Run	Membrane	P_{CH4} (barrer)	P_{N2} (barrer)	N_2/CH_4 Selectivity	Lit. P_{CH4} (barrer)	Lit. P_{N2} (barrer)
1	Kapton	0	-10000000	-	0.00313[34]	0.035[58]
2	Kapton	0	7000000	-	0.00313	0.035
3	Kapton	0	3000000	-	0.00313	0.035
4	Kapton	0	-4000000	-	0.00313	0.035
5	Kapton	0	-5000000	-	0.00313	0.035
6	Kapton	-40000	-10000000	300	0.00313	0.035
7	HPI-BTDA	0	-30000000	-	0.226[35]	0.45[59]
8	HPI-BTDA	0	-20000000	-	0.226	0.45
9	HPI-BTDA	0	-30000000	-	0.226	0.45
10	HPI-ODPA	0	0	-	0.02[36]	0.071[60]
11	HPI-ODPA	0	20000000	-	0.02	0.071
12	PBO-BTDA	0	200000000	-	15[58]	10[53]
13	PBO-BTDA	0	0	-	15	10
14	PBO-ODPA	0	40000000	-	1.25[43]	1.74[38]
15	PBO-ODPA	0	50000000	-	1.25	1.74

For a more detailed account of the steps taken to calculate permeabilities,

please refer to Chapter VI.

Discussion

FTIR Data

Figures 23-25 show that the HPIs probably were not fully thermally

rearranged, since they still have some important peaks from the HPI spectra. The

most distinct of these peaks is that of the wavenumber pertaining to the presence

of phenol/alcohol groups at 2000-3700 cm^{-1}. This peak should be completely

gone for the PBO, since the –OH group is the one that allows an HPI to thermally

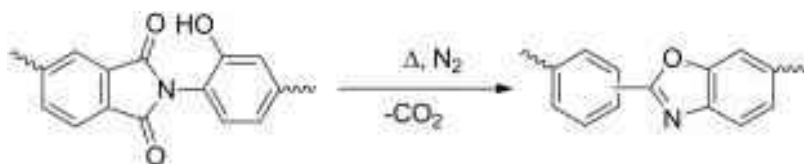rearrange by bonding with the nitrogen of the diamine portion of the HPI. This can be seen in Figure 26.

Figure 26: General mechanism for thermal rearrangement of HPI to PBO[9]

More evidence that the HPIs were not thermally rearranged correctly is that the multiple peaks for carbonyl groups at 1720 cm^{-1} and 1790 cm^{-1} remained in the PBOs. These also should have disappeared during thermal rearrangement. Despite not thermally rearranging completely, all of the spectra for the PBOs contain peaks around 1600 cm^{-1} and 1060 cm^{-1}, which are indicative of the benzoxazole ring[39,41,56,57]. This means that some degree of thermal rearrangement occurred. Another peak that is important to PBO formation is at 723 cm^{-1}. This peak represents the imide ring deformation, which happens as the new benzoxazole ring is formed[58,63].

There are a number of possible reasons for the HPIs not fully rearranging. The most likely is that the oven used for this project was not a vacuum oven and did not have options for alternative atmospheres to air, as did the oven used in the study upon which the procedure was based[43]. In a vacuum or inert atmosphere the transport of CO_2 released during thermal rearrangement would have been better than in an air atmosphere, which would facilitate higher conversion. Another possible reason is that the membranes were too thick, and transport of CO_2 out of the polymer matrix was hindered by the sheer number of

chains present in the membrane. A longer reaction time may have rectified this somewhat.

Permeation Testing

As can be seen in images of casts using HPI-PMDA in Chapter V, such as in Figures 41-43 or Figures 48-51, the membranes created with HPI-PMDA had rather prominent ridges that formed during solvent evaporation. These ridges occurred for all membranes made from HPI-PMDA, and were due to the contraction of the polymer solution as the solvent evaporated. This caused the Teflon that the solution was cast upon to contract and fold slightly, and the solution followed it as the solvent evaporated and the membrane solidified. These ridges proved to be too thick and inconsistent that they prevented the permeation test cell from sealing. As with the HPI-PMDA membranes, the PBO-PMDA membranes were too ridged to allow the permeation test cell to seal, and therefore both were excluded from permeation testing.

Polyimides have nitrogen permeations of 0.035-35 Barrer and methane permeabilities of 0.00313-24 Barrer[6,12,34,35,44,64-66]. As discussed in Chapter II, polybenzoxazoles tend to have nitrogen permeabilities of 0.024-431 Barrer and methane permeabilities of 0.03-463 Barrer[3,37,40]. Even the lowest of the permeabilities calculated in this work is orders of magnitude higher than those values from literature. This means that one of two things happened during the synthesis and/or thermal rearrangement processes of this project. The first possibility is that polyimide and polybenzoxazole membranes with extremely high nitrogen and methane permeabilities, and high N_2/CH_4 selectivities, have been

created. The second, and more likely, possibility is that the method of permeation testing or the capability of the GC used was incapable of accurately measuring the separation properties of the membranes created.

According to the operator of the GC, its lowest detection limit is approximately 0.003 mol%, which accounts for all but one of the P_{CH4} values being zero, as seen in Table 14 in Chapter VI. Even if small amounts of methane were permeating through the membranes, the GC was unable to detect it. In the one run in which the GC detected the methane, the methane content was just barely 0.003 mol%, so it was lucky that enough permeated through the membrane to register.

Additional reasons for the lack of permeation data could be due to the membranes themselves, or due to the method of testing their permeabilities. The membranes were rather thick, compared to those discussed in literature, which had thicknesses of about 1-15 μm[19]. The thicknesses of the membranes in this project were much higher, as can be seen in Table 13 in Chapter VI, with the lowest being 0.254 mm. This was the thickness of the Kapton® commercial membrane; the membranes created were even thicker. These large thicknesses may have rendered the membranes impermeable, or perhaps more time was required to allow the gases to permeate through them than was allowed.

The manifold used in permeation testing was checked for leaks initially and periodically, but some could have developed during use and gone undetected. This would have allowed nitrogen or methane on either side of the membrane to escape into the atmosphere, or allowed air from outside the

manifold to enter into the gas bags. If air entered the gas bags it would have been an amount that would have overwhelmed the already miniscule amount of methane in the bags, thus making it even more difficult for the GC to detect them.

Conclusion

Multiple samples of HPIs were synthesized and cast into membranes for the previous section of this project. Thermal rearrangement was attempted in order to convert these HPIs into PBOs. According to FTIR data, this was partially attained. There were many peaks in the FTIR spectra of the PBOs that indicated thermal rearrangement, but there were also peaks that showed that there remained structure from the HPIs.

The HPI and PBO membranes underwent permeation testing using a manifold setup, but adequate permeation data was not obtained. There are a few possibilities as to why this happened. The membranes may have been impermeable, or they were too thick to allow permeation in the time allowed. Another issue was that the GC used for this project couldn't detect the low concentrations of nitrogen and methane in the permeate gas. A third possibility is that the integrity of the manifold was not high enough to permit accurate collection of gas samples.

CHAPTER V

ADDITIONAL INFORMATION FOR CHAPTER III

Synthesis

Hydroxy-Polyamic Acid Synthesis

The hydroxyl-polyamic acid synthesis generally went well for all of the samples. This synthesis began with measuring out 10 mmol of 2,2'-bis(3-amino-4-hydroxyphenyl)-hexafluoropropane (APAF). The molecular weight of APAF is 366.26 g/mol, so 10 mmol would be 3.66 g. This 3.66 g of APAF was dissolved in N-methyl-2-pyrrolidinone (NMP) and cooled below 10°C in a refrigerator. After it decreased to below 10°C, 10 mmol of the dianhydride (DA) was added, along with enough NMP to dissolve it. The molecular weight of 4,4'-oxydiphthalic anhydride (ODPA) is 310.21 g/mol, so 10 mmol is 3.10 g. The molecular weight of 3,3',4,4'-benzophenone tetracarboxylic dianhydride (BTDA) is 322.23 g/mol, so 10 mmol is 3.22 g. The molecular weight of 3,3',4,4'-biphenyl tetracarboxylic dianhydride (BPDA) is 294.22 g/mol, so 10 mmol is 2.94 g. After sample 17 was synthesized, it was decided that many more membranes would be needed, so samples 18-35 used 20 mmol of APAF and dianhydride instead of 10 mmol. This resulted in sample weights of 7.325 g for APAF, 6.445 g for BTDA, 5.884 g for BPDA, and 6.204 g for ODPA. The masses of APAF and dianhydride and volume of NMP used for each sample are listed in Table 7. Samples 1-7, 17, 26, and 27 used ODPA, samples 8-11 and 18-22 used BTDA, samples 12-16 and 23-25

used BPDA, and samples 28-35 used PMDA (this addition will be discussed

later).

Table 7: Mass APAF, mass DA, and volume NMP for samples

Sample	Mass APAF (g)	Mass DA (g)	Vol NMP (mL)
1	3.769	3.150	40
2	3.718	3.111	35
3	3.788	3.235	70
4	3.724	3.135	45
5	3.730	3.190	40
6	3.758	3.180	40
7	3.731	3.159	50
8	3.677	3.274	50
9	3.674	3.244	45
10	3.665	3.226	45
11	3.670	3.227	40
12	3.663	2.946	60
13	3.663	2.940	65
14	3.667	2.942	70
15	3.666	2.947	60
16	3.665	2.942	70
17	3.667	3.112	35
18	7.327	6.449	70
19	7.329	6.450	70
20	7.329	6.449	60
21	7.328	6.451	70
22	7.330	6.450	75
23	7.331	5.887	90
24	7.328	5.886	80
25	7.328	5.887	80
26	7.330	6.208	50
27	7.235	6.206	50
28	7.329	4.367	70
29	7.329	4.368	75
30	7.239	4.367	75
31	7.328	4.367	70
32	7.328	4.367	70
33	7.327	4.367	75
34	7.329	4.366	75
35	8.810	5.249	90

After all the DA was dissolved, the solution was allowed to react below

10°C for 12 hours. The solution turned yellow for samples using ODPA (HPI-

ODPA), BPDA (HPI-BPDA), and PMDA (HPI-PMDA) and brown for BTDA (HPI-

BTDA).

Hydroxy-Polyimide (HPI) Synthesis

The solution was removed from the refrigerator and added to a 300 mL

round-bottom flask. Then o-xylene (OX) was added to match the volume of NMP

used. The volume of OX used for each sample is shown in Table 8.

Table 8: Volume OX used for each sample

Sample	vol OX (mL)
1	40
2	35
3	70
4	45
5	40
6	40
7	50
8	50
9	45
10	45
11	40
12	60
13	65
14	70
15	60
16	70
17	35
18	70
19	70
20	60
21	70
22	75
23	90
24	80

Table 8 cont.

25	80
26	50
27	50
28	70
29	75
30	75
31	70
32	70
33	75
34	75
35	90

The round bottom flask was submerged into a bath containing 700 mL mineral oil and attached to a Dean-Stark trap and a condenser. This reflux apparatus was then placed on a hot plate. A picture of the apparatus can be seen in Figure 27, and a clear diagram of the apparatus, without the hot plate and oil bath, can be seen in Figure 28. As can be observed from the picture of the apparatus, the Dean-Stark trap has an open bottom with a stopcock.

Figure 27: Reflux apparatus used in the synthesis of hydroxyl-polyimides,

specifically in the conversion of hydroxyl-polyamic acid to hydroxyl-polyimide
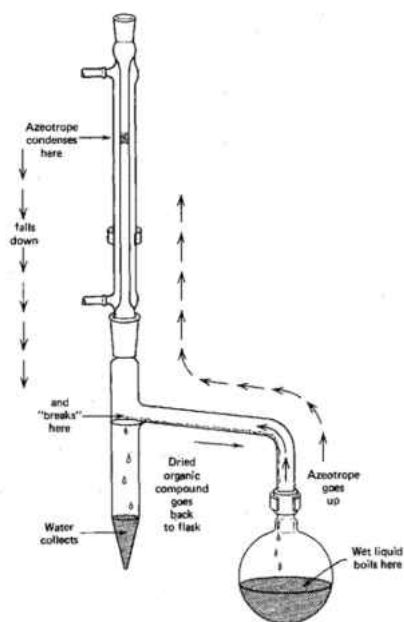
Figure 28: Diagram of reflux apparatus

This reflux apparatus worked by heating the oil bath, which in turn heated the solution in the flask. The water released from the condensation reaction that forms the polyimide formed an azeotrope with the OX and the vapor traveled up the Dean-Stark trap. Once it reached the condenser, the water condensed and fell into the trap, while the OX returned to the flask. The water was removed from the trap via the stopcock. This sequence of events allowed the removal of the water formed without interrupting the reaction.

The hot plate was set to approximately 170°C (or 338°F, since it was a Fahrenheit hot plate). As water accumulated in the trap by the previously described process, it was removed from the trap. As soon as some OX appeared in the trap the solution was ready to begin refluxing. It was allowed to reflux for six hours, then it was removed from the heat source and cooled by the atmosphere.

When it had cooled to room temperature, the solution was transferred from the round-bottom flask to a beaker. Approximately 100 mL of 3:1 water:methanol solution was added the HPI solution. This caused the HPI to precipitate as a solid. This solid was filtered by a vacuum filtration apparatus constructed from some tubing, a T-junction tube piece, a filter with a rubber stopper, and a vacuum flask. One side of the T-junction piece was connected to a water faucet and the faucet was turned on, and another end of the T-junction was connected via tubing to the flask. This created suction that was used to filter the water/NMP/methanol/OX waste from the precipitate. The waste was disposed

of and the precipitate was transferred to a beaker. A picture of the vacuum

filtration apparatus can be seen in Figure 29.

Figure 29: Picture of vacuum filtration apparatus

Another 100 mL of 3:1 water:methanol solution was added to the beaker

and allowed to soak for two days. After two days, the beaker was refilled with

more 3:1 water:methanol solution and placed on a stir plate. The precipitate was

then washed using the stir plate for over twelve hours. After washing, the beaker

sat until almost all of the water/methanol solution was evaporated. It was then

broken up and dried in the oven for twelve hours at 110ºC.

At this point one of the obstacles of the research was reached. The first

sample synthesized was heated in the oven at 150ºC before all of the

water/methanol solution was allowed to evaporate. This caused the HPI to

harden and stick to the beaker. To re-dissolve it, NMP was added. Once it was

dissolved, it was precipitated once more and filtered, but in addition to the yellow

HPI solid there was also a fluffy white solid. This solid was most likely

contamination from the second precipitation, and the sample had to be thrown

out. This mistake was not made again, and the temperature of drying was

lowered.

After the HPI samples were dried, they were broken up as needed,

weighed, and placed in bottles. The weights of HPI samples 2 through 35 can be

seen in Table 9. Note that samples 3, 4, 6, and 7, ended up hardening to the

beaker, and their weights are estimated using the mass of empty beakers. This

may have resulted in small errors, but these errors only affected the composition

of the solution that was cast. Since all solvent is removed during casting, this

error can be considered negligible.

Table 9: Weights of HPI samples

Sample	Mass (g)
1	-
2	4.654
3	9.028
4	7.994
5	6.510
6	3.794
7	4.326
8	7.916
9	8.351
10	7.356
11	8.046
12	6.021
13	7.777
14	7.766
15	6.744
16	9.442
17	8.584
18	18.834

Table 9 cont.

19	17.244
20	19.481
21	11.788
22	19.042
23	-
24	-
25	-
26	17.104
27	19.262
28	15.656
29	16.438
30	9.189
31	14.361
32	-
33	16.208
34	16.294
35	26.064

Samples 23-25 were not included in the previous table for reasons discussed below.

The samples were then subjected to FTIR and TGA measurements, the results of which can be found in the results section of this chapter. The samples that were hardened in the beaker, samples 3, 4, 6, and 7, were not subjected to FTIR as not enough powder could be gathered to use the instrument.

Membrane Formation

The samples were dissolved in NMP to form 20wt%, 30wt%, and 20wt% solutions for HPI-ODPA, HPI-BTDA, and HPI-BPDA, respectively. Once the solution was dissolved, it was stored in the refrigerator overnight to remove any bubbles within the solution. A 4" x 4" glass plate was covered in Teflon®, and the solution was poured onto it until it formed an approximate circle that was slightly more than 2" in diameter. The plate and solution were placed in the oven and

heated for one hour each at 60, 100, 150, 200, and 250°C, with a ramp of 1°C/min.

This step is where a few obstacles were encountered. The first was when the first solution was cast. After heating, the solution and polymer had completely disappeared. It was quickly apparent that the solution had slid off of the plate. This led to the use of a level and some aluminum foil to keep the plate level so the solution wouldn't move. The second obstacle was when the HPI-BTDA solutions were originally dissolved in NMP to make a 20wt% solution. This resulted in only partial membranes formed, so the concentration was raised to 30wt%. A third recurring obstacle was that sometimes the membranes simply wouldn't turn out the required shape or size. It was found that these membranes couldn't be re-dissolved, so they were disposed of. Some membranes were big enough, but not a viable shape. These membranes were simply cut to the required shape with a pair of scissors.

The largest obstacle experienced during the casting step was with the HPI-BPDA. The first sample of powdered HPI-BPDA wouldn't dissolve, so more NMP was added until it did. It was then cast and the cast was unsuccessful due to too low of a concentration. The solution was left out to evaporate over the next few days and eventually enough NMP evaporated such that the solution was back to approximately a 20wt% solution. It was cast once more and failed again. All subsequent casts of HPI-BPDA failed, and when a second group of HPI-BPDA samples were synthesized they became solid right after the HPI synthesis

step. This solid HPI-BPDA proved to be un-dissolvable, and thus samples 12-16 and 23-25 were not included in any further measurements.

Since three dianhydrides were necessary to get significant results from this research, benzene-1,2,4,5-tetracarboxylic acid, also known as pyromellitic dianhydride (PMDA), was chosen as a replacement dianhydride. It was subjected to the exact same synthesis and casting procedures as the other three dianhydrides. PMDA has a molecular weight of 218.12 g/mol, so 20 mmol is 4.362 g.

The masses of NMP used to dissolve each sample are shown in Table 10.

Table 10: Mass of NMP used for casting solution

Sample	Mass NMP (g)
2	17.776
3	36.261
4	32.061
5	23.616
6	15.153
7	17.304
8	28.784
9	15.214
10	15.005
11	16.827
12	17.241
13	19.398
14	-
15	-
16	34.275
17	34.338
18	44.009
19	40.323
20	45.376
21	27.518
22	44.454
23	-
24	-

Table 10 cont.

25	-
26	39.974
27	44.924
28	36.434
29	38.265
30	21.457
31	57.527
32	-
33	37.893
34	38.016
35	60.576

Samples 14 and 15 ended up needing more than the initial amount of NMP to dissolve and it was added periodically and not measured, so the final amount of NMP for these two samples is not known.

Table 11 lists each membrane cast attempt, what sample was used, and whether or not it was successful. Figures 30 through 58 show pictures of successful casts, and Figures 59 through 61 show a few of the failed casts.

Table 11: Successful and unsuccessful membrane casts and their parent sample(s)

Cast	Sample	Successful? (Y/N)
1	3	N
2	3	N
3	3,4	Y
4	4	N
5	4	Y
6	4,6	Y
7	6	N
8	6,7	N
9	7	Y
10	8	N
11	8	N

Table 11 cont.

12	8	N
13	5	Y
14	9	Y
15	9	N
16	5	Y
17	10	Y
18	12	N
19	12	N
20	13	N
21	13,12	N
22	16	N
23	13,12	N
24	11,10	Y
25	11	N
26	2,5	Y
27	2	Y
28	17	N
29	31	N
30	31	N
31	31	N
32	17	N
33	33	N
34	18	N
35	18	Y
36	33	Y
37	18	N
38	31,33	Y
39	31,33	Y
40	18	Y
41	18,19	Y
42	19	Y
43	19	Y
44	28	Y
45	28	Y
46	28	Y
47	28	Y
48	29	N
49	19	Y
50	29	N
51	20	Y
52	29	N
53	20	Y
54	29	Y

Table 11 cont.

55	26,17	Y
56	34	Y
57	34	Y

Figure 30: Cast 3

Figure 31: Cast 5

Figure 32: Cast 6 (slightly folded)

Figure 33: Cast 9

Figure 34: Cast 13
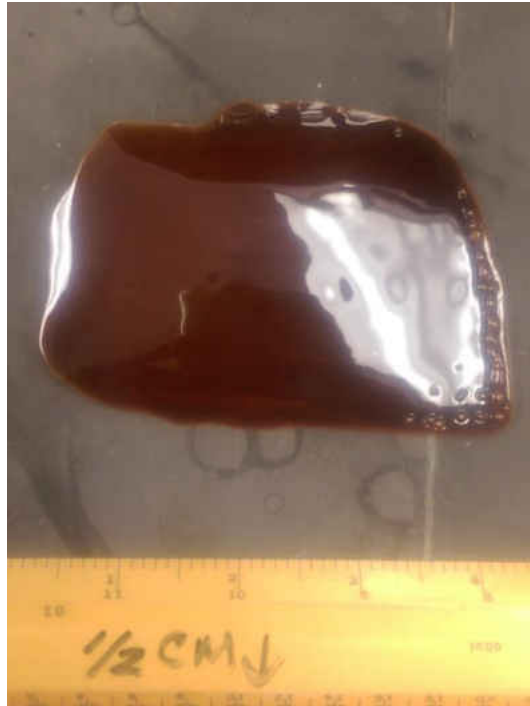
Figure 35: Cast 16 (bubbled portion was removed)

Figure 36: Cast 17 (cut to size)

Figure 37: Cast 24 (oddly shaped)

Figure 38: Cast 26 (cut to size)

Figure 39: Cast 27

Figure 40: Cast 35 (trimmed to fit 2" cell)

Figure 41: Cast 36

Figure 42: Cast 38

Figure 43: Cast 39

Figure 44: Cast 40 (trimmed to fit 2" cell)

Figure 45: Cast 41 (trimmed to fit 2" cell)

Figure 46: Cast 42

Figure 47: Cast 43

Figure 48: Cast 44

Figure 49: Cast 45

Figure 50: Cast 46

Figure 51: Cast 47

84

Figure 52: Cast 49 (cut to produce two pieces that fit 1" cell)

Figure 53: Cast 51 (trimmed to fit 2" cell)

Figure 54: Cast 53 (trimmed to fit 2" cell)

Figure 55: Cast 54 (trimmed to fit 1" cell)

Figure 56: Cast 55 (bubbled portion removed)

Figure 57: Cast 56

Figure 58: Cast 57

Figure 59: Cast 1 (still on plate)

Figure 60: Cast 4

Figure 61: Cast 7 (really bubbly)

Thermal Rearrangement

The first thing done for this section was a test to see if the thermal rearrangement would work. A small piece of a failed membrane cast from each one of HPI-ODPA, HPI-BTDA, and HPI-BPDA were tested for thermal rearrangement. Each piece was pressed between two ceramic plates using only the weight of the plates for pressure, no clamps were used. The sandwiched membrane piece was then placed in the oven and heated at 5°C/min to 300°C and held there for one hour, then heated at 5°C/min to 400°C and held there for two hours. All three pieces blackened some, but otherwise retained their shape and structural integrity.

<div align="center">

Results

</div>

HPI Characterization

The HPI powders were characterized using attenuated total reflectance Fourier transform infrared spectroscopy (ATR-FTIR, referred to from here as "FTIR") and TGA. The FTIR was a Nicolet IR200 and the TGA was a Simultaneous DSC-TGA (SDT) Q600/2960 from Thermo Fisher Scientific. The temperature program run on the TGA matched that of the procedure for thermal rearrangement.

FTIR Data

The FTIR data for HPI samples 2, 5, 8-22, and 26-35 are shown in Figures 62 through 88:
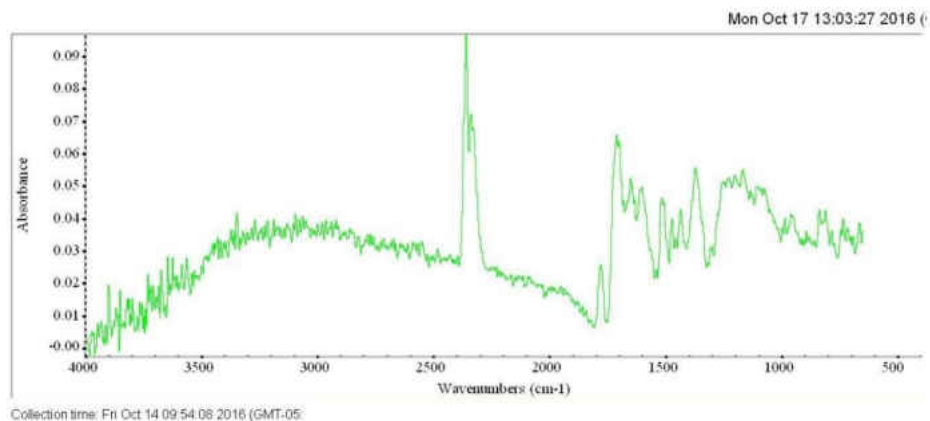
Figure 62: FTIR data for sample 2
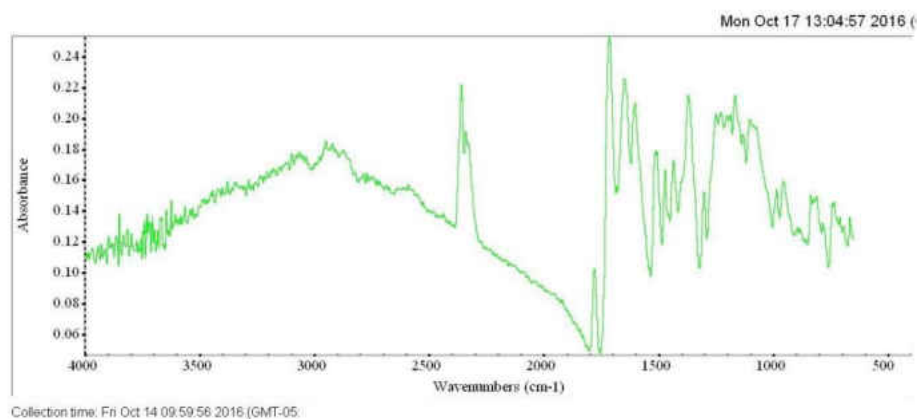
Figure 63: FTIR data for sample 5
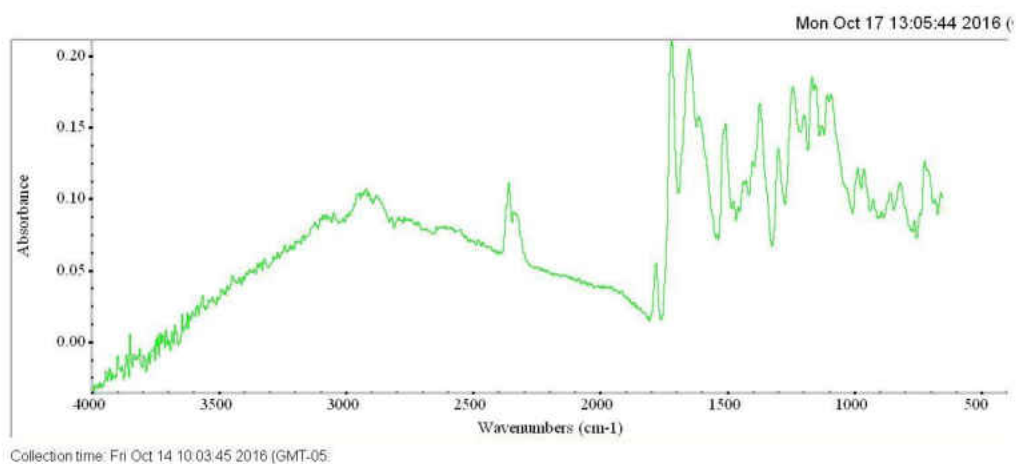
Figure 64: FTIR data for sample 8
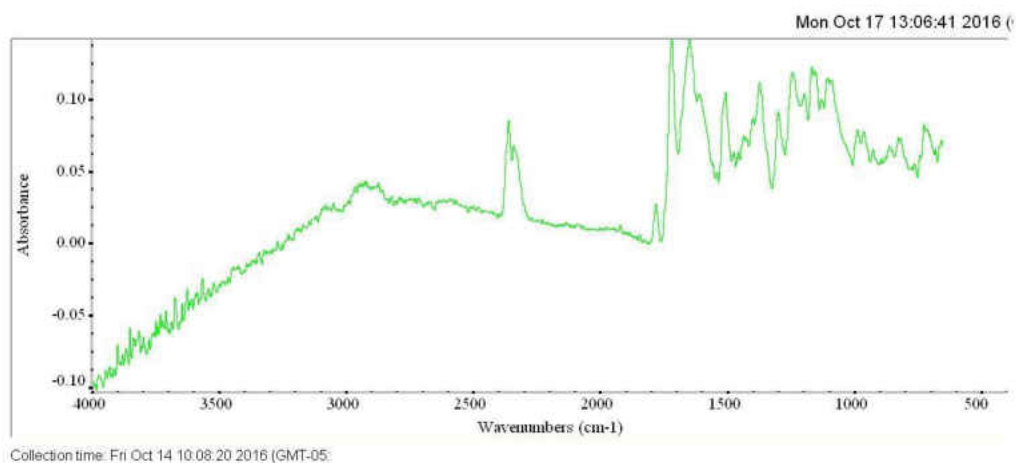
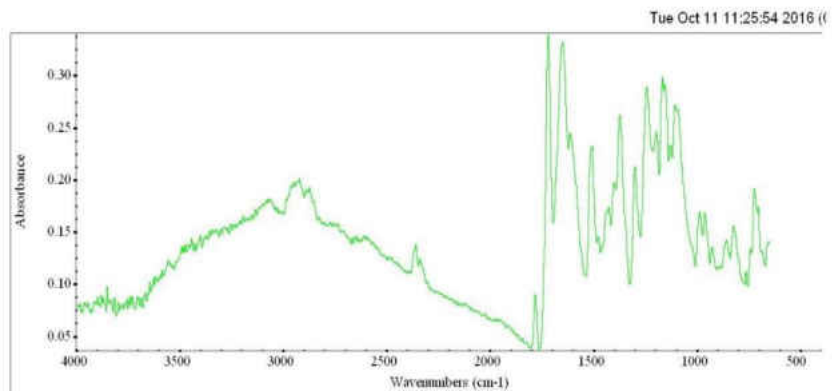Figure 65: FTIR data for sample 9
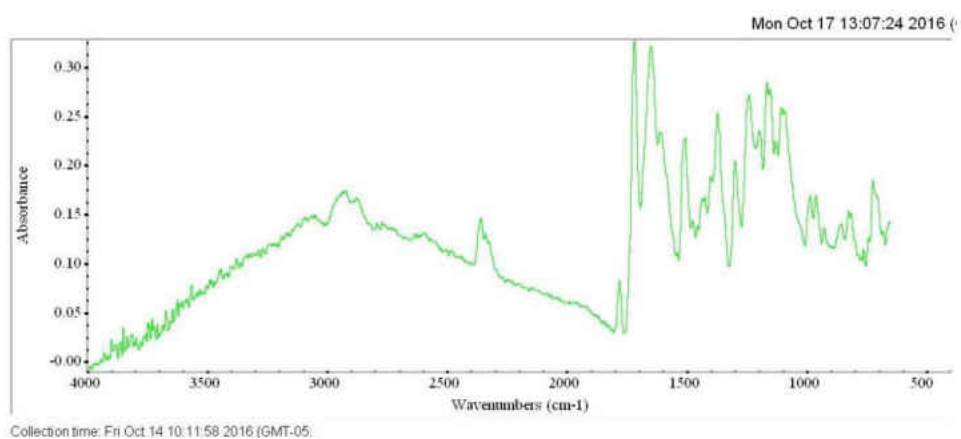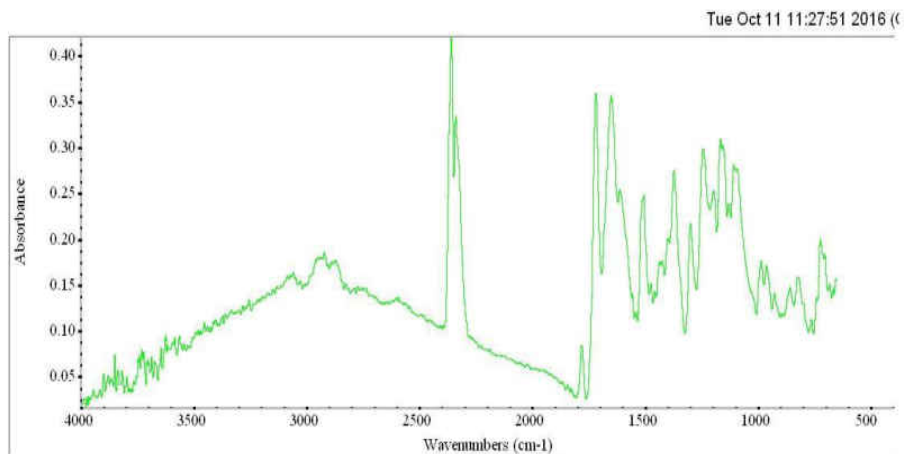

Figure 66: FTIR data for sample 10
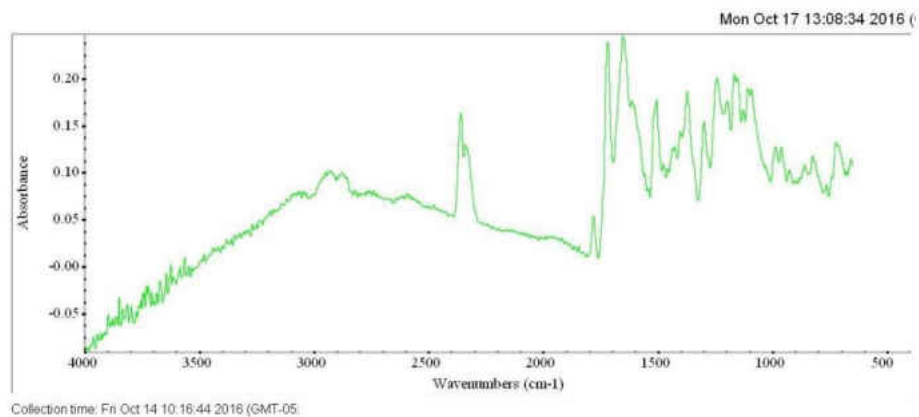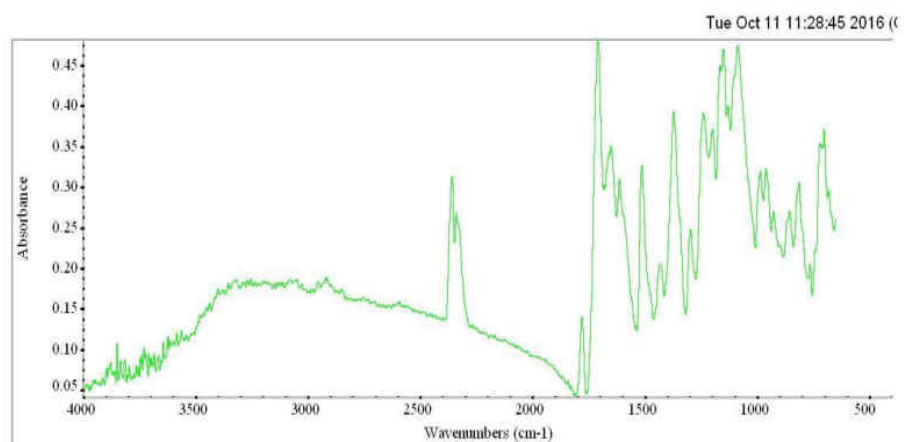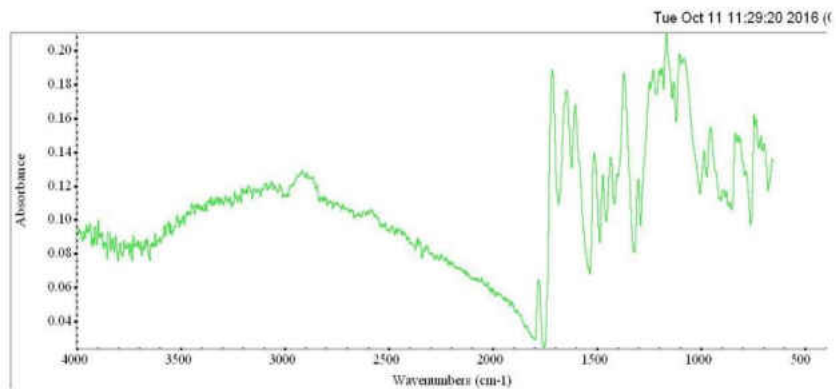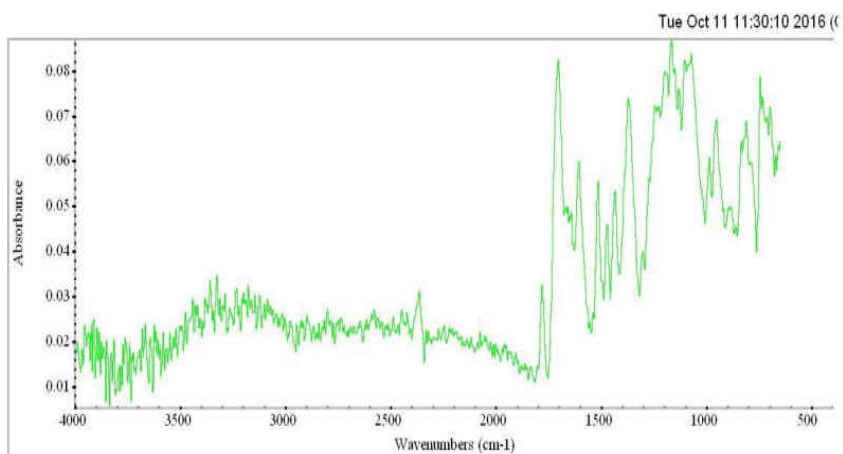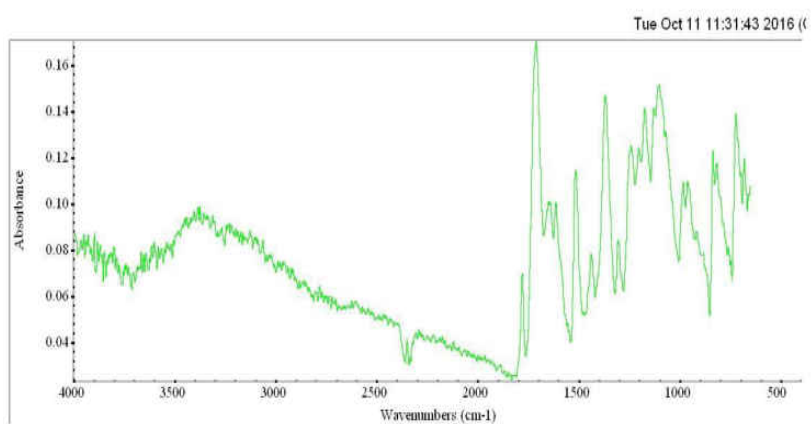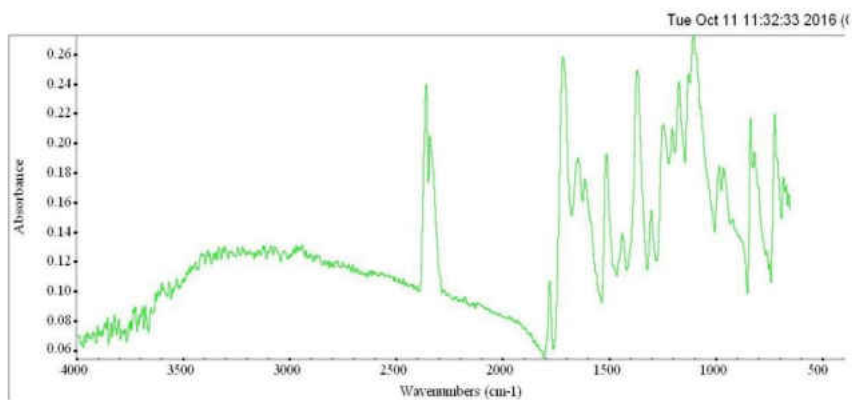

Figure 67: FTIR data for sample 11
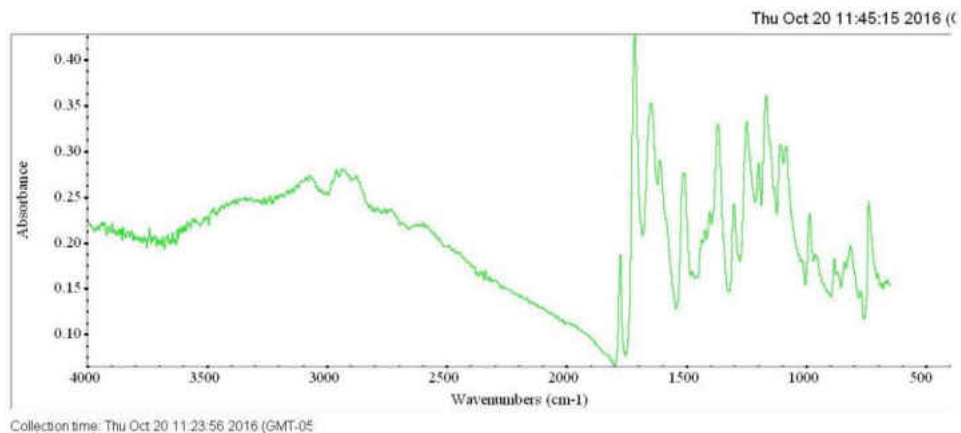
Figure 68: FTIR data for sample 12
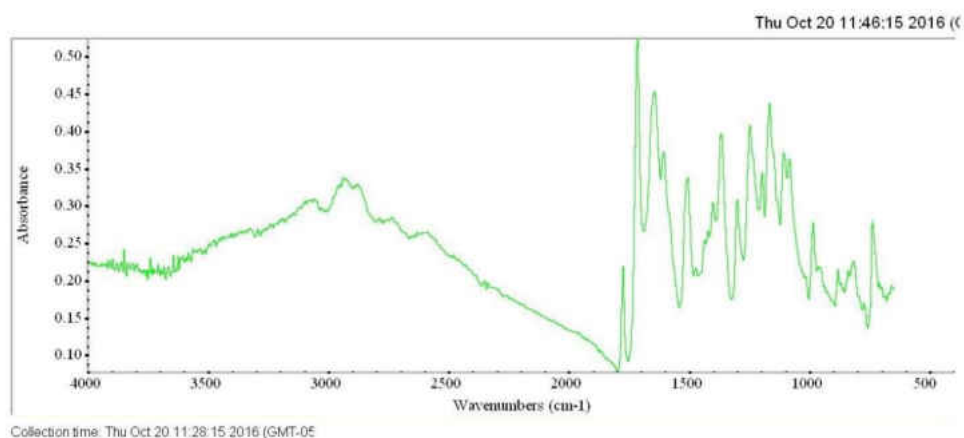
Figure 69: FTIR data for sample 13
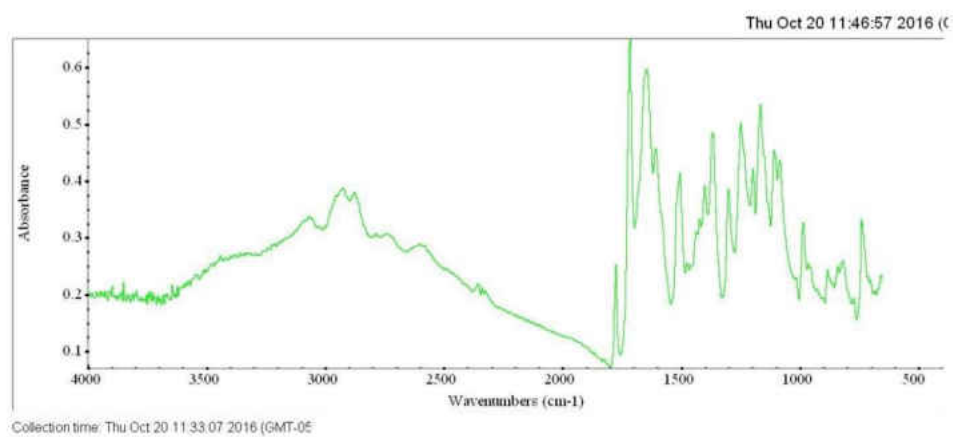
Figure 70: FTIR data for sample 14
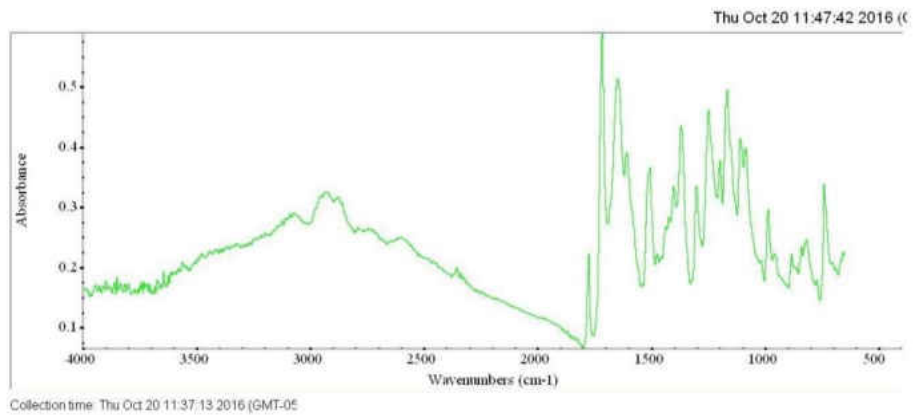
Figure 71: FTIR data for sample 15
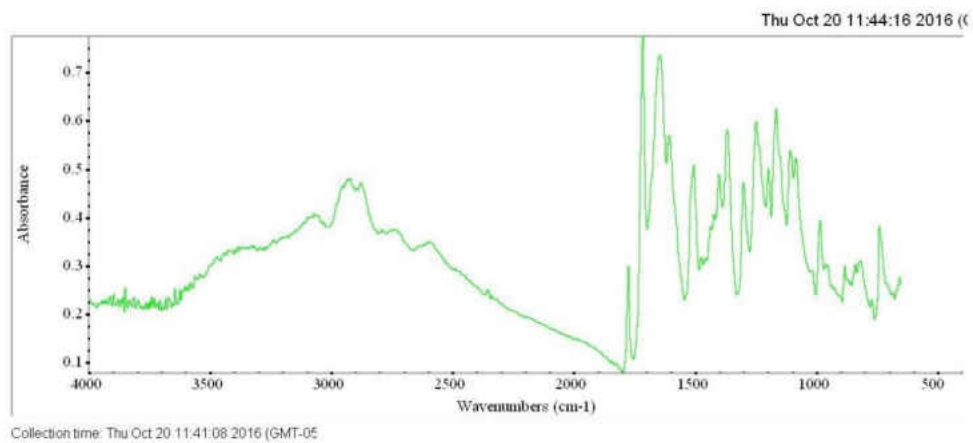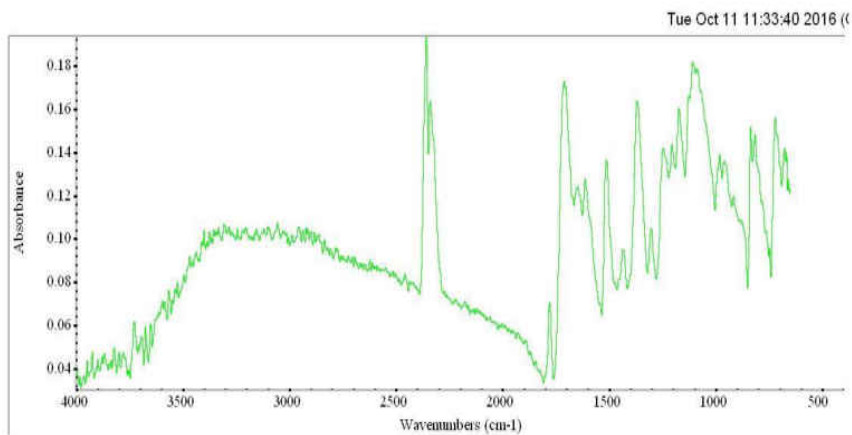

Figure 72: FTIR data for sample 16
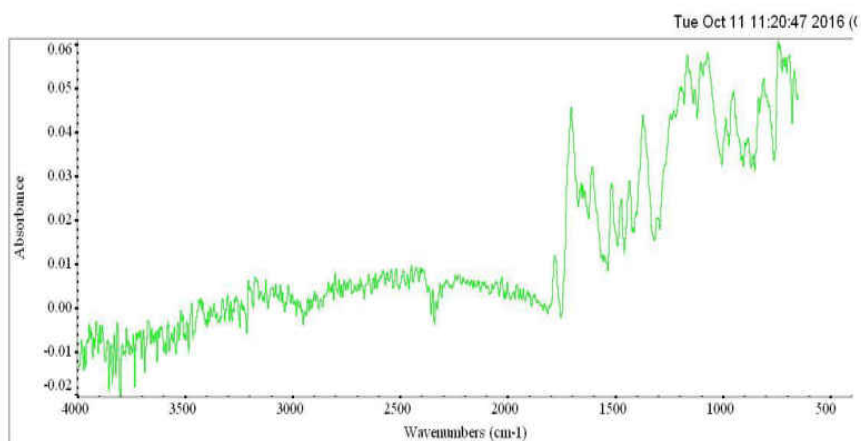
Figure 73: FTIR data for sample 17
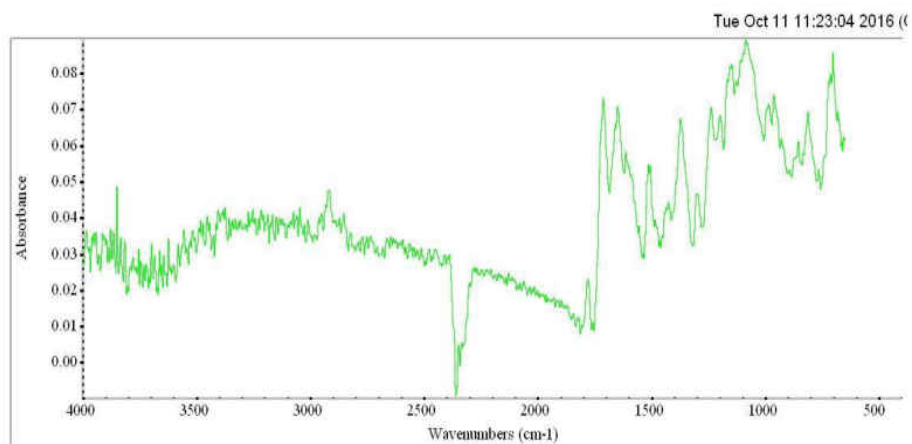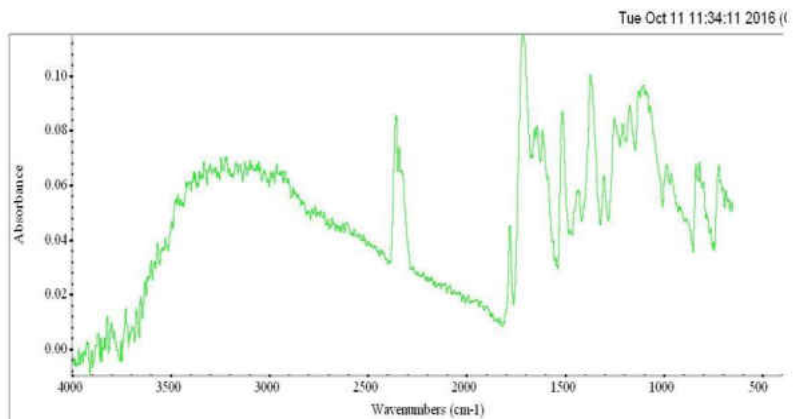
Figure 74: FTIR data for sample 18
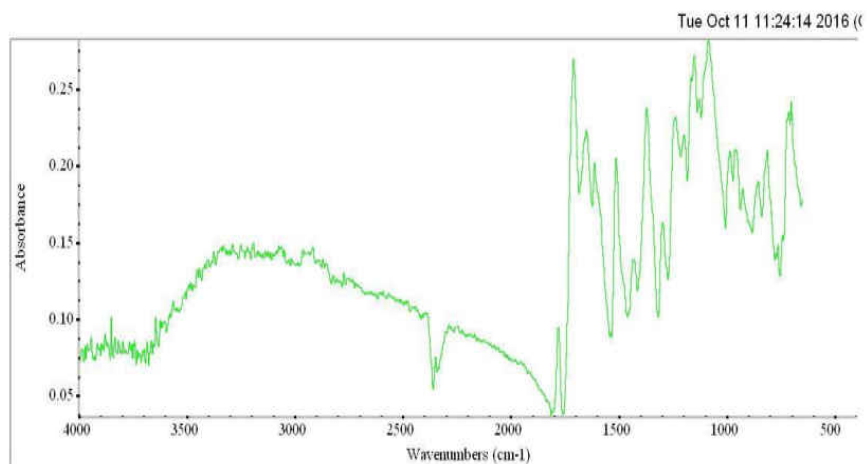
Figure 75: FTIR data for sample 19

Figure 76: FTIR data for sample 20

Figure 77: FTIR data for sample 21

Figure 78: FTIR data for sample 22

Figure 79: FTIR data for sample 26

Figure 80: FTIR data for sample 27

Figure 81: FTIR data for sample 28

Figure 82: FTIR data for sample 29

97

Figure 83: FTIR data for sample 30

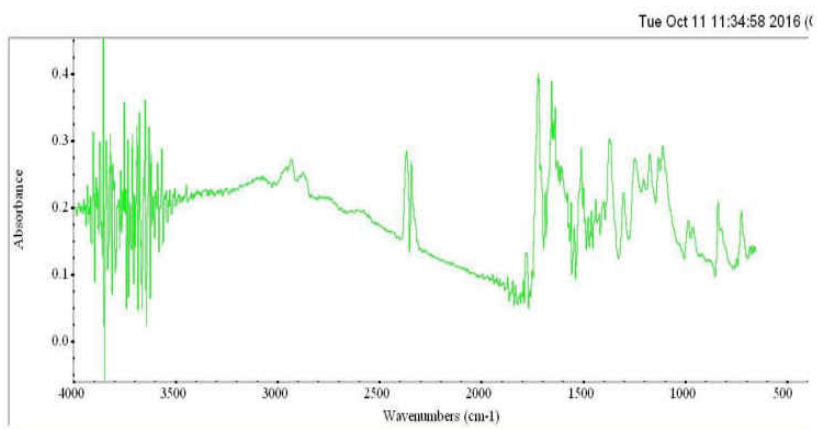Figure 84: FTIR data for sample 31

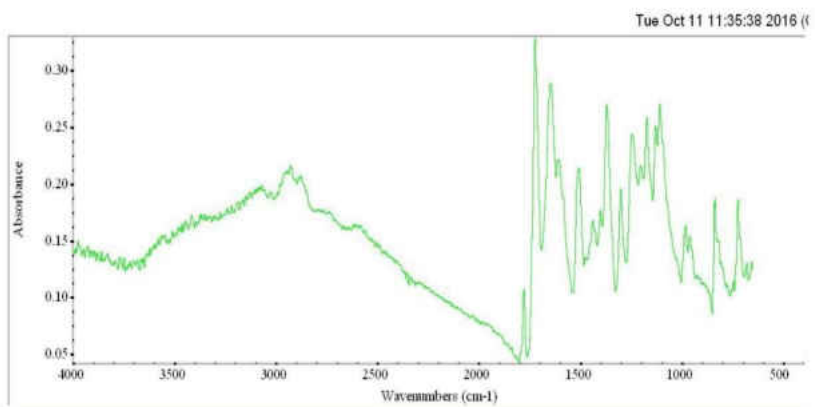Figure 85: FTIR data for sample 32
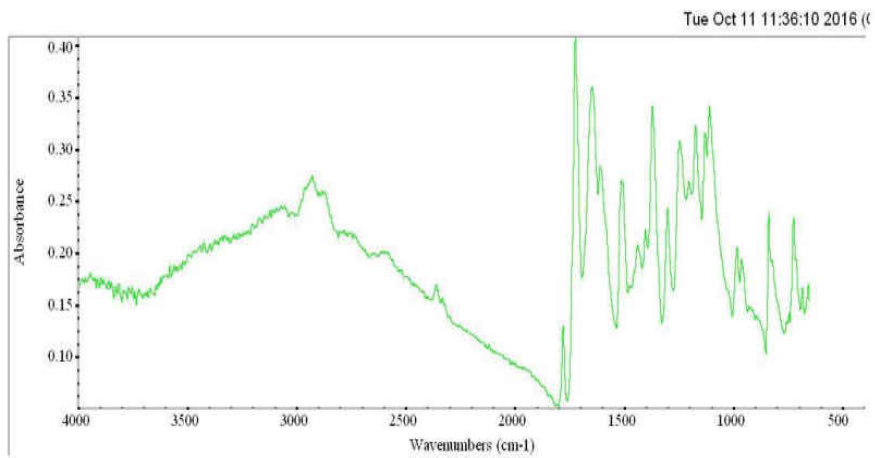
Figure 86: FTIR data for sample 33

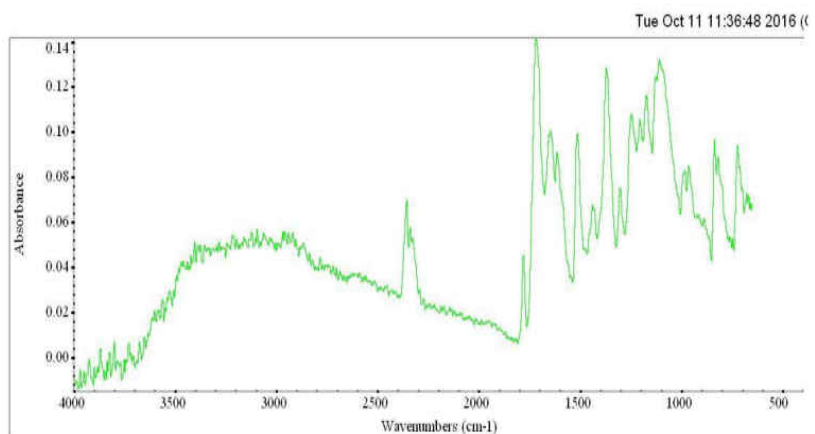Figure 87: FTIR data for sample 34

Figure 88: FTIR data for sample 35

99

TGA Data

The TGA data for HPI samples 2-22 and 26-35 is shown in Figures 89 through 119:
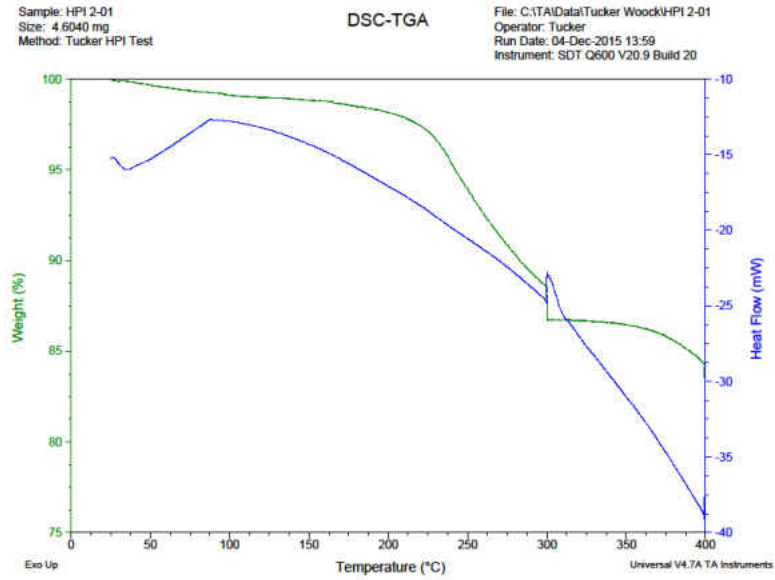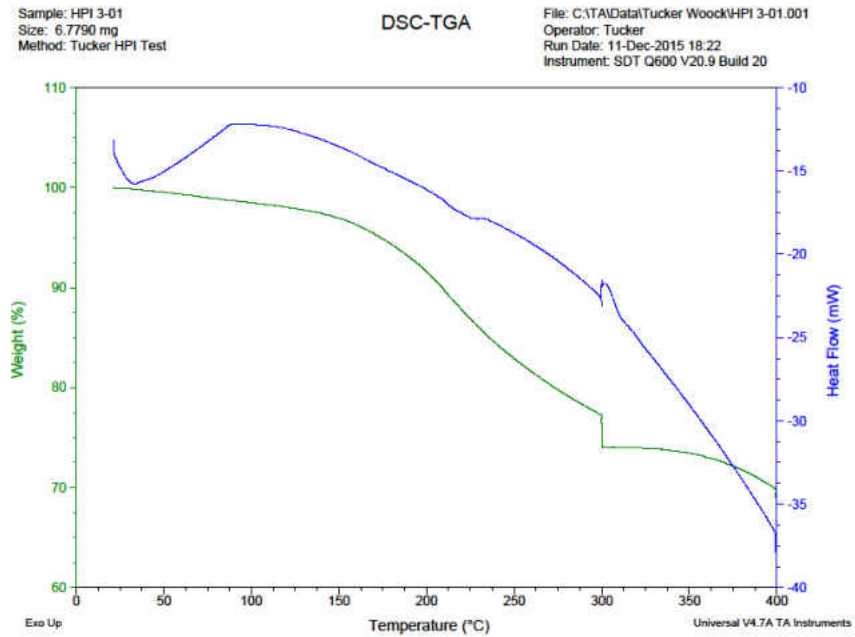

Figure 89: TGA data for sample 2

Figure 90: TGA data for sample 3

Figure 91: TGA data for sample 4

Figure 92: TGA data for sample 5

101

Figure 93: TGA data for sample 6

Figure 94: TGA data for sample 7

Figure 95: TGA data for sample 8

Figure 96: TGA data for sample 9

103

Figure 97: TGA data for sample 10

Figure 98: TGA data for sample 11

Figure 99: TGA data for sample 12
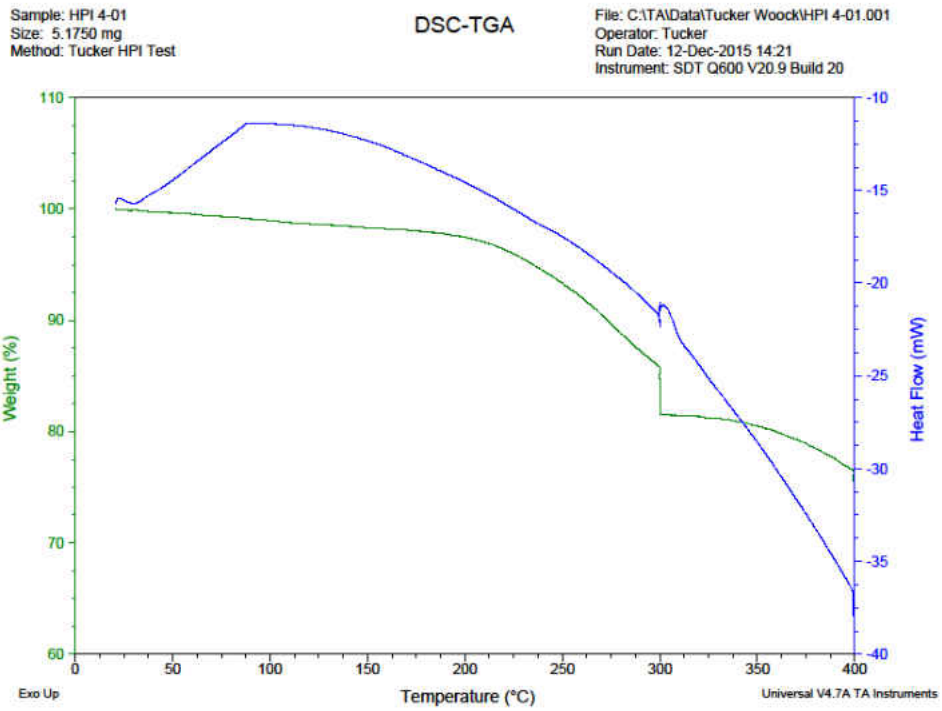

Figure 100: TGA data for sample 13
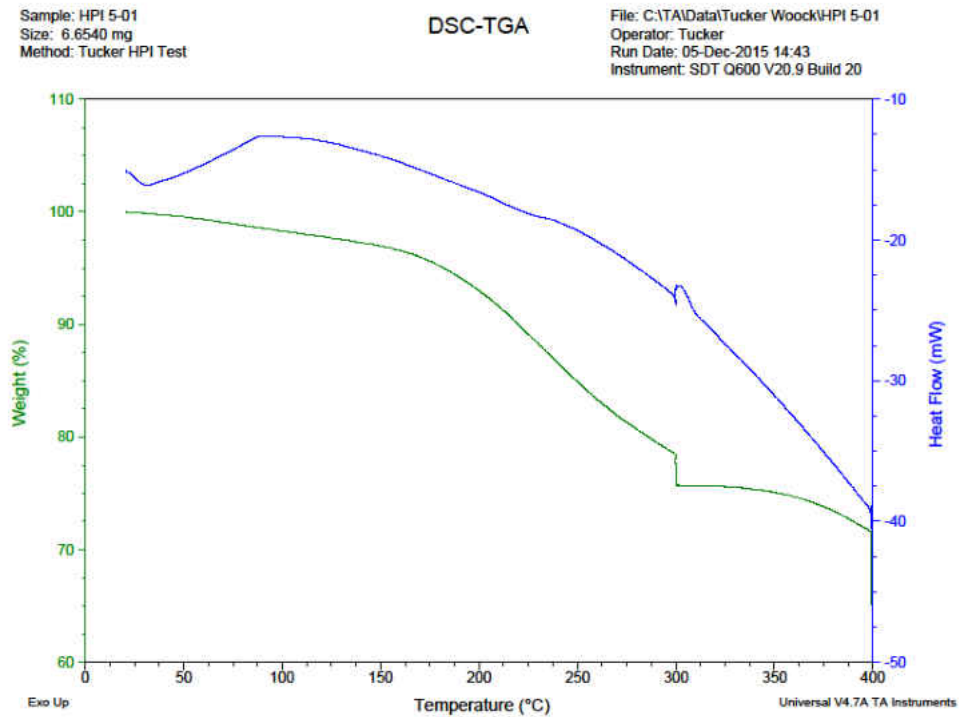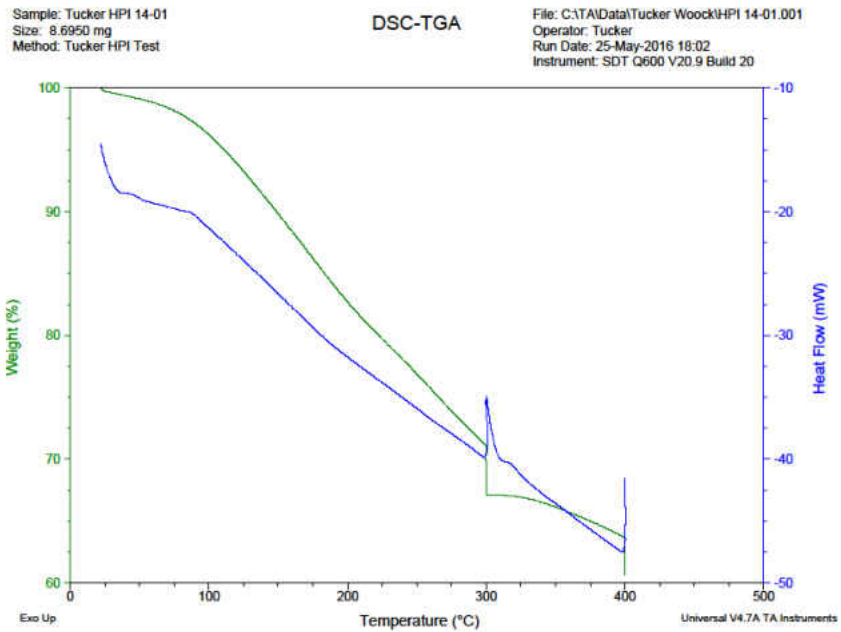
Figure 101: TGA data for sample 14
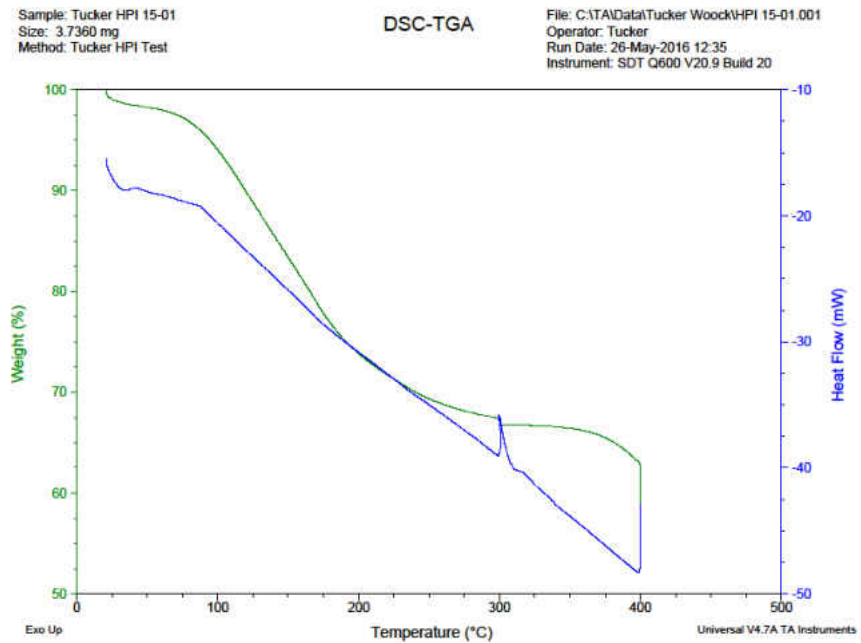
Figure 102: TGA data for sample 15
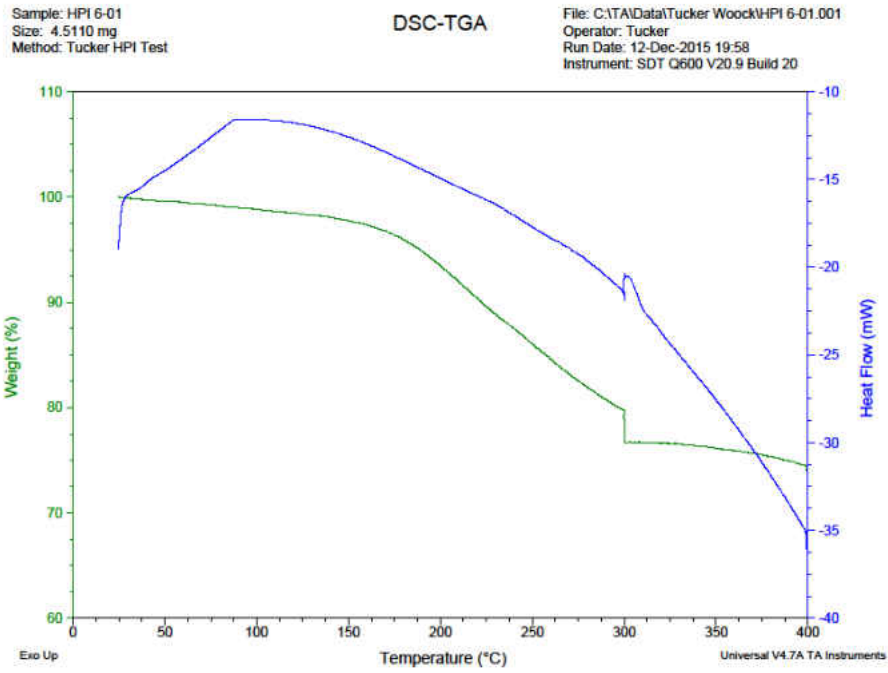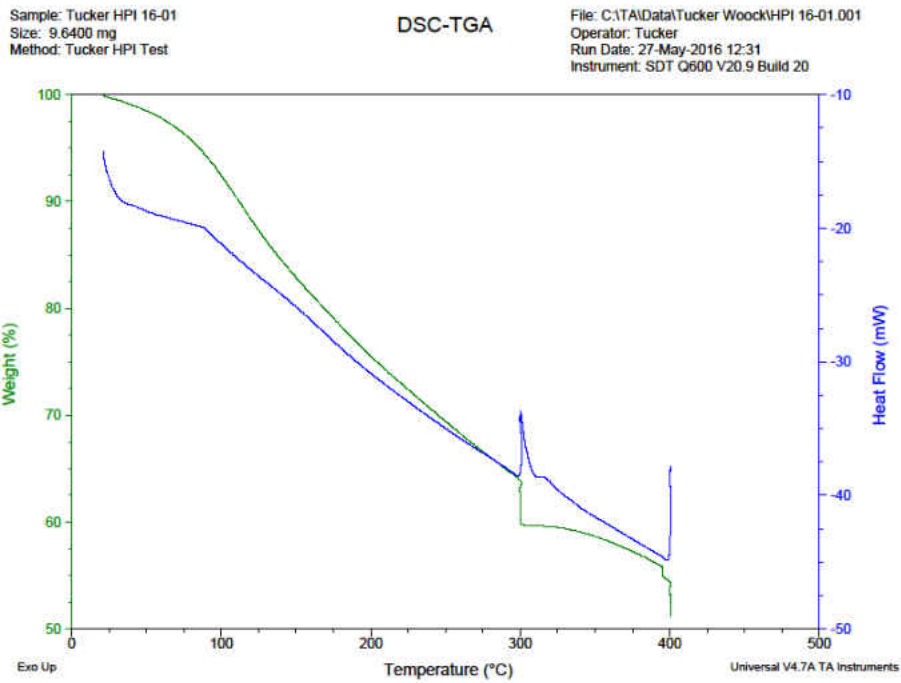
Figure 103: TGA data for sample 16
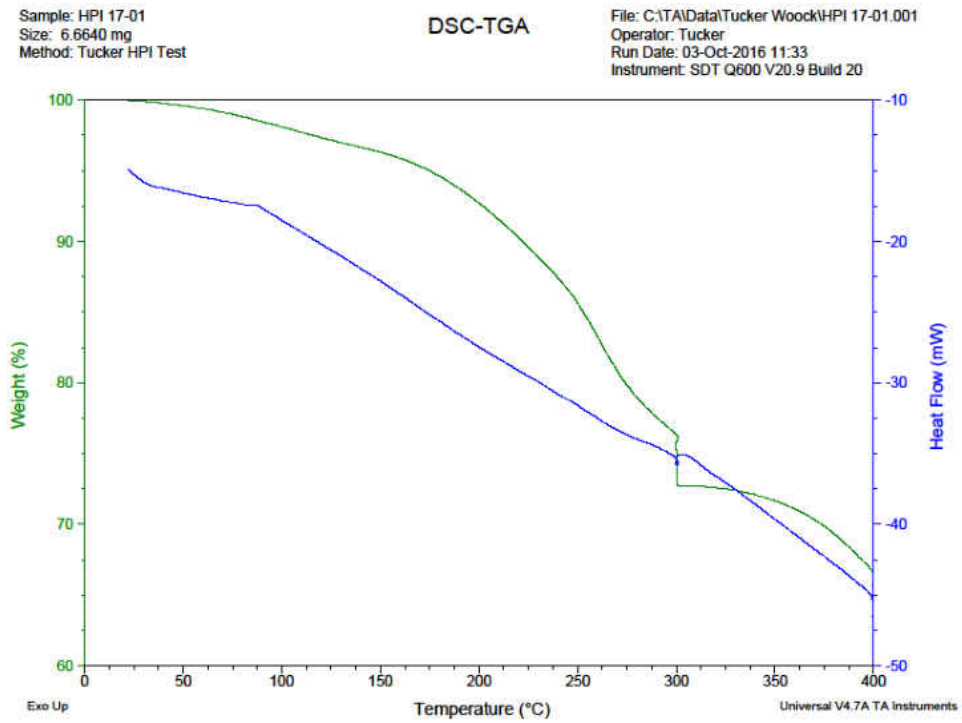
Figure 104: TGA data for sample 17
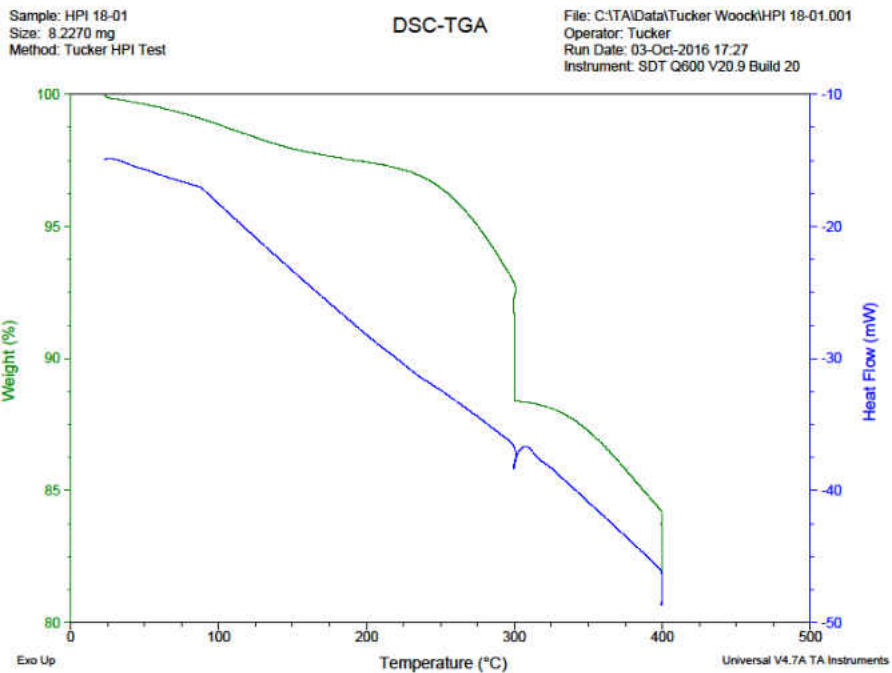
Figure 105: TGA data for sample 18
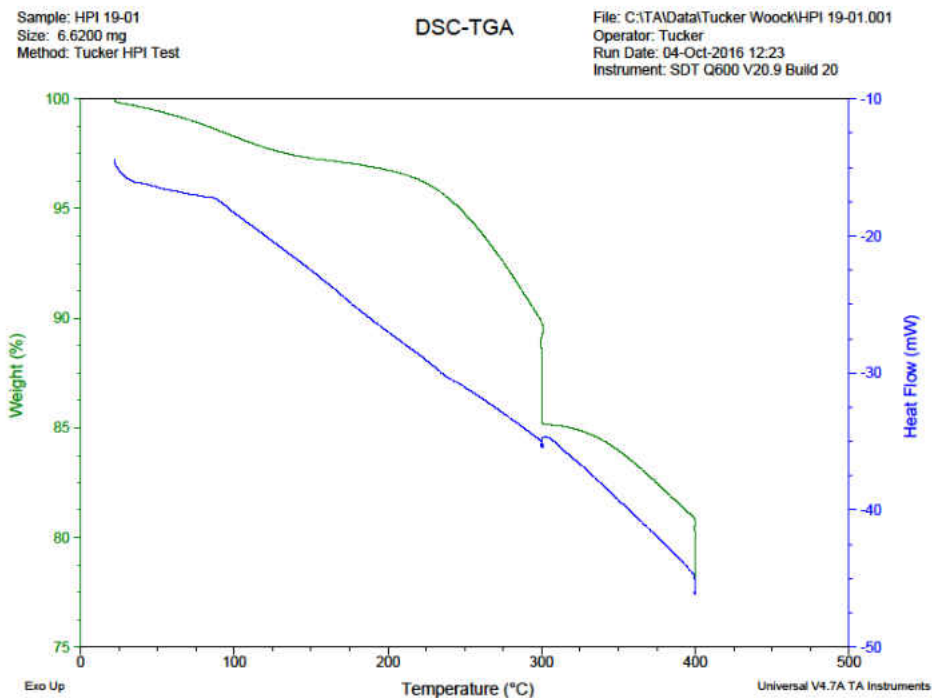
Figure 106: TGA data for sample 19
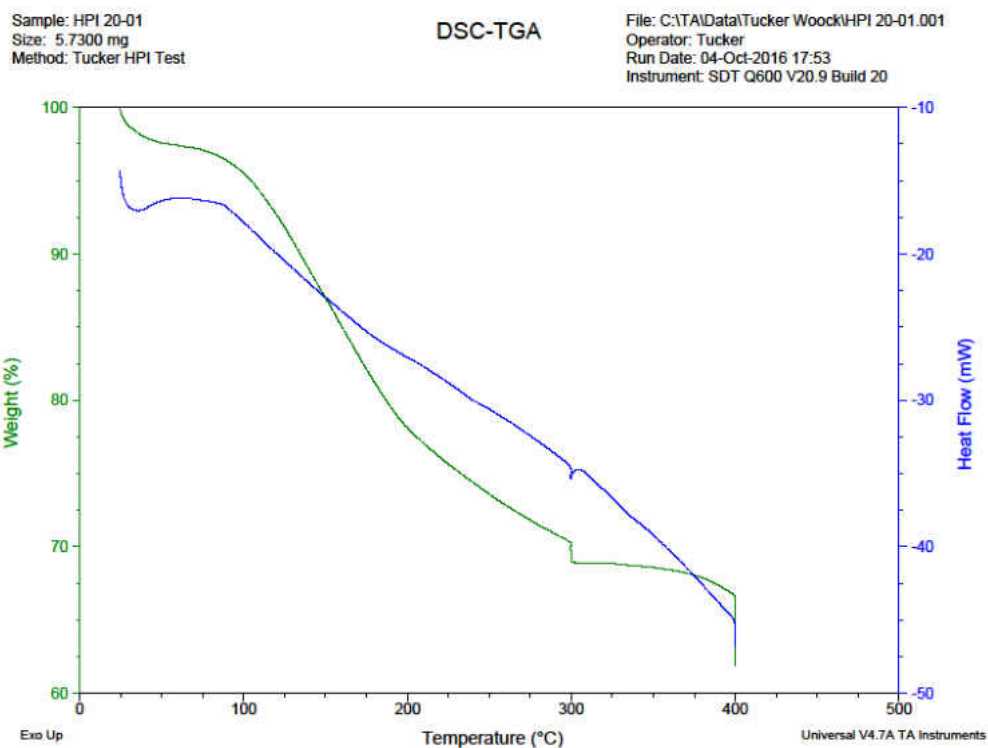
Figure 107: TGA data for sample 20
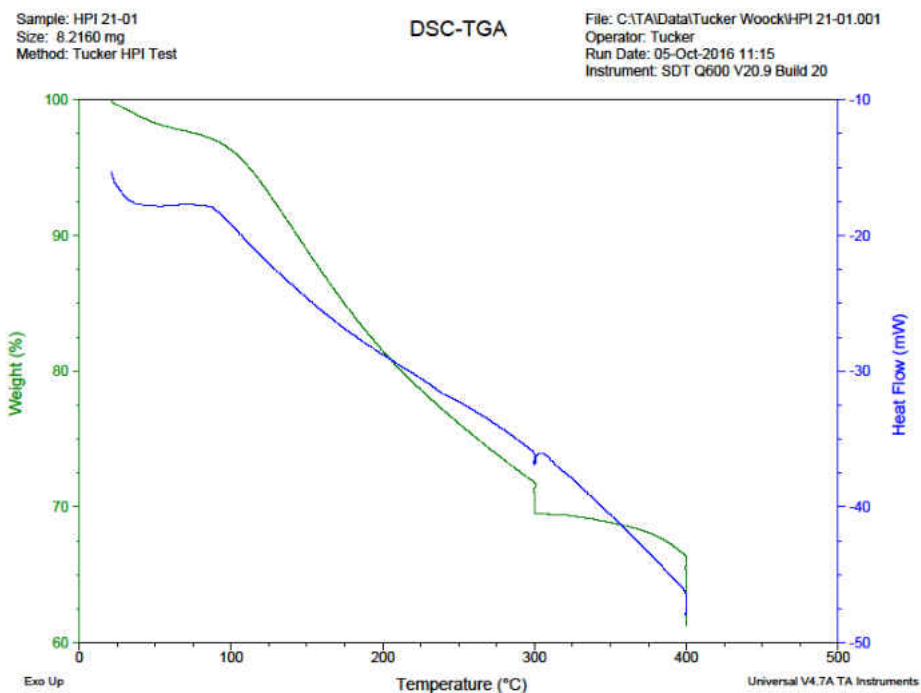
Figure 108: TGA data for sample 21

109
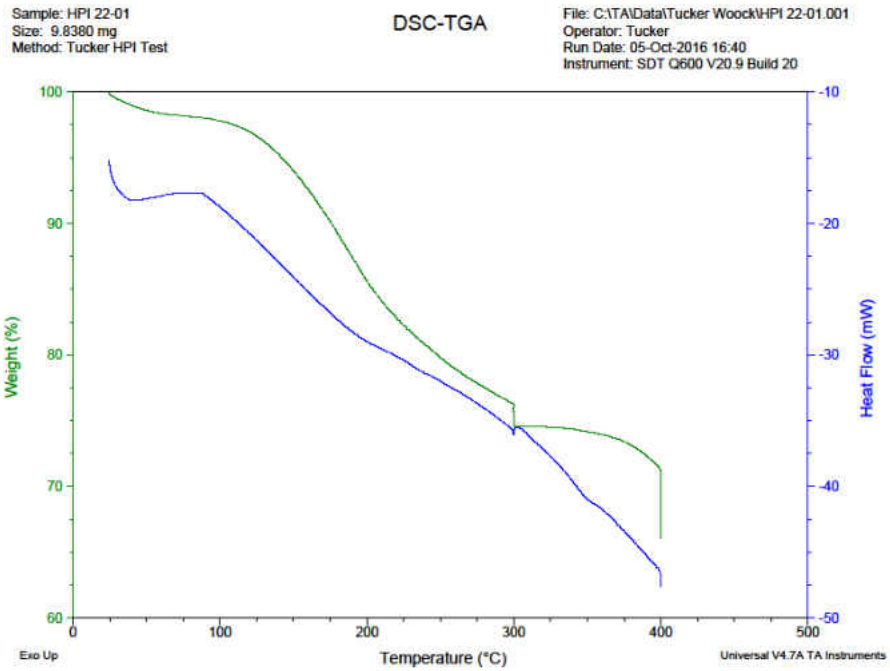
Figure 109: TGA data for sample 22
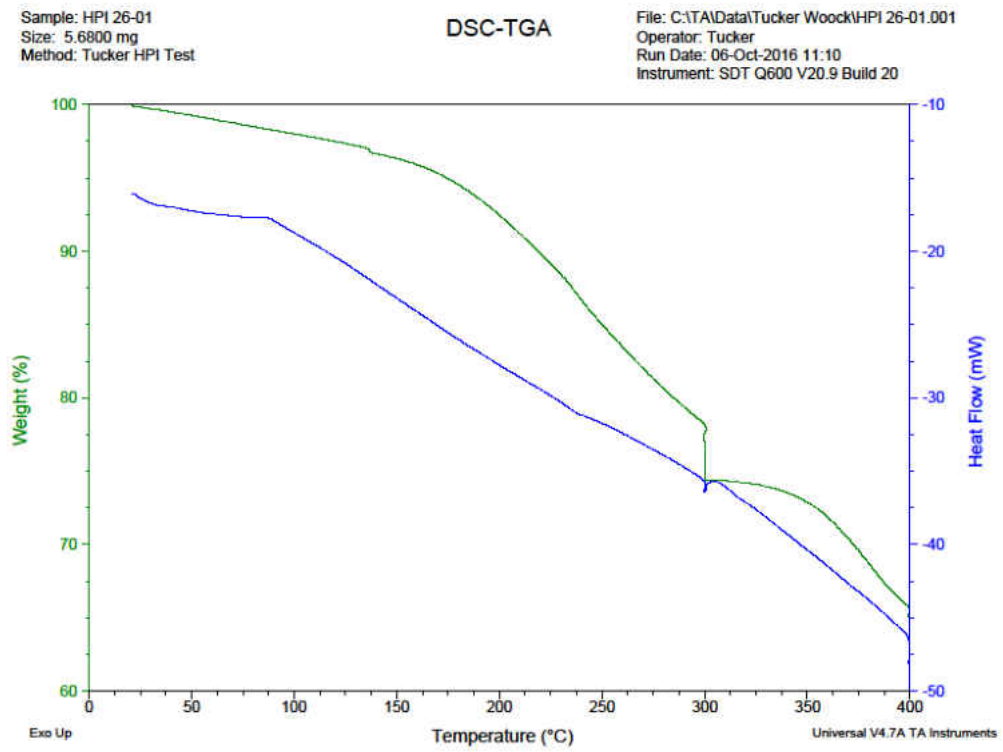
Figure 110: TGA data for sample 26

110
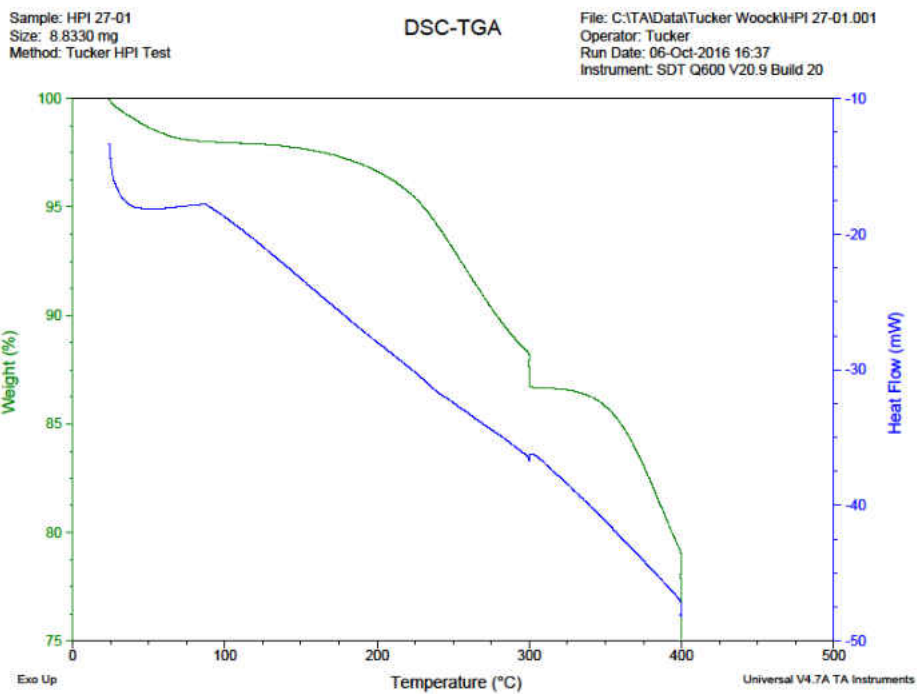
Figure 111: TGA data for sample 27
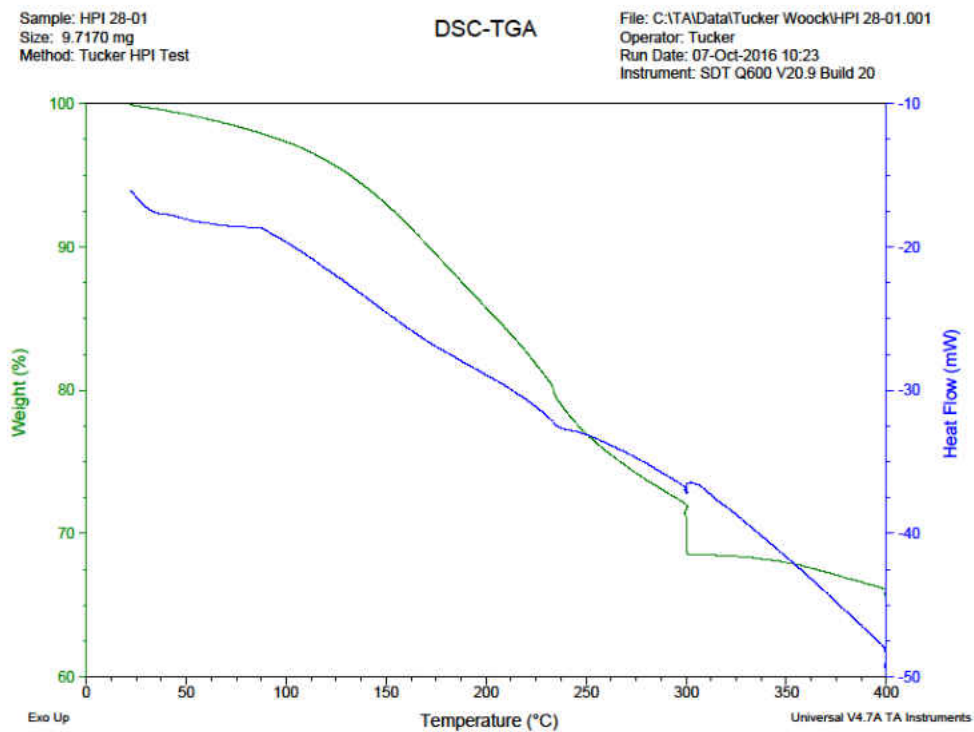
Figure 112: TGA data for sample 28

111
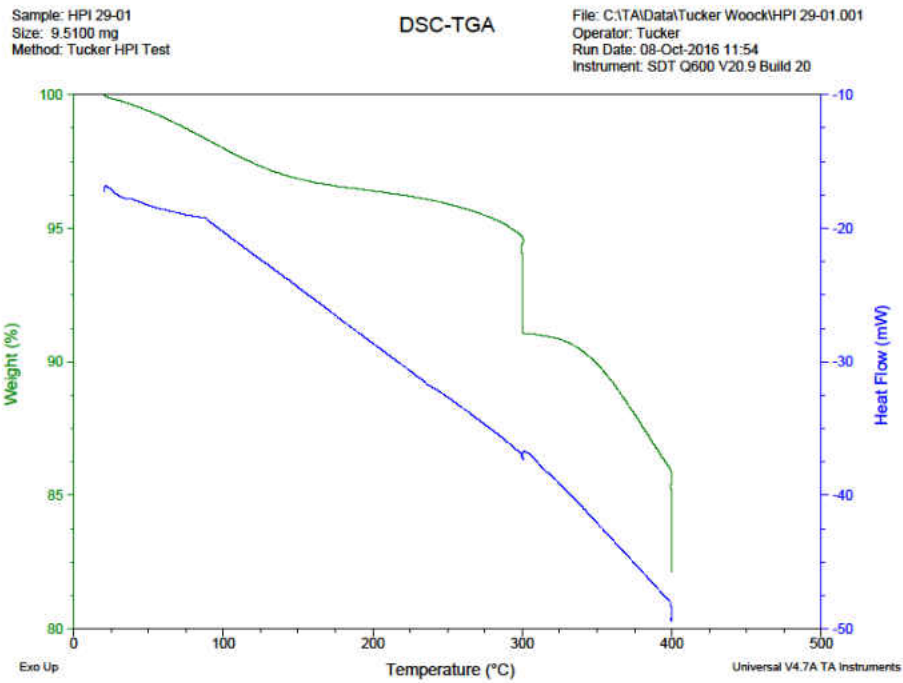
Figure 113: TGA data for sample 29
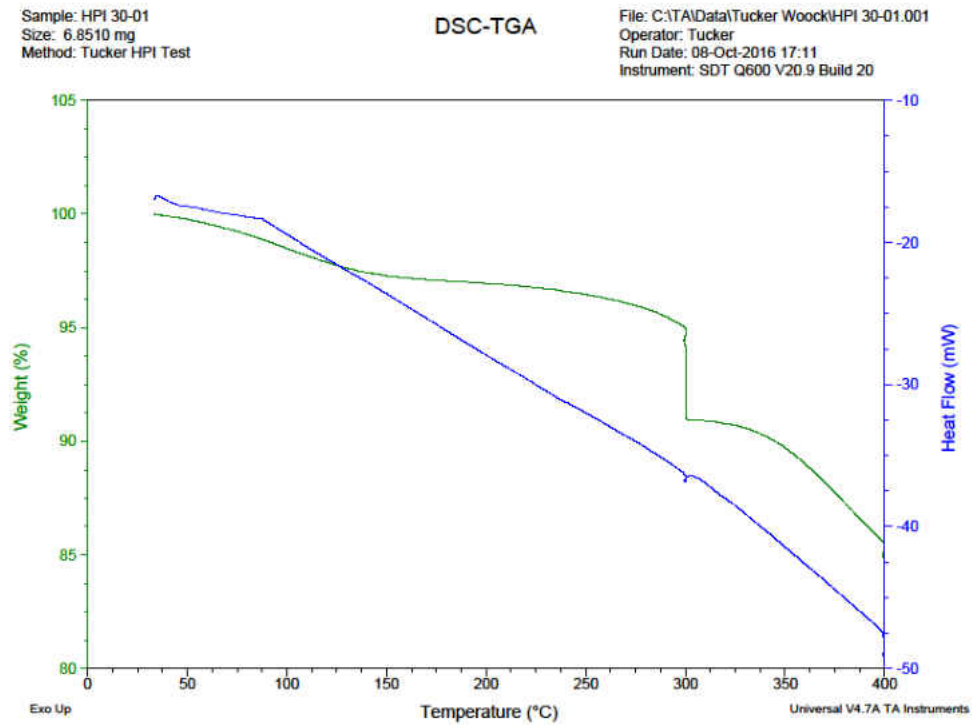
Figure 114: TGA data for sample 30

112

Sample: HPI 31-01
Size: 7.8700 mg
Method: Tucker HPI Test

DSC-TGA

File: C:\TA\Data\Tucker Woock\HPI 31-01.001
Operator: Tucker
Run Date: 09-Oct-2016 11:23
Instrument: SDT Q600 V20.9 Build 20
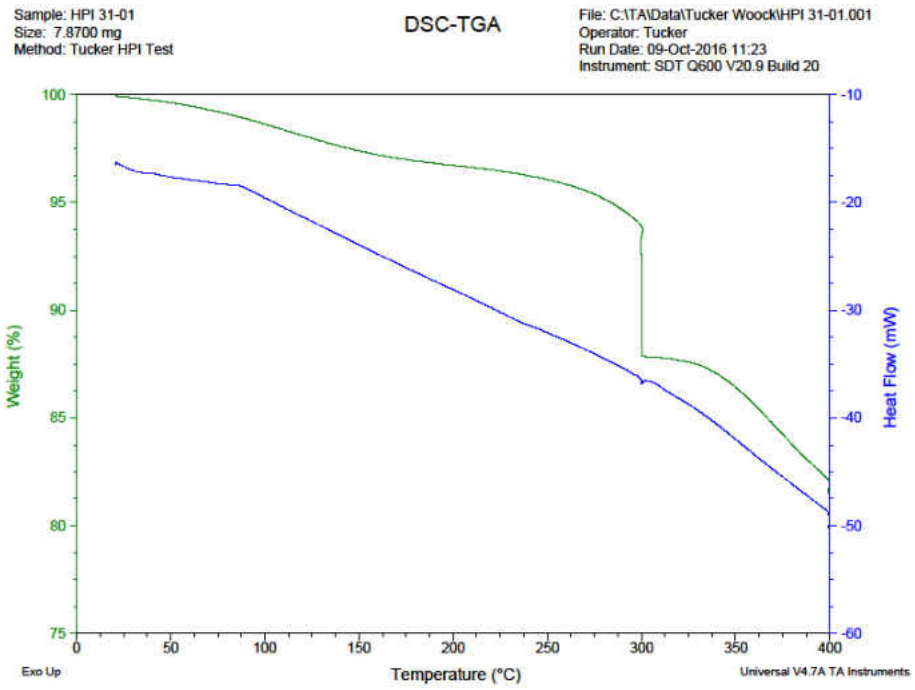
Figure 115: TGA data for sample 31

Sample: HPI 32-01
Size: 8.3540 mg
Method: Tucker HPI Test

DSC-TGA

File: C:\TA\Data\Tucker Woock\HPI 32-01.001

Run Date: 09-Oct-2016 16:32
Instrument: SDT Q600 V20.9 Build 20
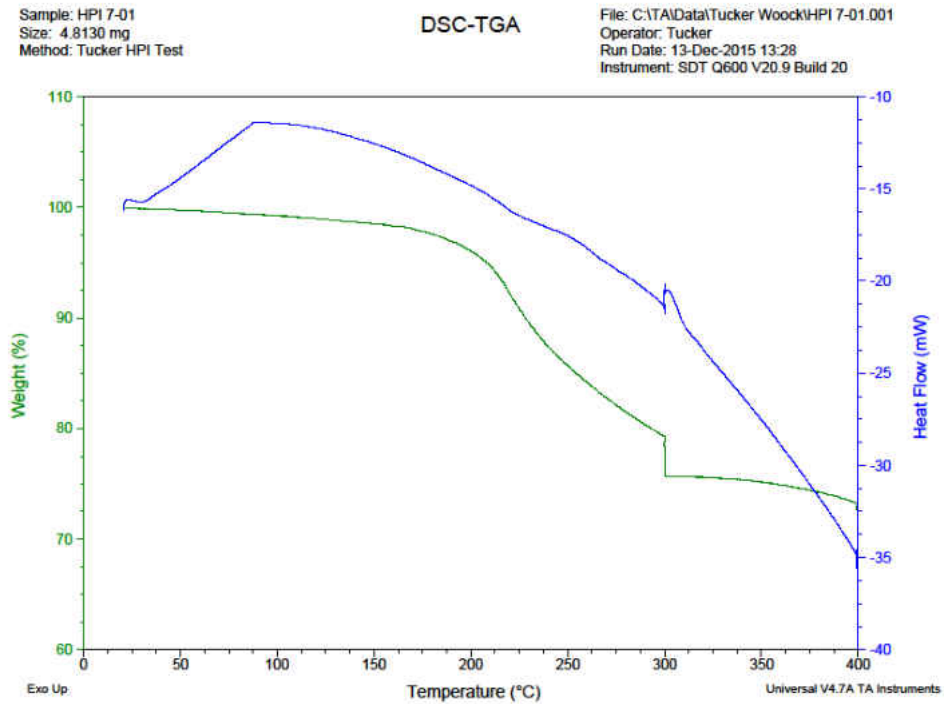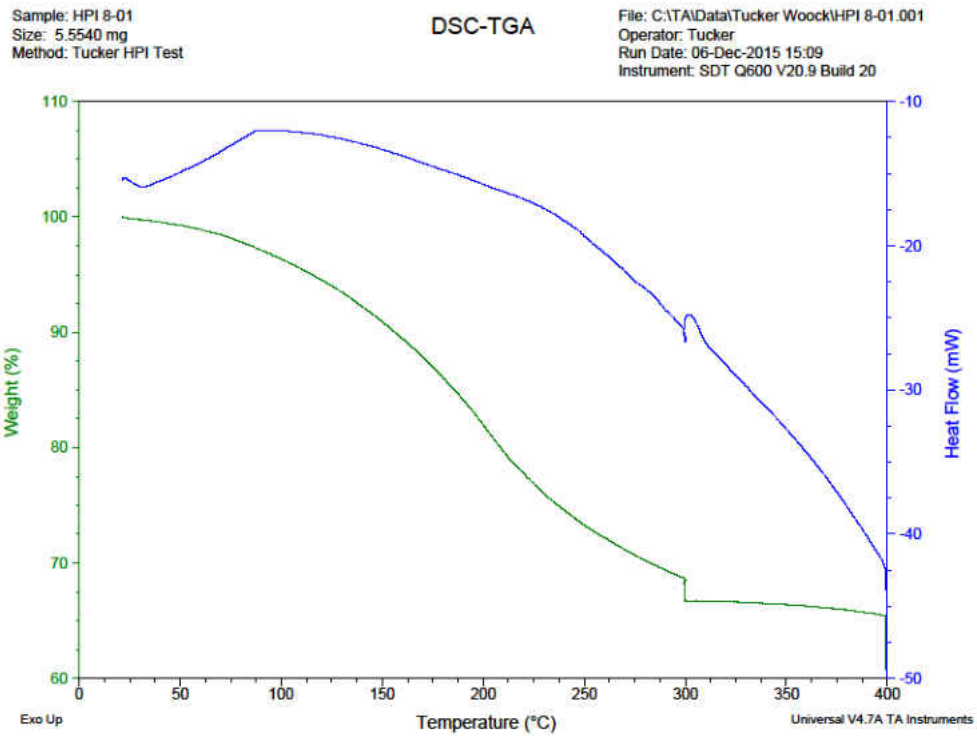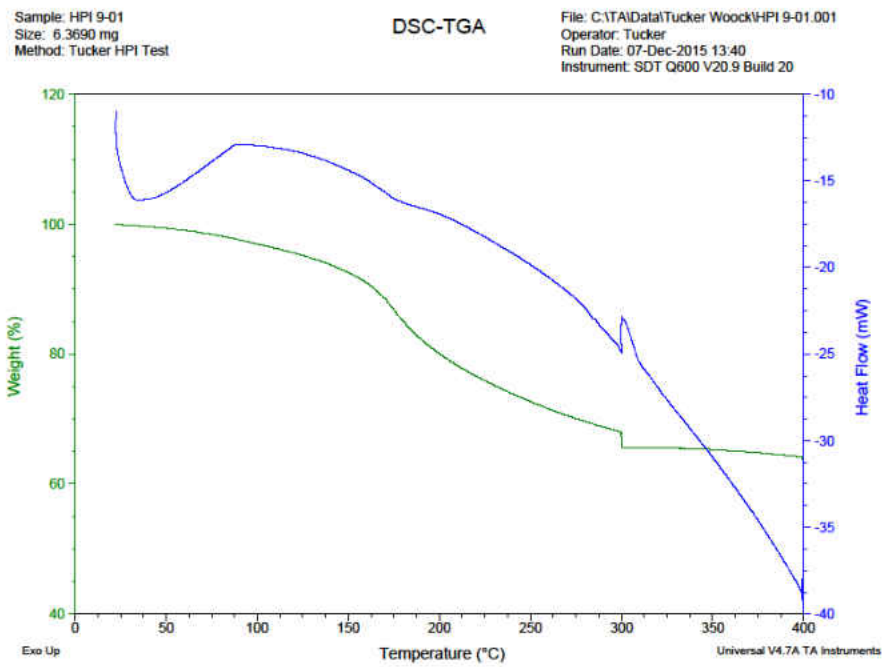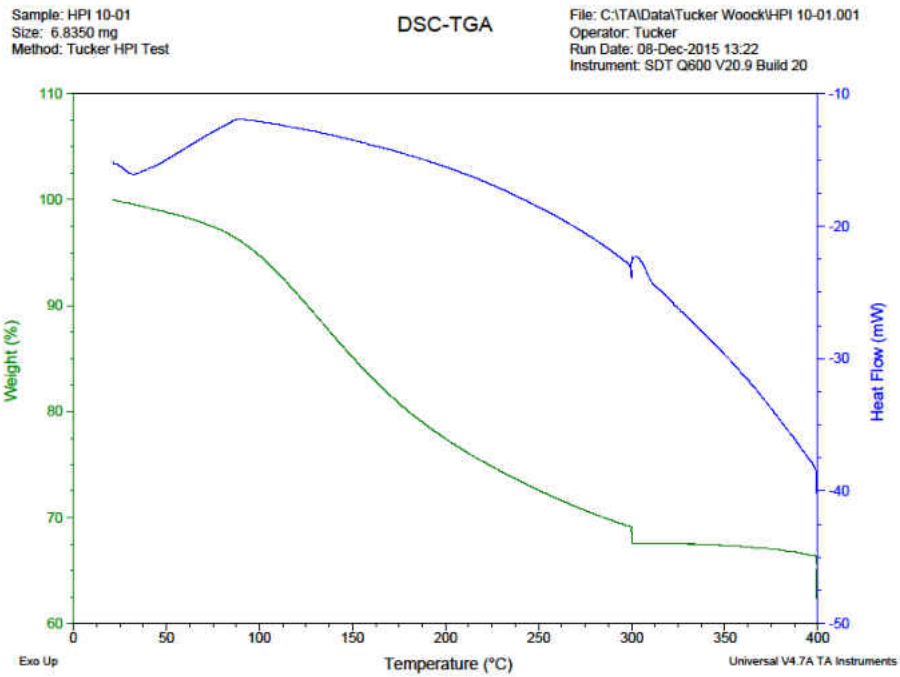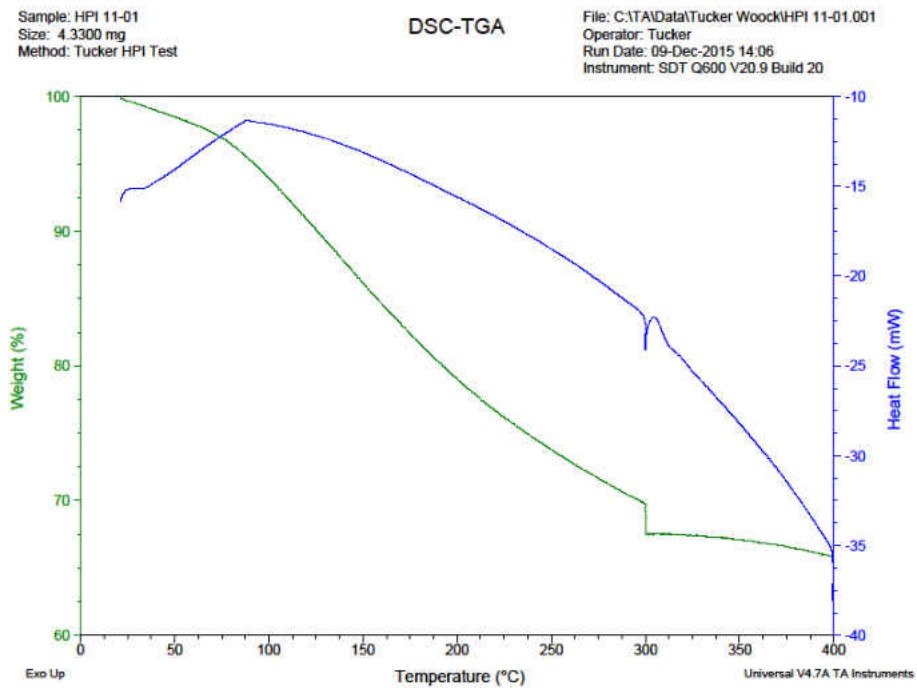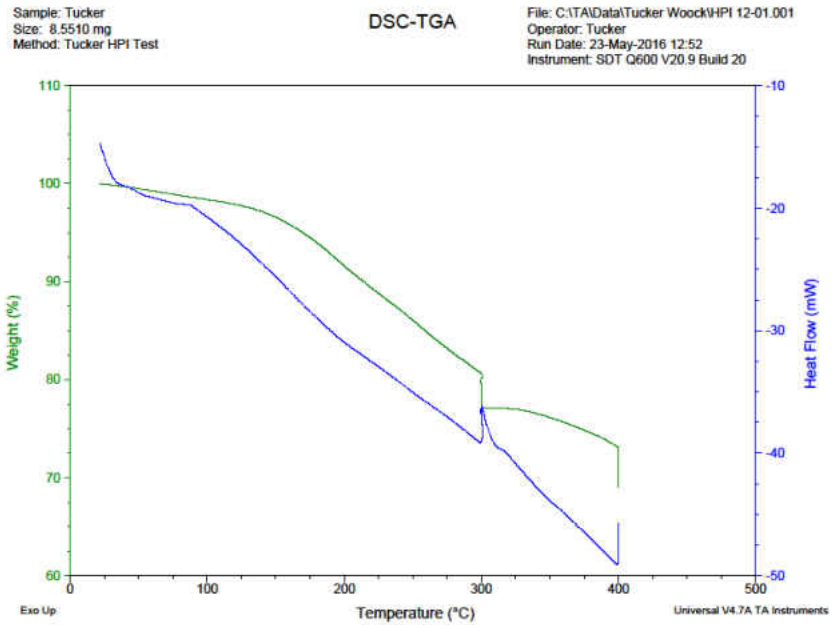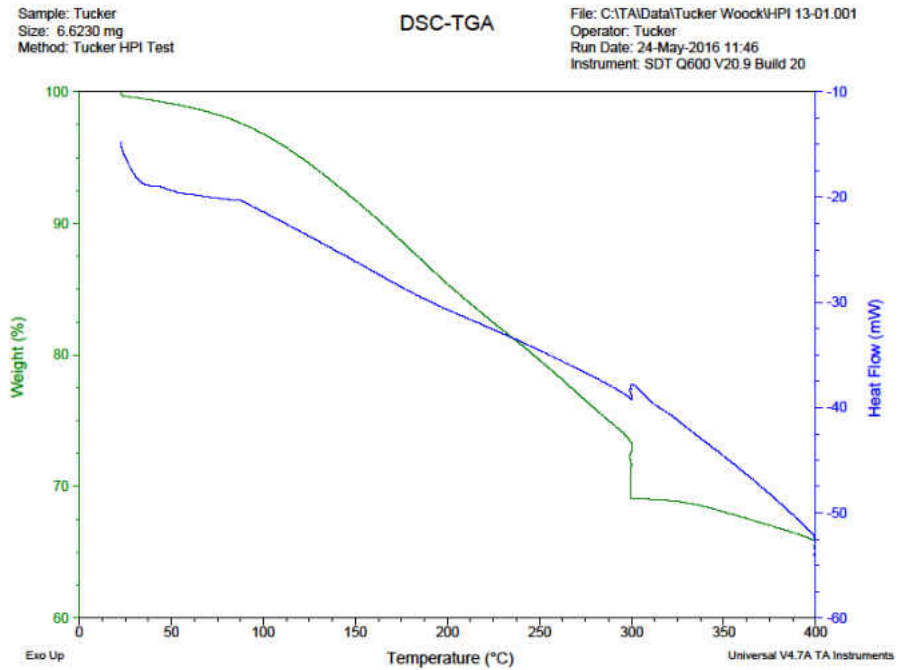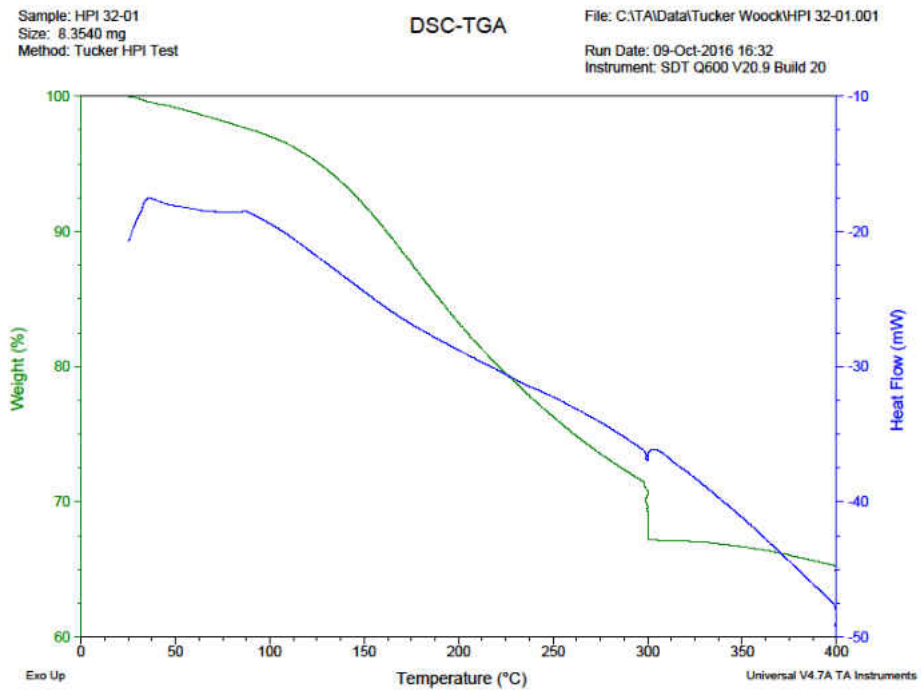

Figure 116: TGA data for sample 32

113
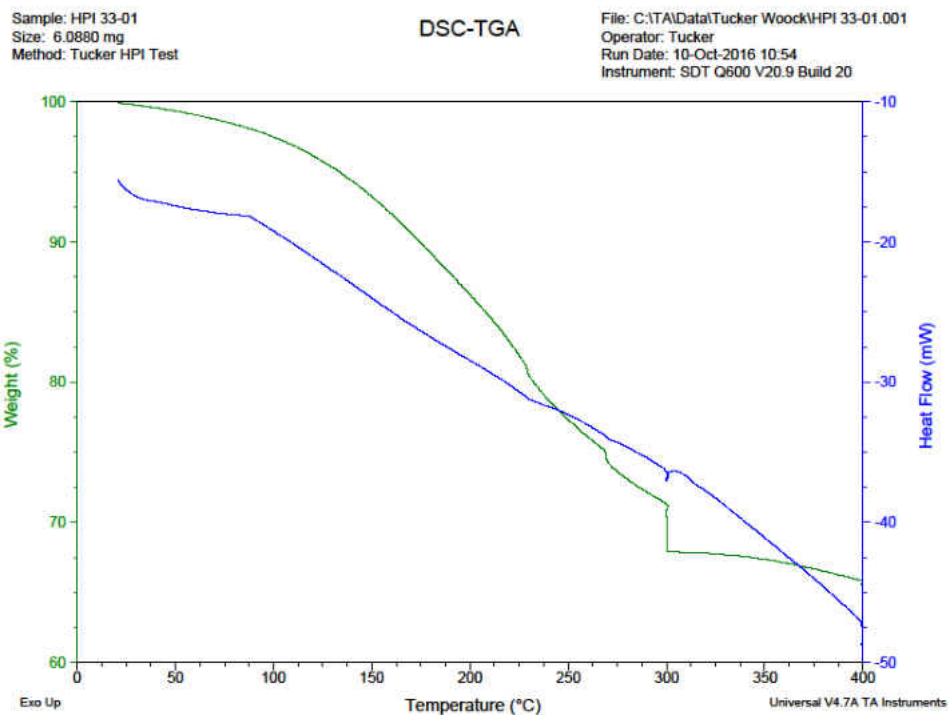
Figure 117: TGA data for sample 33
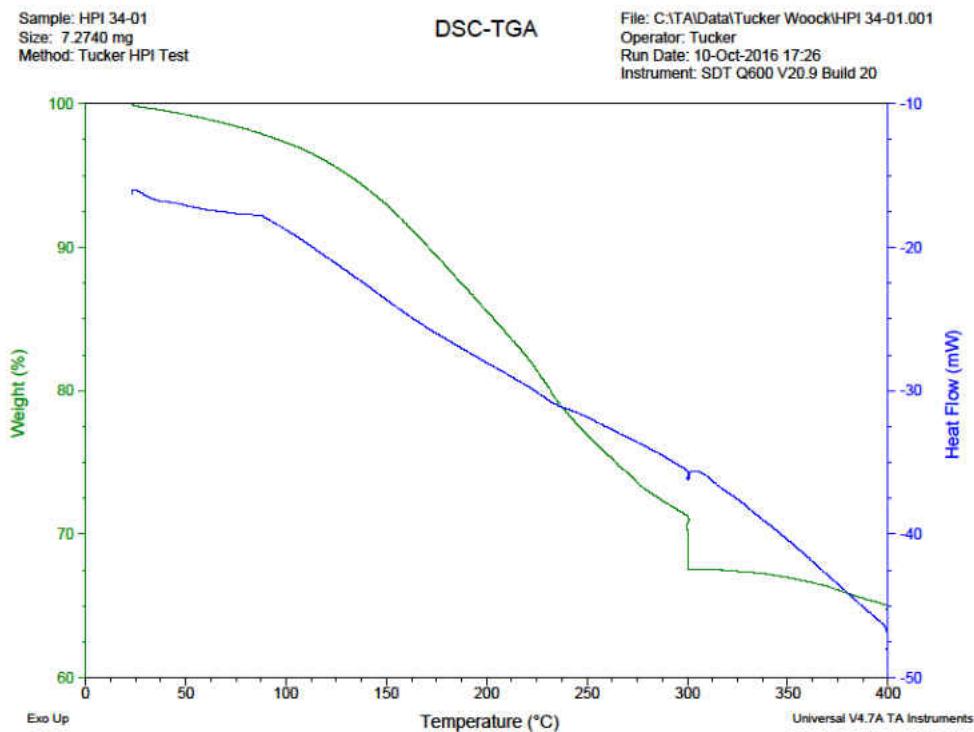
Figure 118: TGA data for sample 34

114
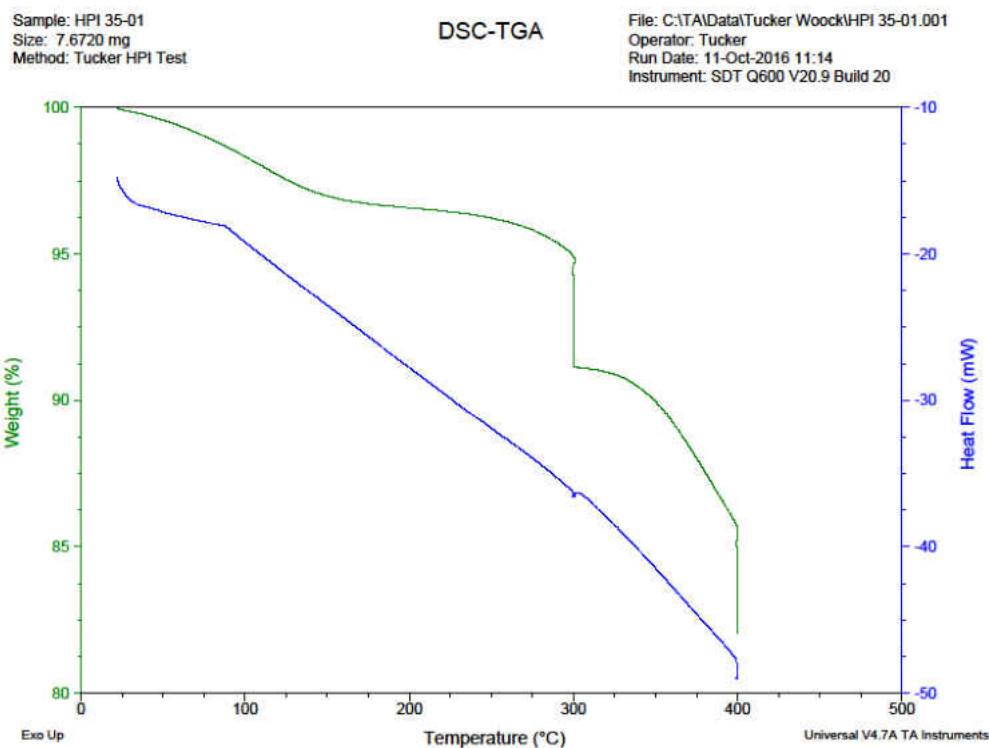
Figure 119: TGA data for sample 35

GPC Data

The GPC used consists of four components and two software packages. The four components are the autosampler, which is a Varian ProStar Model 400, the solvent delivery module, which is from Varian ProStar, the RI detector, which is a Varian ProStar 355, and the mobile phase column, which is also from Varian ProStar. The GPC experimental software is the Galaxie Chromatography Data System. The analysis software is GPC Offline from Cirrus.

Table 12 lists the experimental number average molecular weights (Mn), weight average molecular weights (Mw), and polydispersity index (PDI) for three HPI-ODPA samples, three HPI-BTDA samples, and three HPI-PMDA samples.

Table 12: Mn, Mw, and PDI for nine HPI samples

Sample	Mw (g/mol)	Mn (g/mol)	PDI
HPI-ODPA-01	57000	31000	1.8
HPI-ODPA-02	56000	32000	1.8
HPI-ODPA-03	52000	30000	1.7
HPI-BTDA-01	15000	8400	1.8
HPI-BTDA-02	16000	7200	2.2
HPI-BTDA-03	16000	7100	2.3
HPI-PMDA-01	14000	5900	2.4
HPI-PMDA-02	14000	5900	2.4
HPI-PMDA-03	15000	6000	2.5

CHAPTER VI

ADDITIONAL INFORMATION FOR CHAPTER IV

Thermal Rearrangement

The first thermal rearrangement attempt did not go well. One of the casts of HPI-ODPA was placed between two ceramic plates and placed in the oven. The oven was programmed to ramp at 5°C/min up to 300°C, where it was held for an hour, then to ramp at 5°C/min to 400°C, where it was held for two hours. The oven was set to cool back to room temperature at the end of the program. After the program ended and the oven cooled to room temperature the membrane and sandwiching plates were removed. The membrane was shattered and completely unusable. This was because the membrane was slightly ridged, and during thermal rearrangement the membrane's structural integrity weakened and the ceramic plates crushed the membrane. This was remedied by placing folded pieces of aluminum foil between the plates along with the membrane so the plates wouldn't crush the membrane all the way. Serendipitously, this actually helped the process because it allowed the weight of the plates to flatten some of the more ridged membranes, which made them more usable with the permeation test cell.

The majority of the thermal rearrangements performed after the first were successful. There were only a few that were broken due to the combination of the thermal rearrangement process making the membranes more brittle and human

error in mishandling them. Seven of each of HPI-ODPA, HPI-BTDA, and HPI-

PMDA were thermally rearranged, for a total of 21 polybenzoxazoles (PBOs).

Three PBO-ODPA membranes, three PBO-BTDA membranes, and three

PBO-PMDA membranes were subjected to FTIR to characterize them.

Permeation Testing

The first step of permeation testing was to find and purchase a permeation

test cell. A test cell was purchased from Pesce Labs, Inc. A diagram of a similar

test cell is shown in Figure 120. The left side of the test cell used in this project

looks like the right side of the one in the figure, so both sides match the right side

of the picture. A picture of the whole cell is shown in Figure 121, and a picture of

the open cell is shown in Figure 122.
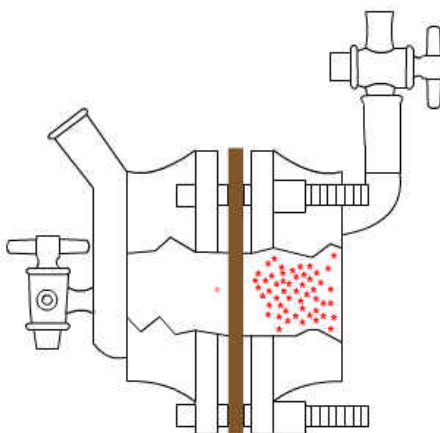
Figure 120: Diagram of similar test cell
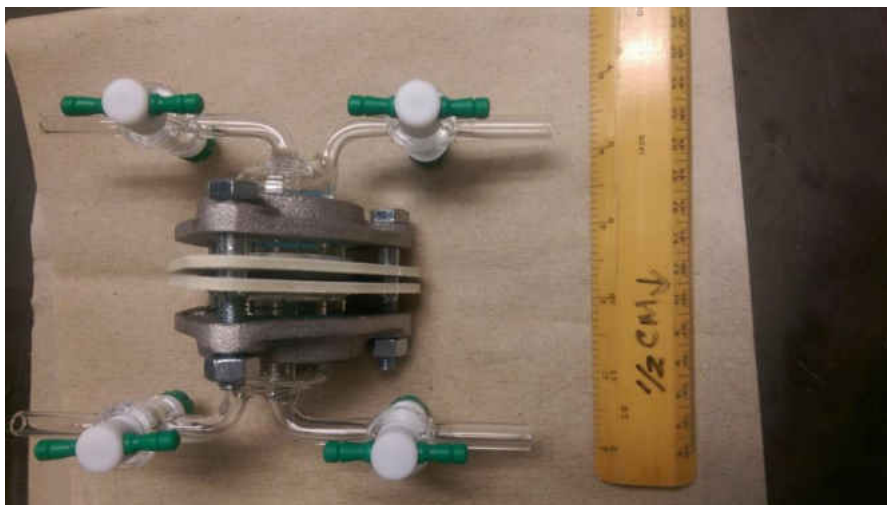
Figure 121: Top view of closed cell

Figure 122: Open cell

Each half of the cell consists of two inlet tubes with valves that connect

into a glass hemisphere. The hemisphere is held in place by an aluminum flange

with three bolt holes, and in the center of the flange, between the flange and the

outside edge of the hemisphere, is an insert that cushions the glass. In front of

the flange, connected with matching bolt holes, is a Teflon gasket. This gasket

has a hole in the middle to allow for gas to reach the membrane. The membrane

is held between the Teflon gaskets of each half of the cell, and the halves are

tightened together with bolts. This tightening creates seals between the glass hemispheres and the Teflon and between the Teflon and the membrane.

The second step in permeation testing was to create a manifold that would control the flow rates to the permeate and retentate sides of the membrane, measure the pressure of all of the streams, and allow collection of the permeate and retentate gases. Figures 123 and 124 show the front and back of the manifold and Figure 125 shows a diagram of the manifold and its connections.

Figure 123: Front of manifold
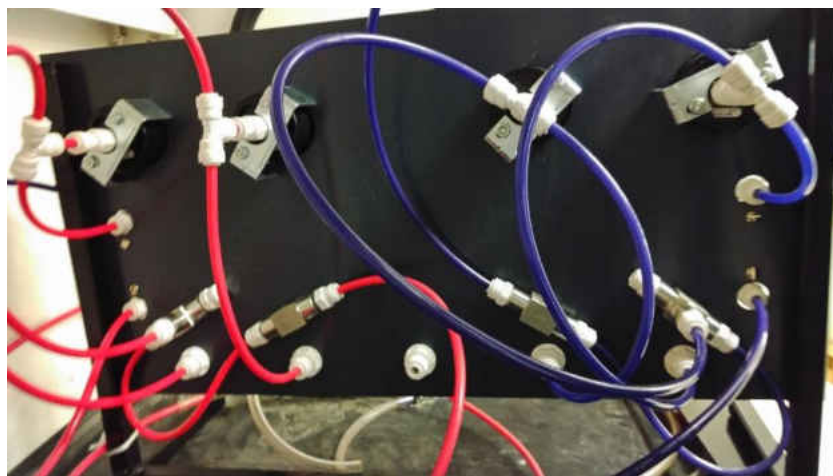
Figure 124: Back of manifold
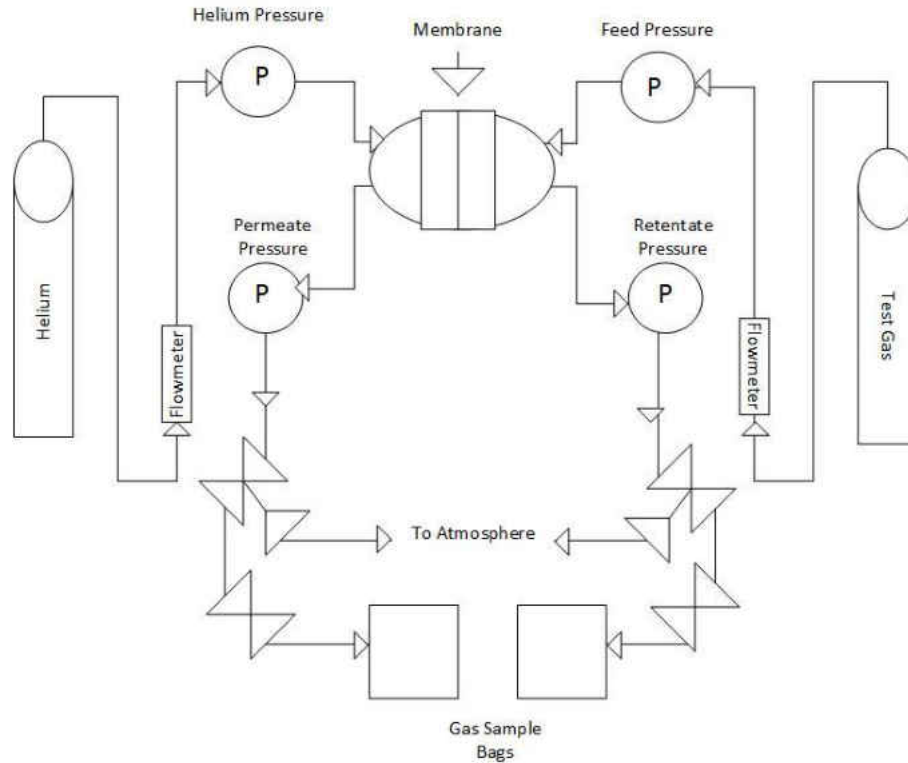
Figure 125: Manifold diagram

The test gas flows from its cylinder into a flowmeter, which begins the right half of the manifold. The gas then passes through a pressure gauge and into the membrane cell. The gas passes across the membrane in the cell, and the retentate travels through another pressure gauge. The gas the flows through two valves, the first of which is a three-way valve that can close the system, open it to the next valve, or vent it to the atmosphere. The second is a two-way valve that opens and closes the flow to the gas sample bags. The left side of the manifold mirrors the right, but controls the flow of the helium carrier gas and directs its flow across the opposite side of the membrane from the test gas.

At first the permeate and retentate gases were collected in mylar balloons, since they are a fraction of the price of gas sampling bags and do not allow

anything to permeate out of them. The first few runs and samples of the test gas

and carrier gas were collected in some of the balloons, but upon testing with the

gas chromatograph it was found that the gas in the balloons was mostly air. This

was because, while the balloons didn't allow any gas to permeate out of them,

there wasn't enough positive pressure within the balloons to prevent air from

entering them. Also, the samples in the balloons had sat for an extended period

of time. After it was discovered that the balloons would not work for the purposes

of this project, aluminum gas sampling bags were purchased.

Another problem that was encountered was that when the flowmeters on

the manifold, which had a scale of 0.05 to 0.4 SCFH, were used to control the

flow of gases, there wasn't enough pressure difference to get readings from the

pressure gauges. This would not work, since the pressure readings were

necessary to calculate the permeability of the membranes. The regulators on the

gas cylinders were used instead to control the flow rates, while the flowmeters

were simply opened all the way to completely allow flow through them. The

regulator on the helium cylinder had a scale for reading the helium flow rate in

SCFH, so the values from that regulator were used as stated. The regulator on

the test gas cylinder, however, did not have a scale for the test gas. The reading

for the scale for the flow rate of Argon was recorded and later converted via a

conversion factor, which is discussed later in this section.

Another issue, which was discussed in Chapter III of this thesis, that

occurred during permeation testing was that the membranes formed using the

dianhydride PMDA developed ridges that caused them to be incompatible with

the permeation test cell. This meant that there were no permeation results for HPI-PMDA or PBO-PMDA membranes.

Results

Thermal Rearrangement

The thermally rearranged membranes look exactly like the original HPI membranes, only black. Therefore no pictures were taken.

FTIR Data

Figures 126 through 134 show the FTIR spectra for the nine PBOs that were subjected to FTIR.
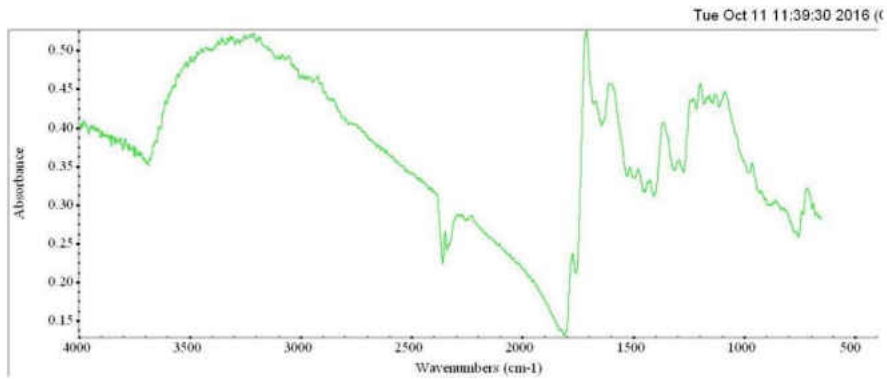
Figure 126: FTIR data for PBO-BTDA-01
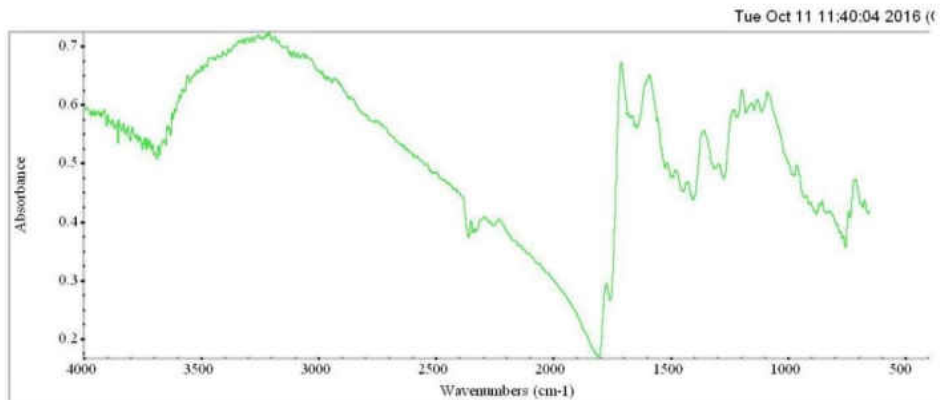
Figure 127: FTIR data for PBO-BTDA-02
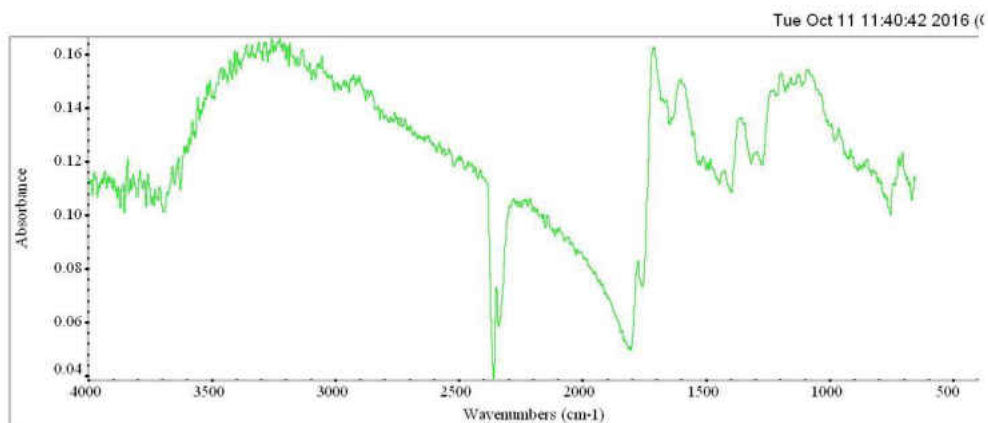
Figure 128: FTIR data for PBO-BTDA-03
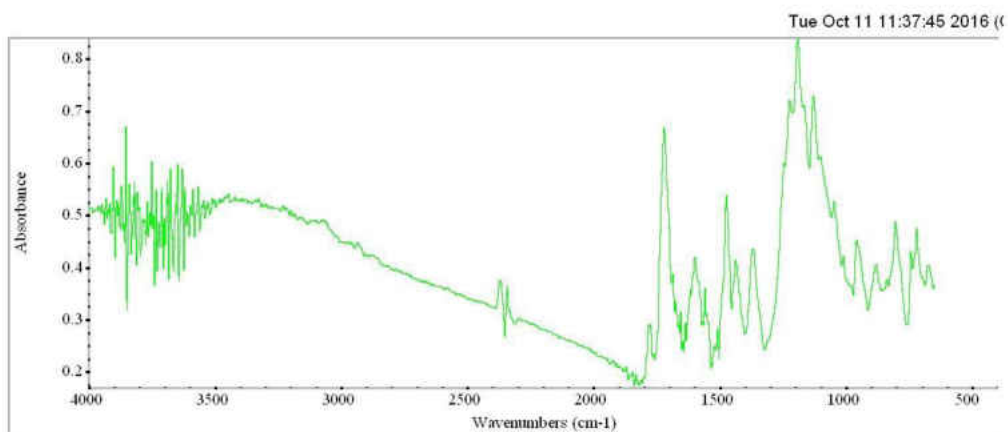
Figure 129: FTIR data for PBO-ODPA-01
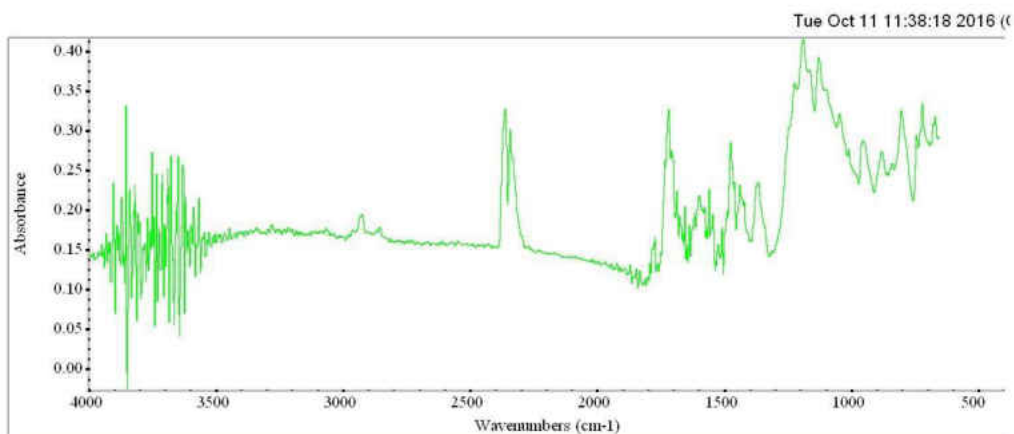
Figure 130: FTIR data for PBO-ODPA-02
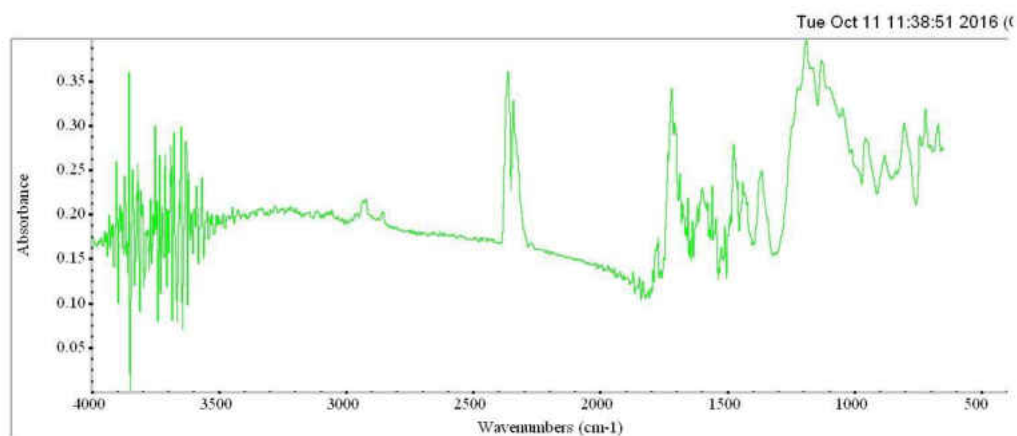
Figure 131: FTIR data for PBO-ODPA-03
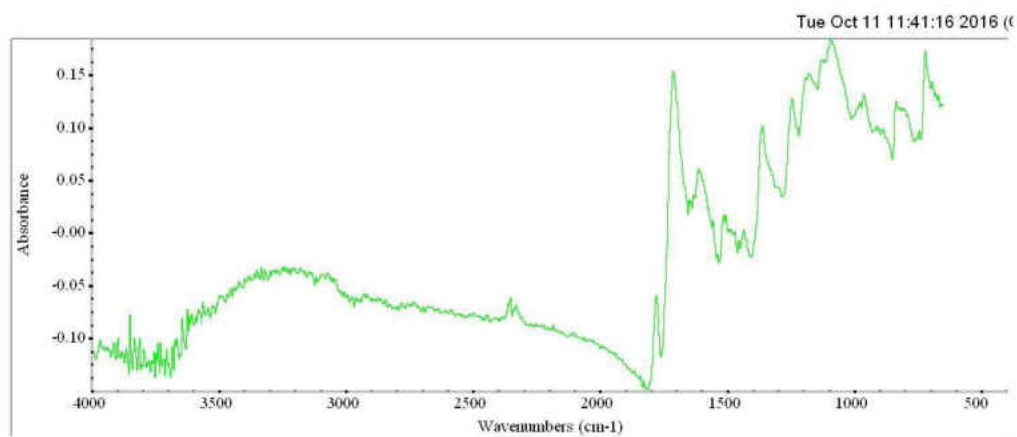
Figure 132: FTIR data for PBO-PMDA-01
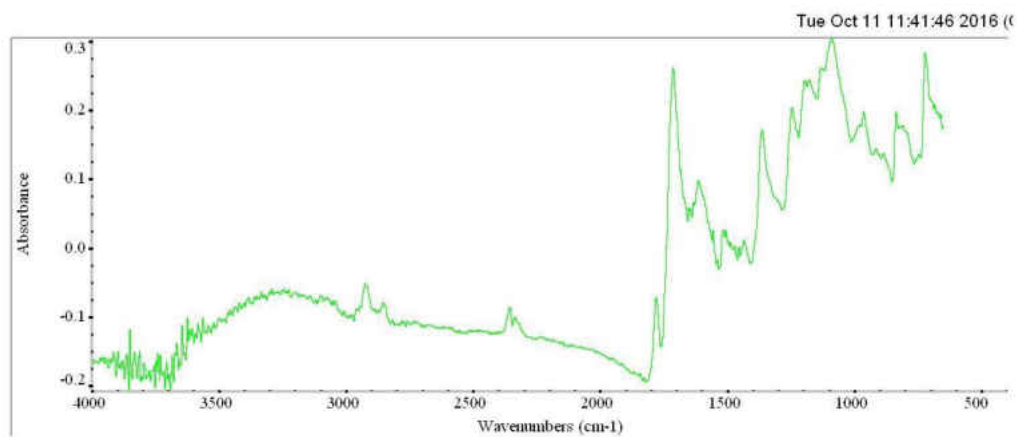
Figure 133: FTIR data for PBO-PMDA-02
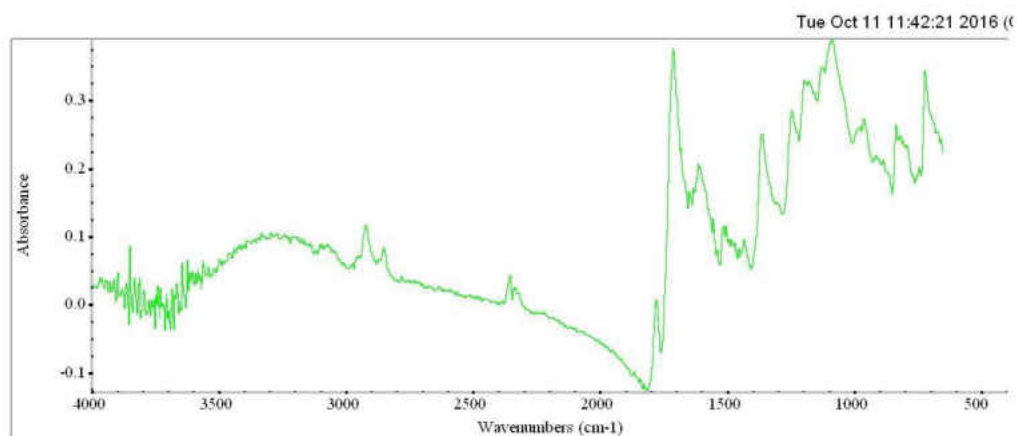
Figure 134: FTIR data for PBO-PMDA-03

Experimental Data

Table 13 shows the data that was recorded for each run. This includes the type of membrane, the thickness of the membrane, the flow rates for the test gas and the carrier gas and their feed pressures, and the retentate and permeate pressures.

Table 13: Experimental data

Run	Membrane	Thickness (cm)	Test Gas Feed (ft^3/h)	Test Gas Pressure (psig)	Retentate Pressure (psig)	Carrier Gas Feed (ft^3/h)	Carrier Pressure (psig)	Permeate Pressure (psig)
1	Kapton	0.00254	5	1.7	1.9	20	3.3	3.3
2	Kapton	0.00254	10	2.3	1.2	30	5	5.2
3	Kapton	0.00254	15	5.6	3.6	40	5.1	5.2
4	Kapton	0.00254	5	0.5	0.7	20	2.1	2.2
5	Kapton	0.00254	5	0.5	0.7	30	4	4
6	Kapton	0.00254	5	0.5	0.7	40	3.2	2.9
7	HPI-BTDA	0.03700	5	0.2	0.6	20	2.6	2.9
8	HPI-BTDA	0.03700	5	0.2	0.6	30	5.1	5.4
9	HPI-BTDA	0.03700	5	0.2	0.6	40	5.5	5.8
10	HPI-ODPA	0.02700	15	3.1	2.7	20	4.6	5
11	HPI-ODPA	0.02700	25	6.2	4.7	30	5.5	6
12	PBO-BTDA	0.03600	15	3.2	2.9	20	4.3	4.6
13	PBO-BTDA	0.03600	25	5.2	4	30	3.5	3.7
14	PBO-ODPA	0.02000	15	2.9	2.4	20	4.6	5
15	PBO-ODPA	0.02000	25	5.5	4.4	30	5.3	5.8

Gas Chromatograph Data

The gas chromatograph used was an Agilent Technologies 7890A Refinery Gas Analyzer Gas Chromatograph. It utilizes a manually fed gas sampling loop and an air-actuated solenoid valve configuration. It contains 9 columns, two capillary columns and seven packed columns, and the sample is split and routed through all the columns at different temperatures utilizing the solenoid valve configuration. It has two TCD detectors and one FID detector. The GC is calibrated for the following compounds: helium, hydrogen, carbon dioxide, propane, propylene, acetylene, iso-butane, carbonyl sulfide, n-butane, hydrogen sulfide, 1-butene, iso-butylene, t-2-butene, iso-pentane, c-2-butene, n-pentane, 1,3-butadiene, ethylene, ethane, oxygen, argon, nitrogen, methane, and carbon monoxide.

Table 14 shows the GC data that was obtained for each run. This includes the molar concentrations of nitrogen, methane, and oxygen in the retentate samples, and the molar concentrations of nitrogen, methane, helium, and oxygen in the permeate samples.

Table 14: GC data

Run	Retentate			Permeate			
	mol% N_2	mol% CH_4	mol% O_2	mol% N_2	mol% CH_4	mol% He	mol% O_2
Test Gas	79.8767	19.5067	0.5772	-	-	-	-
Helium	-	-	-	5.6132	0	92.851	1.5357
1	79.848	19.6363	0.5157	2.9594	0	96.1285	0.9121
2	79.8519	19.8829	0.2652	5.6489	0	92.7051	1.646
3	79.8622	19.6623	0.4755	2.5652	0	96.6372	0.7977
4	80.073	19.66	0.267	1.115	0	98.498	0.387
5	80.0313	19.9687	0	1.3895	0	98.1519	0.4587
6	79.8071	19.851	0.342	3.5444	0.0029336	96.4526	0
7	79.9972	20.0283	0	1.2737	0	98.2965	0.4398
8	79.9471	19.8545	0.1984	0.8034	0	98.8932	0.3003
9	79.844	20.0038	0.1521	1.0813	0	98.5372	0.3815
10	79.8957	19.8928	0.2114	0	0	100	0
11	79.7688	20.0346	0.1966	1.0127	0	98.6373	0.35
12	79.7763	20.0572	0.1665	1.9019	0	97.4753	0.6228
13	79.7334	20.2191	0.0475	1.9171	0	97.5326	0.5503
14	79.886	19.2228	0.8912	1.1999	0	98.3925	0.4076
15	79.8076	19.5498	0.6427	1.9868	0	97.3866	0.6266

Permeability Calculations

The flow rates for the gases were measured with the regulators on the respective gas cylinders. The regulator for the helium cylinder directly measured the helium flow, so the value for the helium flow rate was used directly. The regulator for the test gas cylinder did not read the flow of the test gas directly, so the flow measurement for Argon was used and later converted into flow of the test gas. This was done using the following equation[61]:

$$Q_2 = Q_1 * \sqrt{SG_1/SG_2}$$

Where Q_2 is the converted flow rate of test gas, Q_1 is the observed flow rate of Argon, SG_1 is the specific gravity of Argon (1.379), and SG_2 is the specific gravity of the test gas. The specific gravity of the test gas was found using the following equation:

$$SG_2 = x_{methane} * SG_{methane} + x_{nitrogen} * SG_{nitrogen}$$

Therefore,

$$SG_2 = 0.201 * 0.5537 + 0.799 * 0.9669 = 0.8838$$

Plugging this into the flow rate conversion equation gives:

$$Q_2 = Q_1 * \sqrt{\frac{1.379}{0.8838}} = 1.249 Q_1$$

The following equation, from He *et al.*[62], was used for permeability:

$$P_i = \frac{l * x_{perm\,i} * 273\,K * p_{atm}}{A * \left(x_{feed\,i} * p_{feed} - x_{perm\,i} * p_{perm}\right) * T * 76\,cmHg} * \frac{dV}{dt}$$

Where P_i is the permeability of species i in $(cm^3(STP) * cm)/(cm^2 * s * cmHg)$, l is the thickness of the membrane in cm, $x_{perm\,l}$ is the molar

130

concentration of species i in the permeate gas, p_{atm} is the atmospheric pressure in cmHg, A is the surface area of the membrane in cm^2, $x_{feed\ i}$ is the molar concentration of species i in the feed gas, p_{feed} is the pressure of the feed gas in cmHg, p_{perm} is the pressure of the permeate gas in cmHg, T is the temperature of the system in K, and dV/dt is the flow rate of the feed gas in cm^3/s. Since the hole in the middle of the test cell dictated the exposed surface area of the membrane, it was a constant A = 0.9 in^2 = 4.1043 cm^2. The temperature T and atmospheric pressure p_{atm} were assumed to be constant, with T = 298 K and p_{atm} = 76 cmHg.

Table 15 shows the applicable variables from the experimental data and GC data to be used in the permeability equation, and the calculated permeabilities for each run. The values from the experimental data and GC data tables have been converted to fit the units used in the permeability equation.

Table 15: Converted experimental and GC data for use in the permeability equation and calculated permeabilities

Run	Thickness (cm)	X_{perm} CH$_4$	X_{perm} N$_2$	X_{feed} CH$_4$	Xfeed N$_2$	P_{feed} (cmHg)g	P_{perm} (cmHg)g	Feed flow (cm^3/s)	P_{CH4} (barrer)	P_{N2} (barrer)
1	0.00254	0	0.02959	0.195067	0.798767	-1.0357	0.0000	49.16125	0.00	-9970377.21
2	0.00254	0	0.05649	0.195067	0.798767	5.6964	1.0357	98.3225	0.00	7010670.93
3	0.00254	0	0.02565	0.195067	0.798767	10.3570	0.5179	147.48375	0.00	2596858.73
4	0.00254	0	0.01115	0.195067	0.798767	-1.0357	0.5179	49.16125	0.00	-3730458.00
5	0.00254	0	0.0139	0.195067	0.798767	-1.0357	0.0000	49.16125	0.00	-4681299.97
6	0.00254	2.934E-05	0.03544	0.195067	0.798767	-1.0357	-1.5536	49.16125	-40480.24	-12792760.82
7	0.037	0	0.01274	0.195067	0.798767	-2.0714	1.5536	49.16125	0.00	-30885170.59
8	0.037	0	0.00803	0.195067	0.798767	-2.0714	1.5536	49.16125	0.00	-19566536.29
9	0.037	0	0.01081	0.195067	0.798767	-2.0714	1.5536	49.16125	0.00	-26266671.78
10	0.027	0	0	0.195067	0.798767	2.0714	2.0714	147.48375	0.00	0.00
11	0.027	0	0.01013	0.195067	0.798767	7.7678	2.5893	245.80625	0.00	24281011.69
12	0.036	0	0.01902	0.195067	0.798767	1.5536	1.5536	147.48375	0.00	186063087.29
13	0.036	0	0.01917	0.195067	0.798767	6.2142	1.0357	245.80625	0.00	0.00
14	0.02	0	0.012	0.195067	0.798767	2.5893	2.0714	147.48375	0.00	38661727.53
15	0.02	0	0.01987	0.195067	0.798767	5.6964	2.5893	245.80625	0.00	48462274.54

Table 16 shows the calculated permeabilities and N_2/CH_4 selectivities for each run. The N_2/CH_4 selectivity ($\alpha_{N2/CH4}$) was found using the following equation:

$$\propto_{N_2/CH_4} = \frac{P_{N_2}}{P_{CH_4}}$$

Table 16: Permeabilities and selectivities for each run

Run	Membrane	P_{CH4} (barrer)	P_{N2} (barrer)	N_2/CH_4 selectivity
1	Kapton	0.00	-9970377.21	-
2	Kapton	0.00	7010670.93	-
3	Kapton	0.00	2596858.73	-
4	Kapton	0.00	-3730458.00	-
5	Kapton	0.00	-4681299.97	-
6	Kapton	-40480.24	-12792760.82	316.02
7	HPI-BTDA	0.00	-30885170.59	-
8	HPI-BTDA	0.00	-19566536.29	-
9	HPI-BTDA	0.00	-26266671.78	-
10	HPI-ODPA	0.00	0.00	-
11	HPI-ODPA	0.00	24281011.69	-
12	PBO-BTDA	0.00	186063087.29	-
13	PBO-BTDA	0.00	0.00	-
14	PBO-ODPA	0.00	38661727.53	-
15	PBO-ODPA	0.00	48462274.54	-

CHAPTER VII

CONCLUSION AND FUTURE STUDIES

Conclusion

The intent of this thesis was to determine the effects of the dianhydride used to create hydroxyl-polyimide (HPI) membranes, which were then thermally rearranged into polybenzoxazole (PBO) membranes, on the permeabilities and selectivities of those membranes. The dianhydrides compared in this project were 4,4'-oxydiphthalic anhydride (ODPA), 3,3',4,4'-benzophenone tetracarboxylic dianhydride (BTDA), 3,3',4,4'-biphenyl tetracarboxylic dianhydride (BPDA), and Benzene-1,2,4,5-tetracarboxylic dianhydride (PMDA). The dianhydrides were all combined with the diamine 2,2'-bis(3-amino-4-hydroxyphenyl) hexafluoropropane (bisAPAF) to create HPIs using the same synthesis procedure. The structures of these precursors are shown in Table 17 below. The membranes were all cast in the same manner as well.

Table 17: HPI precursors used in this project
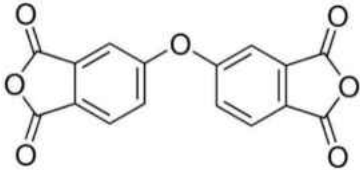
Precursor	Structure
ODPA	

Table 17 cont.

BTDA	
BPDA	
PMDA	
bisAPAF	
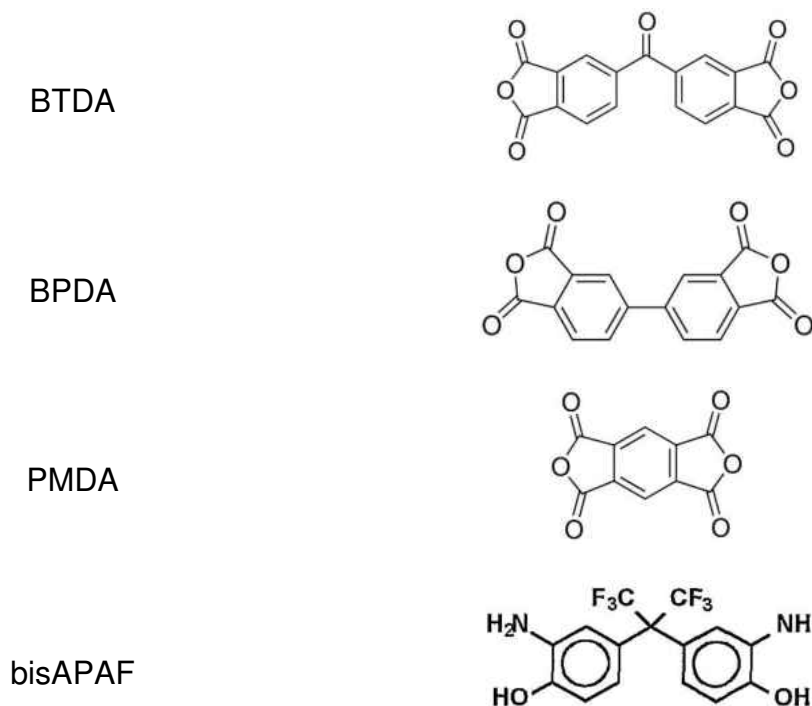
The FTIR and TGA results show that HPIs were successfully synthesized, and should have undergone thermal rearrangement into PBOs. In practice, this was not the outcome. The HPIs, while somewhat thermally rearranging, did not completely thermally rearrange. The reasons for this were discussed in Chapter IV of this thesis.

The permeation testing was almost completely unsuccessful, the reasons for which are also discussed in Chapter IV. Since adequate permeation data was not obtained, the goal of comparing the separation properties of the PBOs made with the candidate dianhydrides was not able to be evaluated.

Future Studies

Future studies that could further the goal of this project include fixes to the project procedure itself, as well as studies that move past the goal of this project. Fixing this project would include using a different oven that can operate under an inert atmosphere or a vacuum. This would create higher degrees of conversion of the HPIs to PBOs. Another thing that would help is to make thinner membranes, whether it's by use of a doctor blade to shear the thickness of the membrane down or by a spinner to increase the surface area of the casting solution, and therefore reducing the thickness of the membrane. A GC more appropriately suited to analyzing the composition of the permeate samples would provide better data for calculating permeabilities. The manifold probably wasn't the biggest problem, but a manifold more resistant to leaks would still help.

Some ideas to further the work of this project, and the research on PBO separation in general, are to compare different combinations of diamines and dianhydrides that have not been tested before.

Another interesting direction that could be taken is to investigate cross-linked PBOs, as begun by Calle *et al*. They tested PBOs that contained small moieties of 3,5-diaminobenzoic acid (DABA) instead of the diamine, and then added 1,4-butylene glycol to connect the DABAs within the polymer chains[39]. Changes to their procedure could include using different cross-linking agents, such as 1,5-pentylene glycol or 1,3-propylene glycol, to see what effect the length of the cross-linking agent has on the separation properties. Another investigation could compare the effect of the target of the cross-linking agent, by

changing DABA to another diamine acid, such as 4,4'-diaminobiphenyl-3,3'-dicarboxylic acid.

REFERENCES

1. Xiao Y, Low BT, Hosseini SS, Chung TS, Paul DR. The strategies of molecular architecture and modification of polyimide-based membranes for CO_2 removal from natural gas—a review. *Progress in Polymer Science*. 2009;34(6):561-580.

2. Woock T, Bjorgaard S, Tande B, Alshami A. Purification of natural gas using thermally rearranged polybenzoxazole and polyimide membranes–a review: Part 1. *Membrane Technology*. 2016;2016(9):7-12.

3. Woock T, Bjorgaard S, Tande B, Alshami A. Purification of natural gas using thermally rearranged polybenzoxazole and polyimide membranes–a review: Part 2. *Membrane Technology*. 2016;2016(10):7-12.

4. U.S. natural gas monthly supply and disposition balance. http://www.eia.gov/dnav/ng/ng_sum_sndm_s1_m.htm. Accessed December 29, 2015.

5. Nitrogen removal from natural gas. http://www.mtrinc.com/nitrogen_removal.html. Accessed December 29, 2015.

6. Sanders DF, Smith ZP, Guo R, et al. Energy-efficient polymeric gas separation membranes for a sustainable future: A review. *Polymer*. 2013;54(18):4729-4761.

7. Paul DR, Yampol'skii YP. *Polymeric gas separation membranes.* CRC press; 1993.

8. Ho WW, Sirkar K. Membrane handbook, 1992. *WNR, New York*. 1992.

9. Park HB, Jung CH, Lee YM, et al. Polymers with cavities tuned for fast selective transport of small molecules and ions. *Science*. 2007;318(5848):254-258. doi: 318/5848/254 [pii].

10. Böddeker KW. *The early history of membrane science: Selected papers celebrating vol. 100: Special issue.* Elsevier; 1995.

11. Wijmans J, Baker R. The solution-diffusion model: A review. *J Membr Sci*. 1995;107(1):1-21.

12. Lokhandwala KA, Pinnau I, He Z, et al. Membrane separation of nitrogen from natural gas: A case study from membrane synthesis to commercial deployment. *J Membr Sci*. 2010;346(2):270-279.

13. Nagel C, Günther-Schade K, Fritsch D, Strunskus T, Faupel F. Free volume and transport properties in highly selective polymer membranes. *Macromolecules*. 2002;35(6):2071-2077.

14. Freeman BD. Basis of permeability/selectivity tradeoff relations in polymeric gas separation membranes. *Macromolecules*. 1999;32(2):375-380.

15. Robeson LM. The upper bound revisited. *J Membr Sci*. 2008;320(1):390-400.

16. Alfrey T, Goldfinger G, Mark H. The apparent second-order transition point of polystyrene. *J Appl Phys*. 1943;14(12):700-705.

17. Curro JG, Lagasse RR, Simha R. Diffusion model for volume recovery in glasses. *Macromolecules*. 1982;15(6):1621-1626.

18. Kim J, Koros W, Paul D. Physical aging of thin 6FDA-based polyimide membranes containing carboxyl acid groups. part I. transport properties. *Polymer*. 2006;47(9):3094-3103.

19. Wang H, Chung T, Paul DR. Physical aging and plasticization of thick and thin films of the thermally rearranged ortho-functional polyimide 6FDA–HAB. *J Membr Sci*. 2014;458:27-35.

20. Wessling M, Schoeman S, Van der Boomgaard T, Smolders C. Plasticization of gas separation membranes. *Gas separation & purification*. 1991;5(4):222-228.

21. Tanaka K, Taguchi A, Hao J, Kita H, Okamoto K. Permeation and separation properties of polyimide membranes to olefins and paraffins. *J Membr Sci*. 1996;121(2):197-207.

22. Tanaka K, Osada Y, Kita H, Okamoto K. Gas permeability and permselectivity of polyimides with large aromatic rings. *Journal of Polymer Science Part B: Polymer Physics*. 1995;33(13):1907-1915.

23. Tanaka K, Kita H, Okano M, Okamoto K. Permeability and permselectivity of gases in fluorinated and non-fluorinated polyimides. *Polymer*. 1992;33(3):585-592.

24. Kawakami H, Anzai J, Nagaoka S. Gas transport properties of soluble aromatic polyimides with sulfone diamine moieties. *J Appl Polym Sci*. 1995;57(7):789-795.

25. Coleman M, Koros W. Isomeric polyimides based on fluorinated dianhydrides and diamines for gas separation applications. *J Membr Sci*. 1990;50(3):285-297.

26. Xu Z, Böhning M, Schultze J, et al. Gas transport properties of poly (phenylene thioether imide) s. *Polymer*. 1997;38(7):1573-1580.

27. Fuhrman C, Nutt M, Vichtovonga K, Coleman M. Effect of thermal hysteresis on the gas permeation properties of 6FDA-based polyimides. *J Appl Polym Sci*. 2004;91(2):1174-1182.

28. Kita H, Inada T, Tanaka K, Okamoto K. Effect of photocrosslinking on permeability and permselectivity of gases through benzophenone-containing polyimide. *J Membr Sci*. 1994;87(1-2):139-147.

29. Won J, Kim MH, Kang YS, et al. Surface modification of polyimide and polysulfone membranes by ion beam for gas separation. *J Appl Polym Sci*. 2000;75(12):1554-1560.

30. Chung T, Ren J, Wang R, et al. Development of asymmetric 6FDA-2, 6DAT hollow fiber membranes for CO_2/CH_4 separation: Part 2. suppression of plasticization. *J Membr Sci*. 2003;214(1):57-69.

31. Takeichi T, Ogura S, Takayama Y. Soluble polyimides that contain curable internal acetylene groups in the backbone. *Journal of Polymer Science Part A: Polymer Chemistry*. 1994;32(3):579-585.

32. Rezac ME, Sorensen ET, Beckham HW. Transport properties of crosslinkable polyimide blends. *J Membr Sci*. 1997;136(1):249-259.

33. Hayes RA. *Amine-modified polyimide membranes*. 1991.

34. Summary of properties for kapton polyimide. http://www.dupont.com/content/dam/dupont/products-and-services/membranes-and-films/polyimde-films/documents/DEC-Kapton-summary-of-properties.pdf. Accessed October 14, 2016.

35. Cecopieri-Gómez ML, Palacios-Alquisira J, Dominguez J. On the limits of gas separation in CO_2/CH_4, N_2/CH_4 and CO_2/N_2 binary mixtures using polyimide membranes. *J Membr Sci*. 2007;293(1):53-65.

36. Smith ZP, Hernández G, Gleason KL, et al. Effect of polymer structure on gas transport properties of selected aromatic polyimides, polyamides and TR polymers. *J Membr Sci.* 2015;493:766-781.

37. Kim S, Lee YM. Rigid and microporous polymers for gas separation membranes. *Progress in Polymer Science.* 2015;43:1-32.

38. Bara JE, Gin DL, Noble RD. Effect of anion on gas separation performance of polymer− room-temperature ionic liquid composite membranes. *Ind Eng Chem Res.* 2008;47(24):9919-9924.

39. Calle M, Doherty CM, Hill AJ, Lee YM. Cross-linked thermally rearranged poly (benzoxazole-co-imide) membranes for gas separation. *Macromolecules.* 2013;46(20):8179-8189.

40. Han SH, Misdan N, Kim S, Doherty CM, Hill AJ, Lee YM. Thermally rearranged (TR) polybenzoxazole: Effects of diverse imidization routes on physical properties and gas transport behaviors. *Macromolecules.* 2010;43(18):7657-7667.

41. Calle M, Lozano AE, Lee YM. Formation of thermally rearranged (TR) polybenzoxazoles: Effect of synthesis routes and polymer form. *European Polymer Journal.* 2012;48(7):1313-1322.

42. Calle M, Chan Y, Jo HJ, Lee YM. The relationship between the chemical structure and thermal conversion temperatures of thermally rearranged (TR) polymers. *Polymer.* 2012;53(13):2783-2791.

43. Soo CY, Jo HJ, Lee YM, Quay JR, Murphy MK. Effect of the chemical structure of various diamines on the gas separation of thermally rearranged poly (benzoxazole-co-imide)(TR-PBO-co-I) membranes. *J Membr Sci.* 2013;444:365-377.

44. Kim S, Han SH, Lee YM. Thermally rearranged (TR) polybenzoxazole hollow fiber membranes for CO_2 capture. *J Membr Sci.* 2012;403:169-178.

45. Merkel TC, Pinnau I, Prabhakar R, Freeman BD. *Gas and vapor transport properties of perfluoropolymers.* John Wiley & Sons: Chichester, England; 2006.

46. García JM, García FC, Serna F, José L. High-performance aromatic polyamides. *Progress in polymer science.* 2010;35(5):623-686.

47. Alentiev AY, Shantarovich V, Merkel T, Bondar V, Freeman B, Yampolskii YP. Gas and vapor sorption, permeation, and diffusion in glassy amorphous teflon AF1600. *Macromolecules.* 2002;35(25):9513-9522.

48. Merkel T, Bondar V, Nagai K, Freeman B, Yampolskii YP. Gas sorption, diffusion, and permeation in poly (2, 2-bis (trifluoromethyl)-4, 5-difluoro-1, 3-dioxole-co-tetrafluoroethylene). *Macromolecules*. 1999;32(25):8427-8440.

49. Pasternak R, Burns G, Heller J. Diffusion and solubility of simple gases through a copolymer of hexafluoropropylene and tetrafluoroethylene. *Macromolecules*. 1971;4(4):470-475.

50. Budd PM, Msayib KJ, Tattershall CE, et al. Gas separation membranes from polymers of intrinsic microporosity. *J Membr Sci*. 2005;251(1):263-269.

51. Ghanem BS, McKeown NB, Budd PM, et al. Synthesis, characterization, and gas permeation properties of a novel group of polymers with intrinsic microporosity: PIM-polyimides. *Macromolecules*. 2009;42(20):7881-7888.

52. Ma X, Swaidan R, Belmabkhout Y, et al. Synthesis and gas transport properties of hydroxyl-functionalized polyimides with intrinsic microporosity. *Macromolecules*. 2012;45(9):3841-3849.

53. Fritsch D, Bengtson G, Carta M, McKeown NB. Synthesis and gas permeation properties of Spirobischromane-Based polymers of intrinsic microporosity. *Macromolecular Chemistry and Physics*. 2011;212(11):1137-1146.

54. Socrates G. *Infrared and raman characteristic group frequencies: Tables and charts.* John Wiley & Sons; 2004.

55. Likhatchev D, Gutierrez-Wing C, Kardash I, Vera-Graziano R. Soluble aromatic polyimides based on 2, 2-bis (3-amino-4-hydroxyphenyl) hexafluoropropane: Synthesis and properties. *J Appl Polym Sci*. 1996;59(4):725-735.

56. Tullos G, Mathias L. Unexpected thermal conversion of hydroxy-containing polyimides to polybenzoxazoles. *Polymer*. 1999;40(12):3463-3468.

57. Lim J, Kim M, Goh M, et al. Synthesis and characterization of polybenzoxazole/graphene oxide composites via in situ polymerization. *Carbon letters*. 2013;14(4):251-254.

58. Park HB, Han SH, Jung CH, Lee YM, Hill AJ. Thermally rearranged (TR) polymer membranes for CO_2 separation. *J Membr Sci*. 2010;359(1):11-24.

59. Carey FA, Sundberg RJ. *Advanced organic chemistry: Part A: Structure and mechanisms.* Vol A. 5th Edition ed. New York, NY: Springer Science and Business Media; 2007:1200.

60. Ghosh MK. *Polyimides: Fundamentals and applications.* 1st Edition ed. New York, NY: Marcel Dekker, Inc.; 1996:912.

61. Frequently asked questions about flowmeters. http://www.Dwyer-inst.com/Product/Flow/Flowmeters/VariableArea/SeriesRM#Questions. Accessed August 1, 2016.

62. Pinnau I, He Z. Pure-and mixed-gas permeation properties of polydimethylsiloxane for hydrocarbon/methane and hydrocarbon/hydrogen separation. *J Membr Sci*. 2004;244(1):227-233.

63. Guo R, Sanders DF, Smith ZP, Freeman BD, Paul DR, McGrath JE. Synthesis and characterization of thermally rearranged (TR) polymers: Effect of glass transition temperature of aromatic poly (hydroxyimide) precursors on TR process and gas permeation properties. *Journal of Materials Chemistry A*. 2013;1(19):6063-6072.

64. Scholes CA, Ribeiro CP, Kentish SE, Freeman BD. Thermal rearranged poly (benzoxazole-co-imide) membranes for CO_2 separation. *J Membr Sci*. 2014;450:72-80.

65. Chern R, Koros W, Yui B, Hopfenberg H, Stannett V. Selective permeation of CO_2 and CH_4 through kapton polyimide: Effects of penetrant competition and gas-phase nonideality. *Journal of Polymer Science: Polymer Physics Edition*. 1984;22(6):1061-1084.

66. Park CH, Tocci E, Kim S, Kumar A, Lee YM, Drioli E. A simulation study on OH-containing polyimide (HPI) and thermally rearranged polybenzoxazoles (TR-PBO): Relationship between gas transport properties and free volume morphology. *The Journal of Physical Chemistry B*. 2014;118(10):2746-2757.